Assembly of Biological Building Blocks for Nano- and Micro-fabrication of Materials

by

Chung-Yi Chiang

SUBMITTED TO THE DEPARTMENT OF MATERIALS SCIENCE AND ENGINEERING IN PARTIAL FULFILLMENT OF THE REQUIREMENTS FOR THE DEGREE OF

DOCTOR OF PHILOSOPHY

AT THE
MASSACHUSETTS INSTITUTE OF TECHNOLOGY

FEBRUARY 2008

Signature of Author: _____
Department of Materials Science and Engineering
January 18, 2008

Certified by: _____
Angela M. Belcher
Germeshausen Professor of Materials Science and Engineering and Biological Engineering
Thesis Advisor

Accepted by: _____
Samuel M. Allen
POSCO Professor of Physical Metallurgy
Chair, Departmental Committee on Graduate Students

Assembly of Biological Building Blocks for Nano- and Micro-fabrication of Materials

by

Chung-Yi Chiang

Submitted to the Department of Materials Science and Engineering on
January 28, 2008 in Partial Fulfillment of the Requirements for the Degree of
Doctor of Philosophy in Materials Science and Engineering

ABSTRACT

Experimental studies were performed to fabricate various material structures using genetically engineered M13 bacteriophage. This virus template showed superior controls of material syntheses from nanoscale to microscale. Structures including nanowires, nanoparticle arrays, hetero-particle arrays, and micro-fibers were fabricated using the engineered M13 virus as the building block and mineralization platform. The mineralization mechanisms were revealed by alternating the types and amounts of peptide motifs displayed on the viral templates. The results showed the importance of a fused peptide motif to mediate the mineralization process of a material, which was dominated by either physical absorption or chemical nucleation. The potential applications of the materials synthesized using the viral template, including energy generation and biosensors, were also demonstrated. For the first time, several types of highly engineered M13 virus were used to fabricate nanostructures such as nanowires, nano-arrays, hetero-particle arrays, and complex nanowires. A type 8 phage library was reported to screen peptide motifs for making nanowires. A multi-functionalized viral template, type 8-3 virus, was engineered and demonstrated to create a variety of nano-archietetures. A type 8+8 virus was used to create complex nanowires embedded with different materials. In addition, the mechanical properties of virus-based materials were evaluated and characterized for the first time. The tunable functionalities and mechanical performances of virus-based materials showed promising capabilities not only to manipulate material syntheses and structures but also to be integrated with other synthetic materials using current processing techniques.

Thesis Advisor: Angela M. Belcher
Title: Germeshausen Professor of Materials Science and Engineering and Biological Engineering

ACKNOWLEDGMENT

Foremost, I thank my advisor, Professor Angela Belcher for mentoring, encouraging, and providing plentiful resources, inspirations, kindness, and unwavering support. I also thank Professor Krystyn Van Vliet for her research guidance on the virus fiber project. I gratefully acknowledge Professor Michael Rubner for his comments and suggestions on my research and teaching. I appreciate all the helps and assistances from my collaborators, Professor Evelyn Hu, Professor Yu Huang, Dr. Charlene Mello, Dr. Yan Gao, Dr. Ki Tae Nam, Dr. Soo-Kwan Lee, Mr. Emilio Silva, and Ms. Jiji Gu. I also appreciate the discussions, inspirations, and encouragements from Dr. Jifa Qi, Dr. Sreekar Bhaviripudi, Dr. Dong-Soo Yun, Dr. Asher Sinensky, Dr. Rana Ghosh, Ms. Jennifer Hsieh, Ms. Amy Shi and all the other members in Belcher's lab. Thank my friends, An-Ling, Miao, Ming, Hong-Ren, Ching-Yin, Kevin, Cheng-Wei, Chia-Hua, Shu-Wei, Tracy, Vivian, Nancy, Yu-Hua, Pei-Chun, Yi-Chun, Liang-Yi, Ivy, for making my MIT life memorable. I also thank my parents for accepting my decisions and forgiving me not sharing the family loads in these years. Finally, I also thank my funding sources from Army Research Office Institute of Collaborative Biotechnologies (ARO-ICB) and David and Lucile Packard Foundation.

There are a lot of changes in my life during these years at MIT. I won some and also lost some. That is the life. Living, is to witness a story of life.

BIOGRAPHICAL NOTE

Education

2002- 2008 **Ph.D. in Bio- and Polymeric Materials Program**
Minor in Applications and Policy of Emerging Technology
Department of Materials Science and Engineering, M.I.T., USA
Thesis: Assembly of Biological Building Blocks for Nano- and Micro-fabrications of Materials
Advisor: Prof. Angela M. Belcher

1997-1999 **M.S. in Chemical Engineering**
National Cheng-Kung University, Taiwan
Thesis: Synthesis and Characterization of Novel Polyurethane Containing Phosphoramide Linkages
Advisor: Prof. Jen-Fong Kuo

1993-1997 **B.S. in Chemical Engineering**
National Cheng-Kung University, Taiwan
Thesis: Drug Controlled-Release of Polyurethane
Advisor: Prof. Jen-Fong Kuo

Awards

2006 Materials Research Society (MRS) Graduate Student Award Silver Winner
1999 Elected Honorary Member of the Phi Tau Phi Scholastic Honor Society
1995 Mr. Ni-Lee Scholarship of Chung Kung Culture Foundation
1994 Outstanding Student Award of National Chung-Kung University

Publication/Patent

Chung-Yi Chiang, Charlene M. Mello, Jiji Gu, Emilio C. C. M. Silva, Krystyn J. Van Vliet, Angela M. Belcher, "Weaving Genetically Engineered Functionality into Mechanically Robust Virus Fibers", *Advanced Materials*, 19(6), pp. 826-832 & cover, 2007

Ki Tae Nam, Dong-Wan Kim, Pil J. Yoo, **Chung-Yi Chiang**, Nonglak Meethong, Paula T. Hammond, Yet-Ming Chiang and Angela M. Belcher, "Virus-Enabled Synthesis and Assembly of Nanowires for Lithium Ion Battery Electrodes", *Science*, 5775(312), pp. 885-888, 2006

Yu Huang*, **Chung-Yi Chiang***, Soo Kwan Lee, Yan Gao, Evelyn L. Hu, James De

Yoreo, and Angela M. Belcher, "Programmable Assembly of Nanoarchitectures Using Genetically Engineered Viruses", *Nano Letter*, 5(7), pp 1429-1434, 2005 (*Equally contribute to this work)

Ki Tae Nam, **Chung-Yi Chiang**, Angela M. Belcher, "Virus Scaffold for Self-assembled, Flexible and Light Lithium Battery" (Patent, WO2006045076)

Teaching Experience

2007 **Teaching Assistant,** *M.I.T., USA*
Organic and Biomaterials Chemistry (Undergraduate Level)

1997 – 1999 **Teaching Assistant,** *N.C.K.U., Taiwan*
Chemical Engineering Thermodynamics (Undergraduate Level)
Process Control (Undergraduate Level)
Process of Chemical Engineering (Undergraduate Level)
Advanced Chemical Engineering Thermodynamics (Graduate Level)

Professional Experience

2006 **Platform and Technological Chief Engineer**
Phototaxis Solar (Start-up), USA
- Finalist in 2006 **Ignite Clean Energy $125K Competition**

2001 – 2002 **Research Engineer,**
Department of Research, CSB Battery Co., Ltd, Taiwan

1999 – 2001 **2nd Lieutenant Reserved Officer**
Army, Taiwan

Table of Contents

List of Tables

List of Figures

Chapter I. Introduction

I.A. Motivation

Nature has developed remarkable controls and means of material syntheses and fabrications for various applications. Nature's engineering is truly amazing. We have observed beautiful archetictures, strong materials, and even functional devices from natural products. Nature precisely constructs complicated but well-organized material structures from nanometric through micormetric to metric scales. One of the examples is the structure of diatom (Figure 1). Diatom is a type of eukaryotic alga and unicellular plankton. The cell wall of diatom is made of silica[1, 2], and the structure of silica is highly ordered and hierarchically constructed on the cell. Another example is the abalone shell (Figure 2). The shell of abalone is made of calcite[3-5]. The mechanical strength of the abalone-made calcite is hundred times stronger than its geological counterpart. The reason why it can be so strong is because of the nanostructured and highly ordered crystallized calcite assembled into the shell. Another example is the magnetotactic bacterium (Figure 3). It mineralizes magnetite in the membrane organelle called magnetosome and secretes a chain of magnetite particles aligning inside the cytoplasm[6, 7]. The magnetotactic bacterium exhibits a special ability to align itself in the direction of the earth magnetic field. It is believed that this bacterium is using the magnetite to navigate itself. From these examples, it is not hard to find that nature can produce various organized, strong and functional materials.

If we trace the synthetic or fabrication routes to see how nature makes these terrific materials, it may end up to find that all these natural structures, components, and functionalities are originally governed by the molecule, DNA. This fabrication mechanism is not only simple but also complicated. It is simple, because DNA only has four types of bases with single type of molecular backbone (sugar and phosphate). It is also complicated, because DNA derives into 20 amino acids, which are the structural units of proteins. Thousands of combinations of the amino acids produce millions of different polypeptides, and hundreds of posterior modifications on the polypeptides are executed by nature to make various proteins. Millions of organelles, cells, creatures and species are therefore created.

From the viewpoints of chemical engineering, I am intrigued by the accuracies of controls on the material syntheses by manipulating a few parameters, the four bases in DNA. From the aspects of materials science and engineering, I am interested in understanding and extending the advantages of these naturally evolved and developed fabrication techniques. How can people use or mimic the natural routes to make various materials that are useful for contemporary material's world, e.g. fabricating nanowires for electronics or producing fibers for functional clothing?

I.B. Scope of Work

This work was focused on using natural templates to create nano- and micro-materials of interesting structures, properties and functionalities. From the route that nature has developed to synthesize materials, proteins are the mediators between the constructing instructions (i.e. DNA information) and the final products (e.g. abalone shell). Proteins are used as the building scaffolds to construct and assemble various components into natural products (Figure 4). There are a lot of choices of bio-organisms potentially can serve as biological templates to manipulate the syntheses of materials. In this thesis, M13 bacteriophage was chosen as the research tool to demonstrate the intelligent designs and controls of material fabrications by manipulating the genome. The filamentous structure of M13 bacteriophage provides a low-dimensional building block, one-dimensional nano-filament, of nanometer scale. Ranging from nanometric to micrometric scales, the exploitation of precise controls on the expressions, conformations, and functionalities of the bacteriophage building block were demonstrated, and the characterizations and applications of the materials fabricated using the M13 bacteriophage were examined and discussed in the thesis.

I.C. Figures

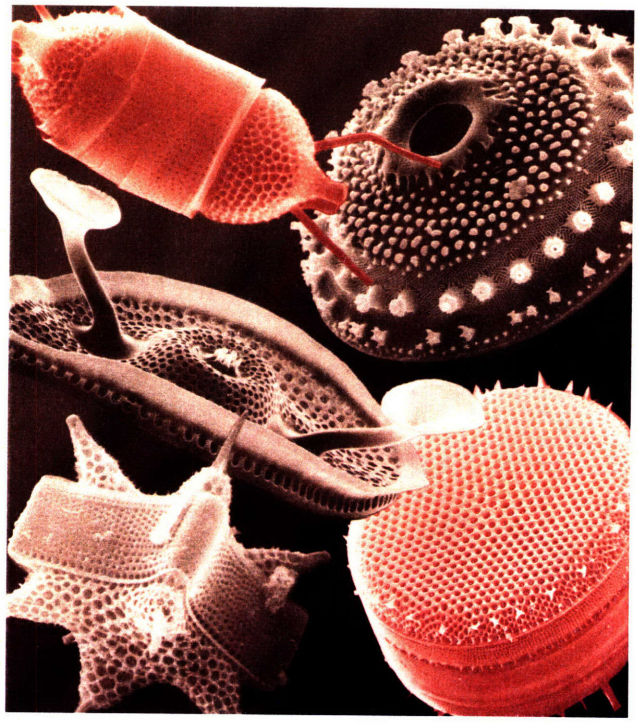

Figure 1. Hierarchically and highly organized silica (SiO_2). Diatoms, unicellular planktons living in the sea. Their cell walls are made of silica through highly organized biomineralizations. (Daniel Morse, UCSB)

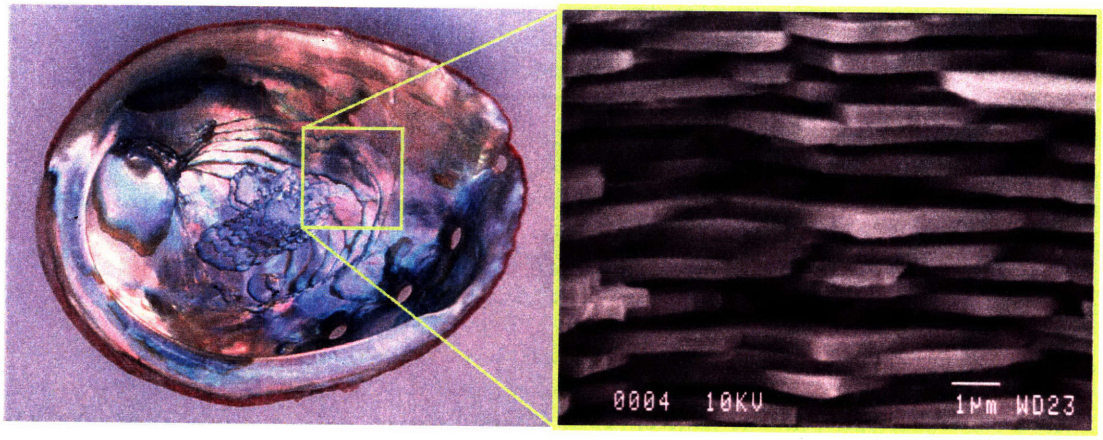

Figure 2. Tough calcite ($CaCO_3$). The abalone shell is comprised of layers of crystallized calcite. Between two calcite sheets is a layer of proteins serving as adhesives

to hold the structures and platforms to mineralize calcite. (Angela Belcher, M.I.T.)

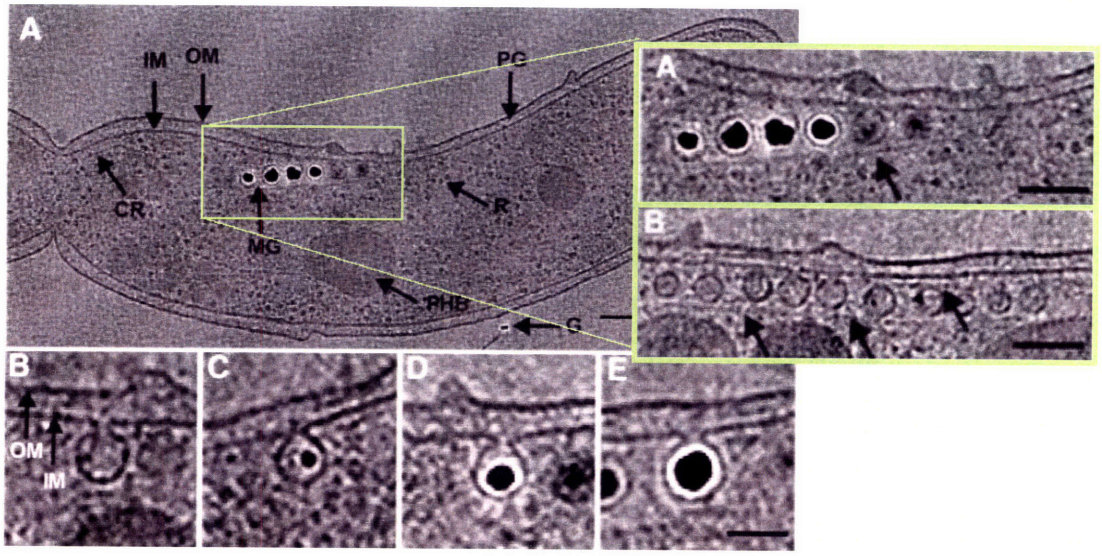

Figure 3. Functional magnetite (Fe_3O_4). A magnetotactic bacterium secretes magnetite nanoparticles in the periplasmic space and aligns these nanoparticles inside the cytoplasm to serve as guiding devices. (Arash Komeili, UC-Berkeley)

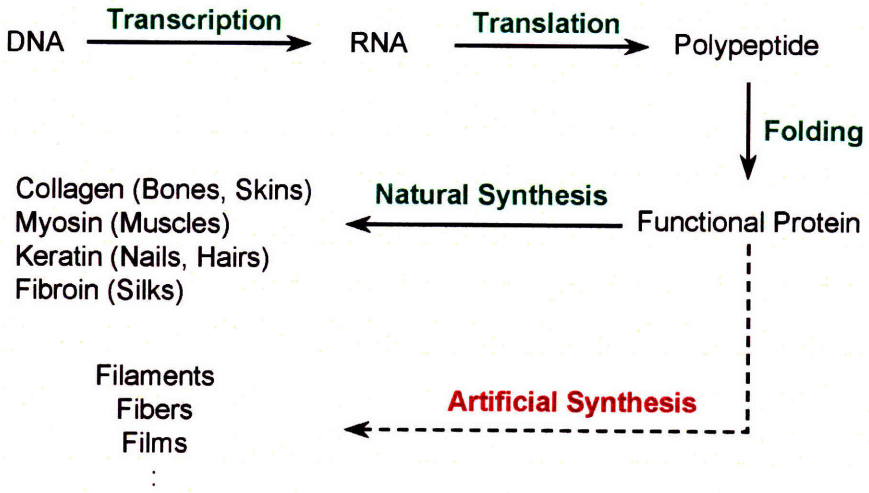

Figure 4. Fabrication lines of natural and artificial materials. New types of synthetic materials can be fabricated through mimicking natural processes and utilizing natural templates, providing outstanding molecular controls at different scales.

Chapter II. Biologically engineered toolkit and preliminary identification of peptides

II.A. Summary

M13 bacteriophage is a well-known filamentous virus. Its whole genome has been revealed and studied for years. It is a non-lytic virus and harmless to mammalian cells. The capsid protein groups on a viral particle can be independently altered by engineering the viral genome. The ease to modify and engineer the M13 bacteriophage makes this virus a powerful biological toolkit. The dimensions and functionalities of a virus can be precisely and simply controlled by manipulating the genome. Unlike the other biological molecules such as protein and DNA serving for templating applications, biological organisms such as M13 viruses have precisely defined structures. Its programmable protein functionalities promise the ultimate flexibility in assembling hetero-functional nanostructures, which makes this viral system an attractive template for synthesis and assembly of various materials and structures. M13 bacterioaphge can be used not only to serve as the templating material for nanotechnology but also to create peptide libraries for biological applications. By displaying random peptides on a certain group of proteins on the bacteriophage, a phage display library can be constructed. Phage display library is the pool of bacteriaphages contains millions of random peptide sequences. A peptide motif of interest to target a specific material is acquired through the evolutionary screening process, biopanning. To select peptides for targeting materials of interest, type 3 phage display libraries are commonly used. However, a peptide selected from a type 3 library may not function correctly when it is expressed on a different type of protein. Therefore, to obtain effective functionalities on the bacteriophage surface, it is essential to design suitable peptides for different types of coat proteins. In this chapter, the methodologies used to select functional peptide motifs and to engineer the viral templates will be discussed. Besides, the type 8-3 engineered virus for hetero-architectures and the type 8 library for biopanning and biomineralization were reported for the first time.

II.B. Introduction

M13 bacteriophage

M13 bacteriophage (or virus) is a type of filamentous virus. The dimensions of M13 bacteriophage are 880 nm in length and 6 to 7 nm in width, giving a high aspect ratio of about 150. The length of this virus is determined by the size of viral DNA (deoxyribonucleic acid), which is about 6,400 nucleotides long for a wild-type strain. M13 bacteriophage has a circular single strand DNA (ss-DNA) enclosed in a cylindrical capsid. The DNA encodes 11 genes for a wild-type M13 virus. The viral DNA stores all the information for signaling the bacterium host to produce various proteins, including DNA replication proteins, capsid proteins and assembly proteins. Figure 1 shows a commercialized DNA vector of M13 bacteriophage. The first group of genes, II, V, and X, producing proteins are required for the replication, transportation and folding of the viral DNA. The proteins produced by the group of genes, III, VI, VII, VIII, and IX, constitute the cpasid proteins of the bateriophage particle. The last group of genes, I, IV, and XI, produces proteins involving in packing the capsid proteins onto the viral DNA to form bacteriophage particles.

The capsid of the virus is comprised of approximately 2,700 copies of the major coat proteins pVIII, capped with about 5 copies each of minor proteins pIII and pVI at one end of the bacteriophage, and about 5 copies each of minor proteins pVII and pIX at the other end. A summary of these coat proteins is listed in the Figure 2. pVIII is the most abundant capsid protein, which is helically packed around the long axis of DNA in a right-handed way (Figure 3). X-ray diffraction and other studies have given well descriptions of the structure of pVIII protein[8, 9]. It exhibits an uninterrupted alpha helical conformation except for the first five amino acids from the N-terminus (Figure 4). pVII and pIX are hydrophobic proteins. The arrangement of these proteins at one end of the capsid is still unknown. pIII and pVI proteins assembled on the other end of the capsid account for 10-16 nm of the bactiophage length. pIII protein is the largest coat protein (about 400 amino acids) in the capsid (Figure 5). It is a globular protein and an essential region for the infection process of virus[10, 11].

The amino acids of these coat proteins residing at different locations on a viral particle can be rationally altered independently via genetic engineering.[12] The methodology to express peptides or proteins on these coat proteins is so called phage display. It is a powerful new technique for carrying out molecular evolution in the laboratory. The display of peptides or proteins on the surface of bacteriophage is achieved by cleaving and recombining DNA fragments through the restriction sites in the viral DNA. The programmable capability and its inherent structural advantages promise the extraordinary flexibility in assembling nanostructures, which makes this viral template an powerful engineering stytem for synthesis and assembly of various materials and architectures.

Modifications of M13 bacteriophage

Various types of vectors are commercially available for peptide fusions on the surfaces of M13 bacteriophage particles. Through standard molecular biological methods, more enzyme restriction sites can be introduced into the viral vector for the convenience of genetic engineering, and therefore various types of phage displays can be achieved. Viral vectors that display fusions in genes III and VIII are termed type 3 and type 8. Bacterial cells carrying these type 3 or type 8 vectors will assemble the virus particles with 100% identical and recombinant pIII or pVIII coat proteins, respectively. In another amplification system, two independent vectors are introduced into a bacterial cell for producing two different pIII proteins (or pVIII proteins) simultaneously. One vector is phagemid vector, which carries a copy of either gene III or VIII but does not have the groups of genes for the assembly of bacteriophage. The other vector is M13 viral vector (referred as helper vector or helper phage), which encodes the full genes (including wild-type gene VIII) for virus amplification. When a bacterial cell harboring the phagemid vector is infected by M13 bacteriophage (helper phage), the amplified bacteriophage particles will carry a mixture of wild-type (from helper phage) and recombinant (from phagemid) pIII or pVIII proteins.[13, 14] The bacteriophages produced using the phagemid system are termed type 3+3 or 8+8. Other types of virus structures such as type 33 and type 88 theoretically could be achieved through genomic

modifications. In this thesis, type 3, type 8, type 8+8, type 8+8-3, and a new type 8-3 phage are used and engineered (Figure 6). Type 8-3 has two distinct peptide motifs displayed on pIII and pVIII proteins. And, type 8+8-3 has two types of pVIII proteins and one type of pIII proteins assembled on the bacteriophage particle.

Recombination and transformation

A M13 bacteriophage particle contains a single-strain deoxyribonucleic acid (ss-DNA), which encodes all the information to replicate the viral DNA itself and produces assistant and coat proteins to assemble viruses in a bacterial host. To modify the genome of M13 bacteriophage, the replicative form DNA (RF DNAs) is first extracted from the infected Escherichia coli (E. coli) and digested by specific restriction enzymes. The designed and synthesized DNA fragment is then recombined with the cleaved RF DNA. The new recombinant DNA containing the inserted DNA fragment is transfected into fresh E. coli using electroporation or heat shock to produce more engineered DNAs and viruses. The whole processing scheme is depicted in Figure 7.

Phage display of random peptides

One important application of phage display is to construct combinatorial peptide libraries. Synthetic oligonucleotides with fixed length and random codons are fused to genes III or VIII of M13 bacteriophage vectors. The fusions are expressed as random peptides on the surfaces of bacteriophage particles to form library pools. The phage display peptide libraries is then used for screening peptides to target materials of interest. Two types of libraries are employed in this thesis. Type 3 libraries are purchased from New England Biolabs. And, type 8 library is constructed by Dr. Soo-Kwan Lee in Prof. Angela M. Belcher's lab at M.I.T.

Biopanning

Biopanning is an evolutionary technique employed to select peptides from peptide libraries in the laboratory (Figure 8). To select a suitable peptide to target a material of interest, the phage library is exposed to the selected material. Some of the phages bind to the selected material and some do not. Unbound phages are washed off the material, and the phages bound to the selected material are eluted from the material surface by changing the environmental pH or temperature. Those phages eluted from the material are then sequenced to characterize the peptide motifs on the coat proteins. Meanwhile, the eluted phages are amplified to serve as the sub-library for the next round of biopanning. This panning process will be repeated until the consensus peptide motif is found.

II.C. Experimental

II.C.1. Biopanning for anti-gold sequence for pIII protein under reduced condition

Materials. Phage display libraries Ph.D.-7C7^{TM} and Ph.D.-12^{TM} were purchased from New England Biolabs. All media and solutions were prepared according to the instruction manuals of the phage libraries. Dithiothreitol (DTT) was purchased from MP Biochemicals. Gold slides purchased from EMF Corp. were cut into 5 mm x 5 mm squares.

Biopanning method. 10 μL phage library was diluted to 1 mL with Tris-buffered saline (TBS). The diluted library solution was added into a microtube containing a gold square. The tube was rocked for 1 hr at room temperature. After transferring the solution to a fresh microtube, the library solution was mixed with DTT (1 M, 10 μL) for 30 min and then incubated with a fresh gold square for 1 hr. The supernatant was discarded, and the gold square was washed with 1 mL TBS 10 times. After the washing steps, the gold square was incubated with Glycine-HCl (pH = 2.2, 0.2 M, 500 μL) for 10 min to elute the phages physically bound to the gold substrate. The supernatant of glycine-HCl solution was discarded. The gold square was then incubated with bacteria culture for amplification (bacterial elution). After 4.5 to 5 hr, the amplified phages were purified and concentrated to make the sub-library. The sub-library was tittered and the clones in this sub-library were sequenced. The sub-library was then used to pan for the next round. The procedure was repeated until a consensus of peptide sequences was found.

Binding affinity test. The selected virus clone from the biopanning was incubated with DTT (the final concentration was 10 mM) for 30 min. The reduced virus was then incubated with gold squares for 1 hr. The same virus without incubating with DTT was used as the negative control sample in this experiment. The supernatant was discarded and the gold substrate was washed 10 times with 1 mL TBS buffer. Glycine-HCl solution was added to elute the bound virus and neutralized to pH 7 with Tris-HCl (pH = 9.2). The elution was added to the bacteria culture for amplifying the virus, followed by purification, titration and sequencing. Meanwhile, the gold substrate was incubated in bacteria culture for bacterial elution and phage amplification, also followed by

purification, titration and sequencing. Both the virus eluted from the Au surface and remaining on the Au substrate were quantified.

II.C.2. Amplification of type 8+8 and 8+8-3 virus

Materials. Bacteria clone carrying pMoPac16 vector (phagemid) with anti-gold motif, LKAHLPPSRLPS (termed p3-Au12), selected by Dr. Daniel Solis, was used as the host. The helper phage used to induce the amplification in bacterial cells was the wild-type virus (M13KE, from New England Biolabs) or the virus clones selected in section **II.C.1**.

Amplification condition. A hundred-fold dilution of the overnight bacterial culture harboring the phagemid with anti-gold sequence was prepared in Terrific Broth. The bacterial culture was grown to mid-log phase (OD_{600} ~ 0.5). 10 μL helper phage (~10^8 pfu/μL) was added into the bacterial culture and incubated at 37°C for 5 minutes without shaking. Isopropyl β-D-thiogalactoside (IPTG, 100 mg/mL) was added to make the final concentration of 100 μg/mL in the amplification culture. The culture was then incubated at 37°C for 1 hr without shaking, followed by 5 – 6 hours incubation in the 37°C incubator shaker. All virus clones were amplified to the concentration of ~10^9 pfu/μL.

SDS-PAGE electrophoresis. The fusion of p3-Au12 onto the pVIII proteins was verified and quantified using electrophoresis. Novex® 16% Tris-Glycine Gels purchased from Invitrogen were used in electrophoresis. The virus sample was denatured at 95°C for 2 min before loading. Mark12™ (Invitrogen) was used as the protein standard. The electrophoresis was carried out at 125 V, and the gel was stained using SilverQuest™ Silver Staining Kit (Invitrogen).

II.C.3. Biopanning for anti-gold sequence using type 8 phage library

Materials. Gold squares (5mm x 5mm) were used for the panning. Type 8 phage library constructed by Dr. Soo-Kwan Lee was used for the biopanning. In this type 8 phage display library, peptides containing eight random residues are fused to the major coat

protein. The random octa-peptides are expressed at the N-terminus of pVIII protein where the first residue of the fusion is preceded by an alanine and the last residue is followed by the wild-type pVIII sequence. The sequencing primer was -96 gIII sequencing primer purchased from New England Biolabs. All media and solutions used were the same as those used for the type 3 libraries.

Panning method. The anti-gold M13 bacteriophage was selected via the screening of a type 8 phage display library. The type 8 library was exposed to the gold substrate in Tris-buffered saline (TBS, pH 7.5) containing 0.1% (v/v) Tween-20. After rocking for one hour, the gold substrate was washed 10 times with TBS (pH 7.5). The bound phage was eluted by addition of 1 mL Glycine-HCl (0.2M, pH 2.2) containing 1mg/mL bovine serum albumin (BSA). The eluate was neutralized by adding 300 μL Tris-HCl (1 M, pH 9.1). A small amount (~10 μL) of the eluate was plated on LB XGal/IPTG plates. Plaques on the plates were randomly picked and DNA sequenced. The rest of the eluate was mixed with Escherichia coli ER2537 (New England Biolabs) host to amplify the concentration to approximately 10^9 pfu/uL. This sub-library was used for the next round of biopanning.

II.C.4. Construction of type 8-3 M13 bacteriophage

Materials. The replicative form DNA of gold binding virus (p8#9) selected from the type 8 library in **Chapter II.C.3.** was extracted from the bacterial cells infected by p8#9 clone. The restriction enzymes Eag I and Acc65 I were purchased from New England Biolabs. The synthetic oligonucleotide s1 and s1-primer were synthesized by Integrated DNA Technologies. The sequence of oligonucleotide s1 was 5'-CATGTTTCGGCCGAACCT CCACCCTACGATGCTGCAGCAAATGAGAATAAGGATCCCAAGAGTGAGAATA GAAAGGTACCCGGG-3', and that of the s1-primer was 5'-CATGCCCGGGTACCTTT CTATTCTC-3'. XL-1 Blue electrocompetent bacteria used for transformation were purchased from Stratagene.

Genetic modification. The DNA of p8#9 clone was a derivative of M13SK vector, a

modified vector from M13KE. The M13SK vector contains Eag I and Acc65 I restriction sites in gene III. The RF DNA of p8#9 was digested by Eag I and Acc65 I and purified using electrophoresis. The PCR product of oligonucleotide s1 and s1-primer was also digested by Eag I and Acc65 I. This ds-DNA fragment containing the gene to express the anti-streptavidin peptide (WDPYSHLLQHPQ, termed p3s1) on pIII protein was then ligased into the digested ds-DNA of p8#9. The recombinant DNA was electroporated into XL-1 Blue bacteria for amplification. The produced type 8-3 phage was named #9s1 phage.

MALDI mass spectrum. The peptide display on pVIII proteins was confirmed using mass spectrometry. 500 μl of the phage-containing supernatant was added with 200 μL PEG/NaCl (20% (w/v) polyethylene glycol-8000, 2.5M NaCl) to precipitate phage particles. The phage pellet was suspended thoroughly with 100 μL iodide buffer (10 mM Tris-HCL (pH=8.0), 1 mM EDTA , 4 M NaI) and then added with 250 μL ethanol. After incubating 10 minutes at room temperature, the sample was centrifuged for 10 minutes to spin down unwanted DNA. The supernatant was collected for MALDI analysis. The mass spectrum of the phage proteins in the supernatant was acquired using an applied biosystem model Voyager DE-STR instrument for matrix assisted laser desorption/ionization time of flight (MALDI-TOF) mass spectrometry operated at linear mode.

Enzyme-linked immunosorbent assay (ELISA). The streptavidin-binding motif on pIII protein was verified using ELISA. Streptavidin-coated 96 plate wells (purchase from Pierce Biotechnology, Inc.) were blocked with blocking buffer (TBS + 0.05% Tween + 0.1% BSA) for 1 hour and washed with washing buffer (TBS + 0.05% Tween) 3 times. 2-fold serial dilutions of each phage clone were carried out in a row of ELISA plate wells and incubated for an hour. After washed with washing buffer 3 times, each well was added with 200 μL horseradish peroxidase (HRP) conjugated anti-M13 antibody (diluted 1:5000 in blocking buffer) solution, incubated for 30 minutes and then washed with washing buffer 3 times. 200 μl 2', 2'-azino-bis (3-ethylbenzthiazoline-6-sulphonic acid) diammonium salt (ABTS) solution containing H_2O_2 (hydrogen peroxide, Sigma-Aldrich) was added to each well to develop color. HRP turns ABTS substrate from colorless to

green at the presence of H_2O_2. Green coloration indicated the presence of the M13 bacteriophage in the well. The intensities of coloration were measured using microplate reader set at 405 nm.

II.D. Results and Discussion

The genetically controllable functionalities of the M13 bacteriophage make this virus an interesting templating material. The goal was set to design a virus which could be anchored onto the gold surface through its pIII proteins and mineralized to bind/grow Au nanoparticles on its pVIII proteins to form conductive nanowires on the gold substrate. To reach this goal, the gold-binding affinity and mechanism of the peptide displayed on pIII protein should be distinct from that on pVIII protein. A wild-type pIII protein contains 8 cysteines, forming four disulfide bonds to stabilize the tertiary structure of the protein. Three of four disulfide bonds are located in the N-terminal domain (Figure 5).[10, 11] When treated with reduction agents, the disulfide bond will be reduced to two sulfhydral (or thiol) groups. Besides, with the presence of reduction agents, the structure of pIII protein will change due to the dissociation of the intra-crosslinkages of disulfide bonds. The change of protein conformation will change the interaction between pIII protein and the surrounding material.

Additional parameters were therefore introduced in the regular biopanning process for selecting a distinct peptide motif. The sequences screened from the biopanning for the anti-gold peptide under reduced condition are shown in Table 1 and 2. The consensus sequence from Ph.D.-C7C™ library was SHLHSPL, named p3-Au7C1r, and that from Ph.D.-12™ library was TMGFTAPRFPHY, named p3-Au12r. Both sequences were rich in positively charged amino acids such as histadine (H), arginine (R) and lysine (K). In addition, amino acids containing hydroxyl groups, such as serine (S), threonine (T) and tyrosine (Y), were also frequently observed. The results of the modified biopanning have high similarities to that of regular panning performed by others[15, 16]. One of the sequence screened using regular panning process in the laboratory was LKAHLPPSRLPS, termed p3-Au12. This sequence also contains mostly positively charged and hydroxyl groups.

It is well-known that thiol (-SH) group can covalently bind to gold metal. Thus, introducing cysteines to the N-terminal displayed peptide will also promote the binding affinity to the gold. To examine the binding affinity of the selected peptide to the gold could be promoted under the reduced condition, binding affinity tests were carried out.

Experiments showed that p3-Au7C1r clone had the best on-and-off gold-binding capability. Without treating with the reduction agent, p3-Au7C1r showed no binding affinity to the gold substrate (Figure 9). In the other words, the gold binding activity was only triggered in the presence of reduction agent. This peptide would be engineered onto the M13 bacteriophage to anchor the viral particle on the gold surface through the pIII protein as discussed in **Chapter IV**.

The type 8+8-3 virus carrying two distinct anti-gold motifs were engineered using the phagemid system. This was the virus designed to have two distinct anti-gold binding mechanisms on pIII and pVIII. A mixed displays of wild-type and p3-Au12 fusion were exhibited on pVIII proteins. The helper phage used during the amplification was the virus containing p3-Au7C1r on the pIII proteins, producing amplified virus with mixed expressions (wild-type and p3-Au12) on pVIII and p3-Au7C1r on pIII. The SDS-PAGE protein electrophoresis was used to examine the amount of p3-Au12 fused pVIII proteins. The results showed that the recombinant pVIII proteins displayed on the virus were less than 5% overall (Figure 10). This estimation was based on the comparison of band intensities between the wild-type pVIII band and the p3-Au12 fused pVIII band. The expression ratio of the fused pVIII proteins was about 27-fold lower than that of wild-type proteins. For a M13 bacteriophage containing 2700 copies of pVIII protein, there were about 100 copies of fused p3-Au12 pVIII protein. This low expression ratio resulted in deficient gold mineralization performed on this engineered virus. The details of the gold mineralization on virus templates to make Au nanowires are discussed in **Chapter III**. The low expression ratio might result from the low yield of recombinant pVIII proteins produced from the phagemid vector or other unknown viral assembly factors.

Although the type 3 library is the most commonly used screening pool, which is based on a combinatorial library of random peptides fused to pIII proteins, peptide motifs screened from a type 3 library cannot be directly translated to pVIII proteins because pIII and pVIII proteins have their distinct structure information. Fusing binding motifs chosen from the type 3 phage library to pVIII proteins may cause a deviation in the functionality of the displayed motifs and vice versa.[17] Therefore, to identify the desirable peptide

motifs for pVIII proteins in addition to avoiding the problem of low expression ratio mentioned above, a type 8 engineered library was exploited. It was used for the first time to select the gold-binding peptide for pVIII proteins.

The type 8 library was constructed by fusing eight random amino acids into the N-terminus of all the 2700 copies of the pVIII proteins[18] with a random population of 10^7-10^8. This library employed a modified M13KE phage vector (referred as the wild-type in the following chapter) by generating restriction sites, PstI and BamHI, in gene VIII through mutagenesis for the insertion of random codons ($Gnm(nnm)_6nnG$), where n = G, C, A or T and m = T or G. Unlike the previously described phage engineered using a phagemid system, phage in the type 8 library employ genome engineering that produces 100% expression and monodispersed viral dimensions.[12] Through the use of a general biopanning technique by exposing the type 8 phage library to gold thin films, anti-gold binding motifs on pVIII proteins were selected. The peptide sequence VSGSSPDS, which is named p8#9, emerged as the dominant binding motif after the forth round of the selection. The sequences screened from the panning process are listed in Table 3. This gold-binding motif contains four serines, each of which has a hydroxyl group on the side chain (Figure 11). Hydroxyl-rich peptides have been reported to have high affinity to gold lattices.[15, 16] Other data obtained from the biopanning of the type 3 library also show that hydroxyl-rich motifs are favorable for binding gold surfaces. Similar to the results that were obtained from the type 3 phage display libraries, the consensus peptide motif evolved from the biopanning of type 3 library was also rich in hydroxyl groups. Unlike the previous engineering scheme to transform the peptide selected from pIII protein to pVIII protein, the peptide selected from type 8 library is directly to be used on pVIII.

To extend the applications of this type 8 phage, p8#9, another peptide motif can be integrated into its pIII proteins. The pIII protein was genetically engineered with anti-streptavidin motif.[19] This new type 8-3 phage was hence named #9s1 clone (Figure 12). The anti-streptavidin motif displayed in pIII protein, which is named p3s1, can bind streptavidin independently with the existence of peptide p8#9 in pVIII proteins in the same phage particle. The functionality of the p3s1 binding motif was verified by an

enzyme-linked immunosorbent assay (ELISA)-based method (Figure 13). Each well of the ELISA plate was coated with streptavidin that can be bound by p3s1 motif. Green coloration indicated positive interaction, and the intensity of the green color represents the amount of the bound phage in the well. The result showed that both #9s1 and p3s1 had predominant binding affinities to streptavidins. It also proved the successful expression of s1 motif on pIII proteins in clone #9s1. Furthermore, the expression of the p8#9 motif on pVIII proteins was proven by mass spectroscopy. The peak at 5655.25 Da in the mass spectrum of #9s1 corresponded to the molecular weight of the engineered pVIII proteins, indicating that the anti-gold motif (p8#9) was 100% displayed on the pVIII proteins of bacteriophage (Figure 14). Another peptide motif, p3-Au7C1r was integrated into this p8#9 clone to create another type 8-3 clone, named #9-Au7C1r. This virus was used for grafting gold nanowires onto a gold substrate for biosensor in the **Chapter IV**.

II.E. Conclusion

Biopanning has greatly accelerated the design of peptide or protein for various applications. However, the success of a biopanning relies on the choice of library. It is extremely essential to have various types of libraries to fit the needs of peptide designing and engineering. Using the peptides selected from libraries also can avoid the problems of compatibility issues and mutations occurring in the transformations of rationally designed peptides. In addition, mutagenesis studies assisted with biopanning can be carried out to reveal the importance of individual amino acid in selected peptides for specific binding affinity/mechanism.

M13 bacteriophage is an ideal template that can be easily manipulated and modified to accommodate the needs of engineering. Engineering viral template can be accomplished and precisely controlled at molecular and nanometric scale. Several types of engineering on the M13 virus were demonstrated and proved in this chapter. In the following chapters, the applications of this viral template will be used to make materials for electronics, sensors, and fibers.

II.F. Tables and Figures

	Sequence								
Round 2	C	H	P	T	H	S	H	P	C
	C	P	D	L	K	L	P	S	C
	C	N	T	Y	G	R	H	E	C
	C	P	L	P	L	P	L	L	C
	C	P	G	S	G	I	Q	M	C
	C	T	L	G	T	P	H	L	C
Round 3	C	S	H	L	H	S	P	L	C
	C	S	H	L	H	S	P	L	C
	C	N	P	T	M	S	K	T	C
	C	N	T	Y	G	R	H	E	C
	C	S	H	L	H	S	P	L	C
	C	S	H	L	H	S	P	L	C
	C	N	P	T	M	S	K	T	C
	C	S	H	L	H	S	P	L	C
	C	S	H	L	H	S	P	L	C
	C	S	H	L	H	S	P	L	C
Round 4	C	S	H	L	H	S	P	L	C
	C	N	P	T	M	S	K	T	C
	C	S	K	L	H	S	S	L	C
	C	S	H	L	H	S	P	L	C
	C	S	H	L	H	S	P	L	C
	C	S	H	L	H	S	P	L	C
	C	S	H	L	H	S	P	L	C
	C	N	P	T	M	S	K	T	C
	C	N	P	T	M	S	K	T	C
	C	H	S	H	S	T	S	K	C

Table 1. Biopanning of Ph.D.-7C7™ library for gold binding sequence under reduced condition. Positively charged amino acids, histidine (H), lysine (K), and arginie (R), and hydroxyl amino acids, serine (S), threonine (T), and tyrosine (Y) frequently observed in the peptides screened from the library. Successive positively charged and hydroxyl amino acids were mostly present in these peptides.

	Sequence											
Round 2	S	M	V	Y	G	N	R	L	P	S	A	L
	S	I	P	P	S	R	D	Q	P	S	H	K
	S	T	T	I	A	G	T	N	L	P	P	W
	T	P	L	P	P	R	N	L	Q	S	A	P
	Y	K	P	P	H	Q	P	Y	M	N	S	H
	I	A	H	T	T	S	S	A	N	T	H	I
Round 3	T	M	G	F	T	A	P	R	F	P	H	Y
	Q	A	N	P	A	H	P	S	I	N	P	P
	T	M	G	F	T	A	P	R	F	P	H	Y
	T	M	G	F	T	A	P	R	F	P	H	Y
	S	I	N	P	A	P	Q	L	W	A	G	R
	T	M	G	F	T	A	P	R	F	P	H	Y
	S	I	N	P	A	P	Q	L	W	A	G	R
	A	A	N	S	R	Q	A	A	H	P	G	Q
	K	P	I	Q	Y	N	N	G	L	Q	A	F
	S	I	N	P	A	P	Q	L	W	A	G	R
Round 4	Y	A	G	A	A	D	Q	Q	D	F	F	P
	T	P	I	S	K	G	I	Q	L	S	R	A
	T	M	G	F	T	A	P	R	F	P	H	Y
	T	M	G	F	T	A	P	R	F	P	H	Y
	G	H	N	G	L	H	P	F	T	A	S	V
	D	R	A	P	L	I	P	F	A	S	Q	H
	T	M	G	F	T	A	P	R	F	P	H	Y
	A	S	S	N	S	P	L	Q	W	L	P	M
	T	M	G	F	T	A	P	R	F	P	H	Y
	D	R	A	P	L	I	P	F	A	S	Q	H

Table 2. Biopanning of Ph.D.-12™ library for gold binding sequence under reduced condition. Positively charged amino acids preceding or following hydroxyl amino acids were observed in the peptides screened from the library. However, no specific peptide motif predominated in the biopanning.

	Sequence								
Round 1	E	S	A	Q	P	G	P	M	
	-	-	E	G	D	-	-	-	X 9
Round 2	E	P	T	S	D	G	P	V	
	V	S	G	S	S	P	S	D	X 6
	-	-	E	G	D	-	-	-	X 14
Round 3	G	L	D	G	S	A	P	V	
	V	S	G	S	S	P	S	D	X 7
	-	-	E	G	D	-	-	-	X 12
Round 4	V	S	G	S	S	P	S	D	X 19
	-	-	E	G	D	-	-	-	X 1

Table 3. Biopanning of type 8 library for gold binding sequence. In the first round, wild-type virus was dominant. A sequence, named p8#9, started dominating in the second and rest of rounds. The sequences observed in this biopanning also contained hydroxyl amino acids as observed in the biopannings using type 3 libraries shown in Table 1 and 2.

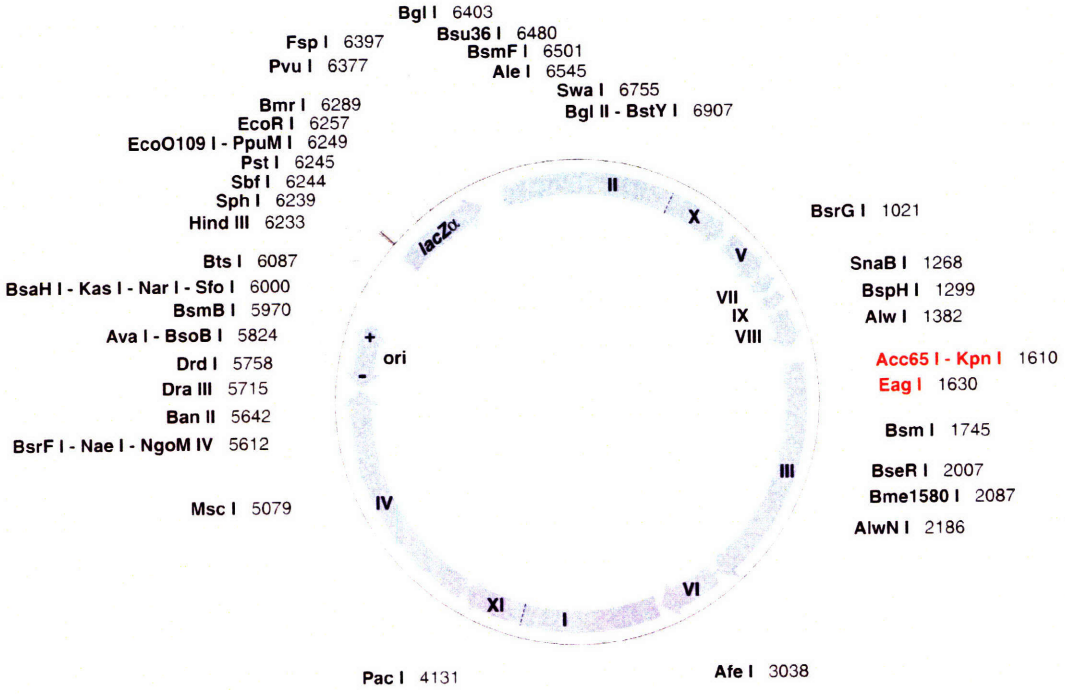

Figure 1. Commercialized M13 bacteriophage vector M13KE. It was designed for the convenience to insert an engineered peptide into pIII protein through Acc65 I and Eag I restriction sites. M13KE vector was used to construct the new vector M13SK for type 8 library and other types of engineered viruses. (Source: New England Biolabs catalog)

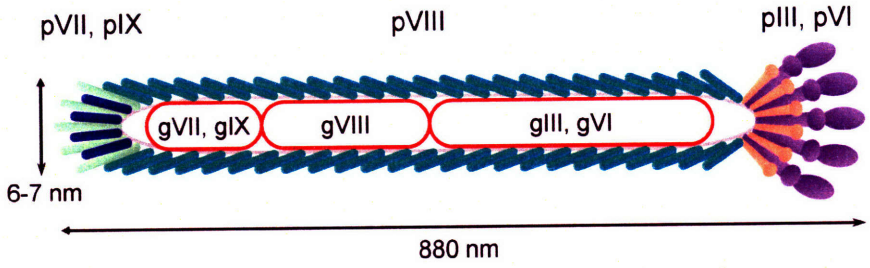

Protein	pVII	pIX	pVIII	pIII	pVI
Residues	33	32	73	427	112
No. of Copies	5	~5	~2,700	3-5	~5

Figure 2. Schematic representation of M13 bacteriophage and summary of coat proteins. M13 bacteriophage is a filamentous virus with 880 nm in length and 6 - 7 nm in diameter. It has five types of coat protiens encasing the viral DNA. pVIII protein is the major coat protein, which has 2,700 copies per bacteriophage. Other proteins are the minor coat proteins.

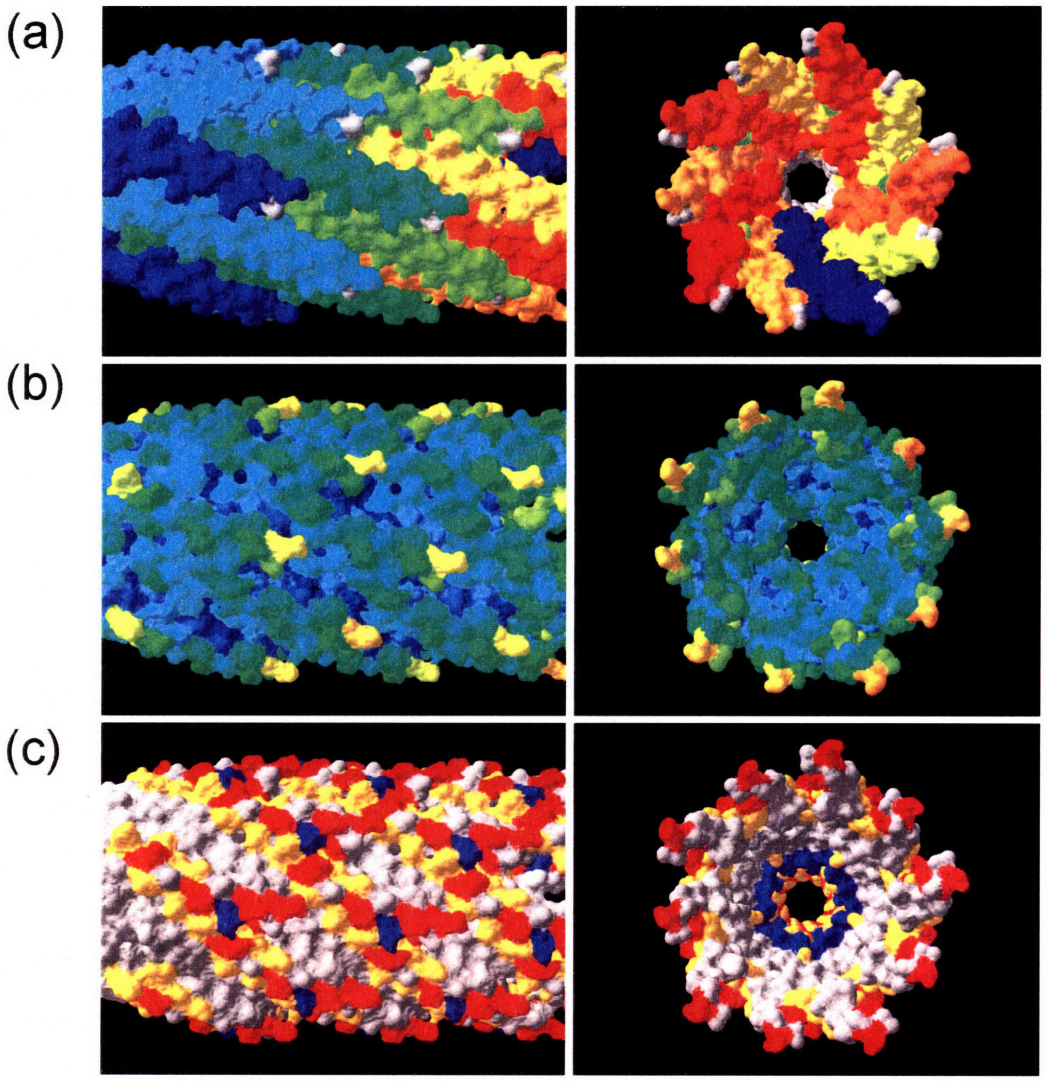

Figure 3. Molecular models of pVIII proteins packed on M13 bacteriophage. Side view (left) and cross section (right) of the assembled pVIII proteins. The molecular surfaces were colored by (a) individual pVIII proteins, (b) accessibilities to the surrounding environment, (c) types of amino acids. In figure (c), negatively charged amino acids (red) are mostly present on the outer surface, and positively charged amino acids (blue) are densely located in the core of virus capsid to stabilize the viral DNA,

which is negatively charged. Hydrophilic amino acids (yellow) are present both in the outer and inner regions of coat proteins. (Software: Swiss-PDB; Structure Model: 1IFJ)

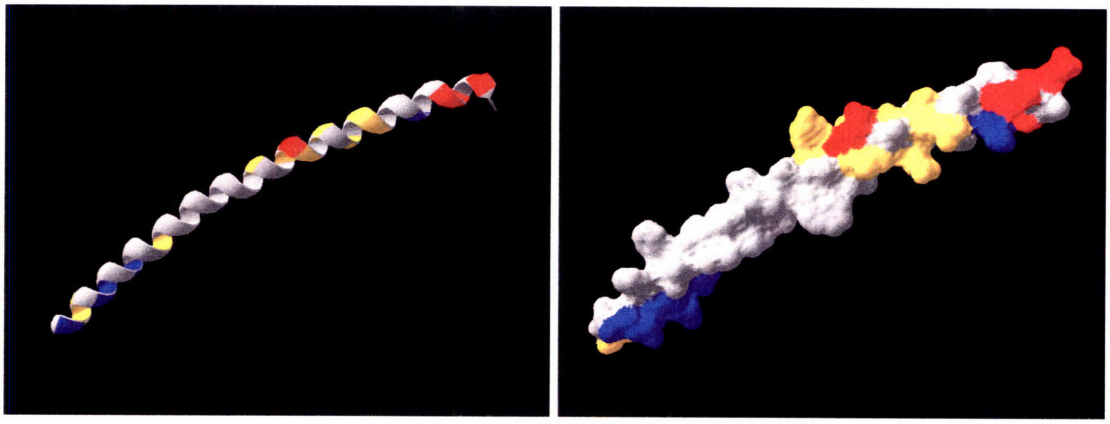

Figure 4. Molecular model of single pVIII protein. (Left) The ribbon structure colored by the types of amino acids shows alpha helical structure of pVIII protein. (Right) The molecular surface colored by the types of amino acids shows that negatively charged amino acids and hydrophilic amino acids are mostly present in the N-terminal region. Hydrophobic amino acids for adhering neighboring pVIII proteins are present in the middle to C-terminal region of pVIII protein. Positively charged amino acids are located at the C-terminal region. (Software: Swiss-PDB; Structure Model: 1IFJ)

Figure 5. Molecular model of the N-terminal domain of pIII protein in ribbon structure. pIII protein is a globular protein containing alpha- and beta-structures. In the

N-terminal domain, there are three disulfide bonds (in blue) comprised of six cysteines to hold the tertiary structure of pIII protein. The peptide insert is commonly displayed in the coil region following the alpha helix at N-terminus shown on the right of the picture. (Software: Swiss-PDB; Structure Model: 1G3P)

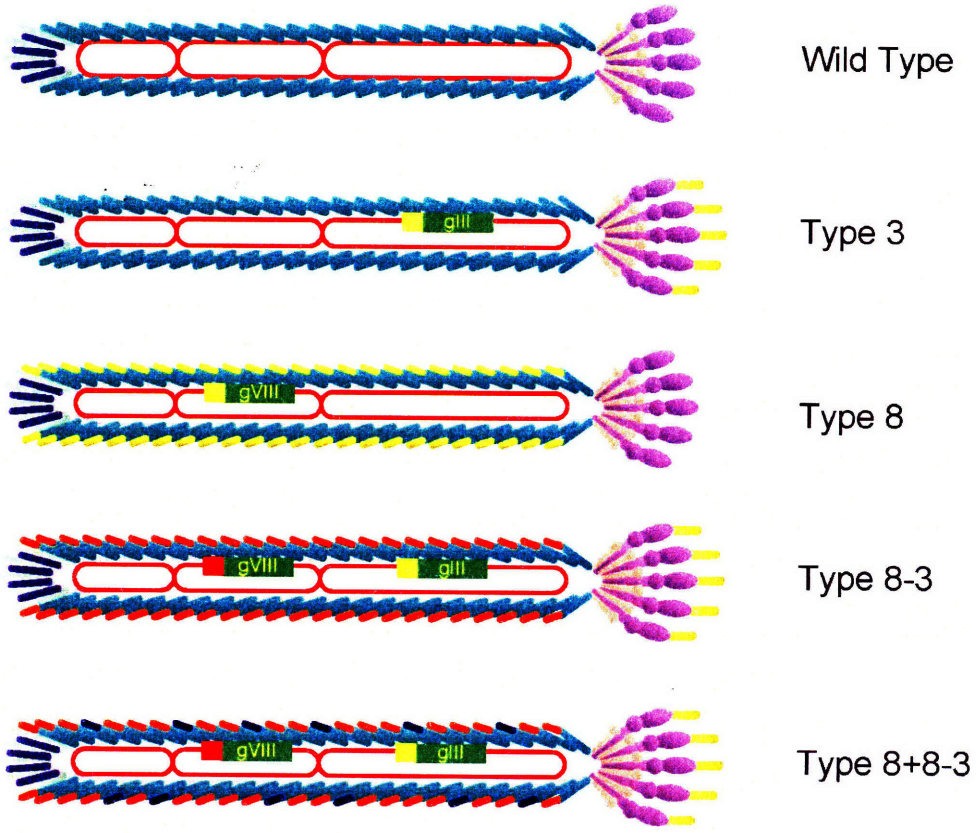

Figure 6. Various types of genetic modifications. Four types of engineering schemes are illustrated. Type 3 virus contains engineered peptides on pIII proteins, and type 8 has modified pVIII proteins. Type 8-3 contains two distinct peptide motifs on pIII and pVIII proteins engineered through the viral genome. Type 8+8-3 is a derivate of type 8-3 virus. It contains two peptide motifs displayed in pVIII proteins. One is originated from the phagemid, and the other one is from the viral vector.

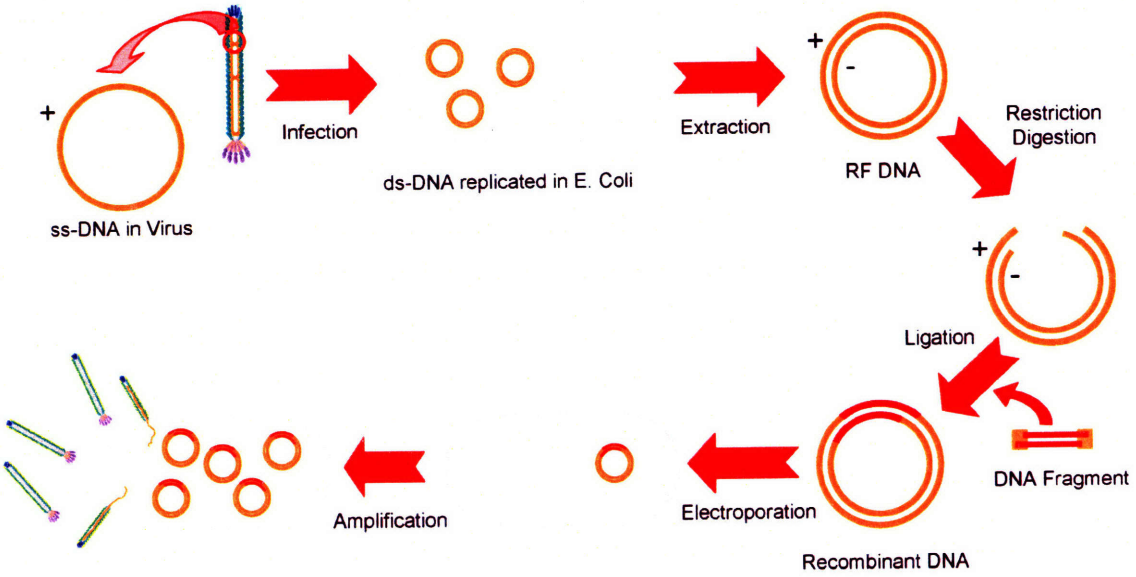

Figure 7. Recombination and transformation. A flow chart of genetic engineering procedure. The virus containing a single-stranded DNA (ss-DNA) infects an E. Coli host and produces double-stranded DNAs (ds-DNAs) in the bacterial cell. The ds-DNA (replicative form DNA) is extracted and digested with restriction enzymes. Synthesized DNA fragment is ligased into the digested ds-DNA. And, the recombinant DNA is electroporated into a fresh E. Coli to produce engineered M13 bacteriophages.

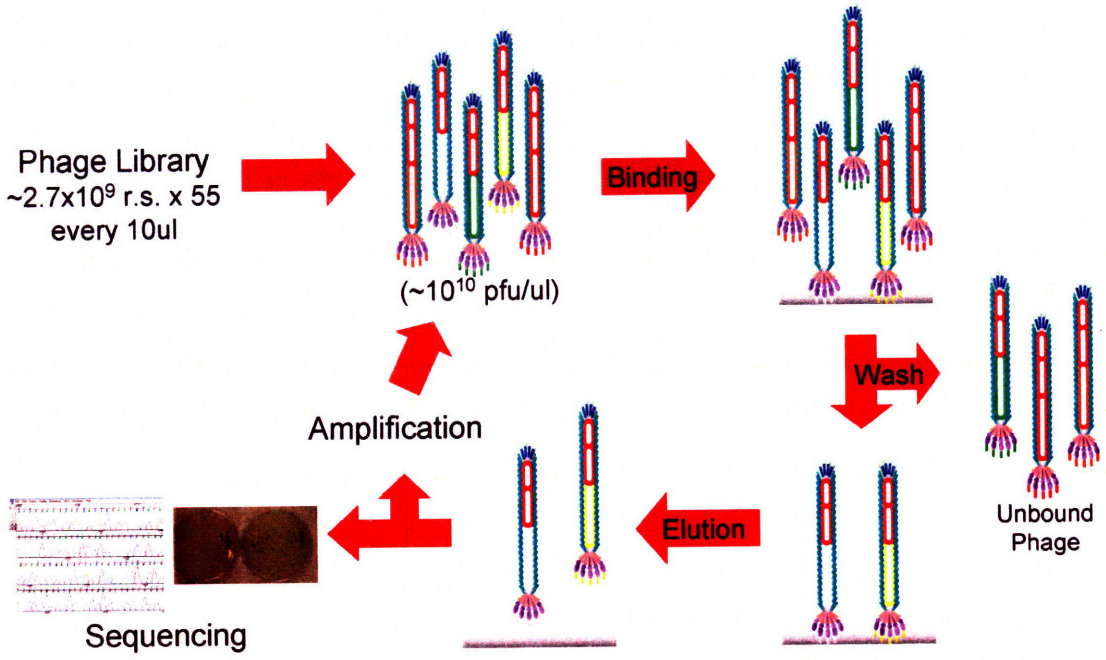

Figure 8. Procedure of biopanning. Phage library containing about millions of random sequences is exposed to the material of interest. After washing unbound phages, the bound phages are eluted from the surface and sequenced to analyze the peptides. The eluate is amplified and then used for the next round of biopanning. The panning steps are repeated until a consensus sequence is found.

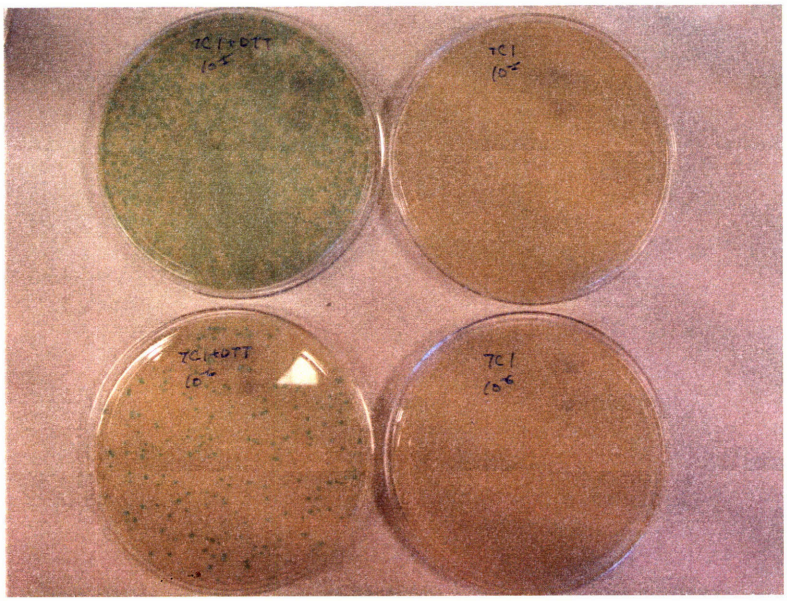

Figure 9. Titration of virus p3-Au7C1r bound to gold surface. Two samples were prepared: one was treated with DTT, and the control was treated without DTT. Plates on the left hand side were tittered from the sample treated with reduction agents (DTT) before binding, and the plates on the right hand side were tittered from the other sample treated without reduction agents. The virus showed no affinity to gold surface if it was not treated with DTT. The binding affinity to gold would increase when the virus was treated with DTT.

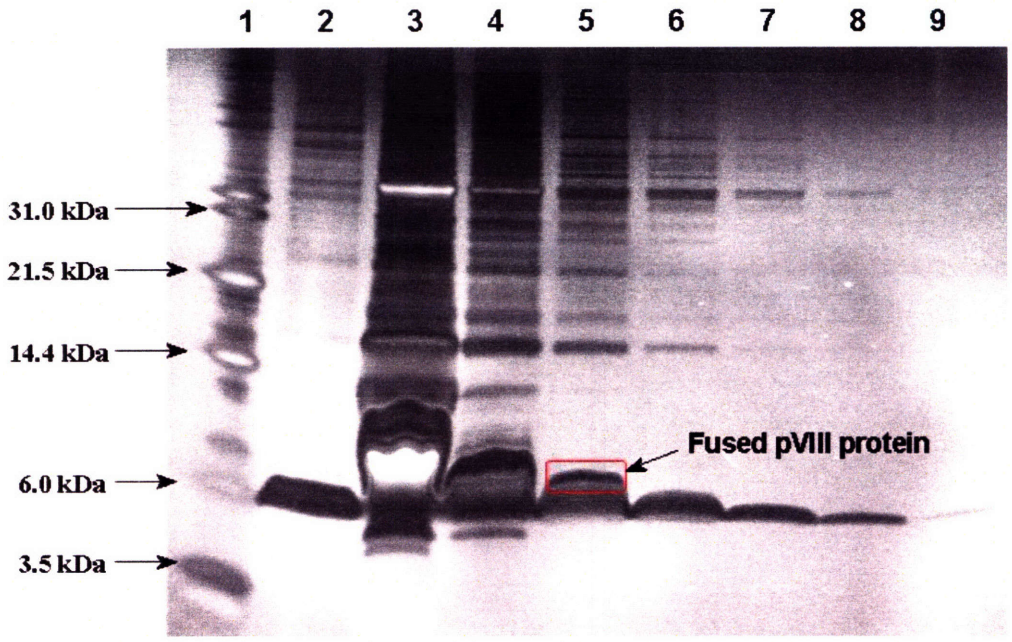

Figure 10. SDS-PAGE electrophoresis for analyzing displayed pVIII protiens. Lane 1 was the DNA standard (Mark12^{TM}). Lane 2 was p3-Au7C1r virus. Lanes 3 to 9 were the 3-fold serial dilutions of type 8+8-3 virus amplified using phagemid system. The band of recombinant pVIII protein (p3-Au12, circled in red) in lane 5 showed approximately the same intensity of the wild-type pVIII protein in lane 8, indicating that the estimated expression ratio of fused pVIII proteins was approximately 3^3=27-fold lower than that of wild-type pVIII proteins. Given the pVIII protein of about 2,700 copies for M13 bacteriophage, the number of fused pVIII proteins was approximately 100 copies per bacteriophage.

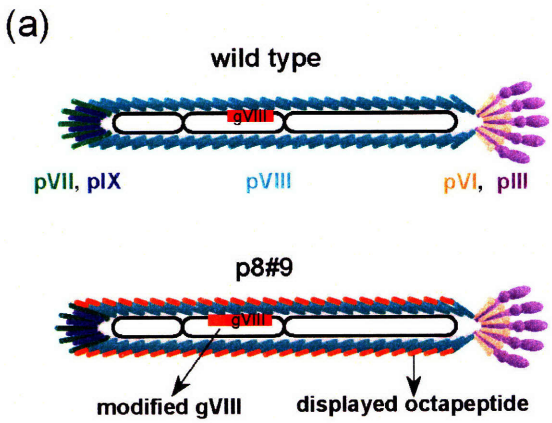

(b)

wild type (M13KE)

gVIII 5'-	GCT	GAG	GGT	GAC	GAT	CCC	GCA	AAA	GCG	GCC	TTT	AAC	TCC	CTG	CAA	GCC	TCA	GCG	....	**-3'**
pVIII N-	Ala	Glu	Gly	Asp	Asp	Pro	Ala	Lys	Ala	Ala	Phe	Asn	Ser	Lys	Gln	Ala	Ser	Ala	....	**-C**

p8#9

gVIII 5'-	GCA	GTG	TCG	GGG	TCG	TCG	CCG	GAT	TCG	GAT	CCC	GCA	AAA	GCG	GCC	TTT	AAC	TCC	....	**-3'**
pVIII N-	Ala	Val	Ser	Gly	Ser	Ser	Pro	Asp	Ser	Asp	Pro	Ala	Lys	Ala	Ala	Phe	Asn	Ser	....	**-C**

Figure 11. The comparison of wild-type (M13KE) and p8#9. (a) Schematic representations of wild type and type 8 engineered bacteriophages. Type 8 engineered bacteriophage bears an insertion in gVIII genome, which leads to a displayed octa-peptide motif (shown in orange color) on each major coat protein. (b) The comparison of gVIII sequences and corresponding peptide sequences between a wild type phage and a p8#9 phage. The differences are highlighted in grey. Type 8 gold-binding virus p8#9 contains octa-peptide, which replaces the tri-peptide in the wild-type pVIII proteins of M13KE virus.

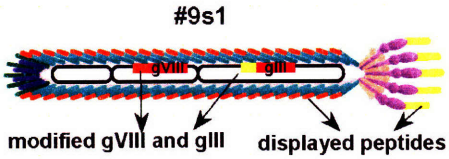

gVIII 5'-	GCA	GTG	TCG	GGG	TCG	TCG	CCG	GAT	TCG	GAT	CCC	GCA	AAA	GCG	GCC	TTT	AAC	TCC	....	-3'
pVIII N-	Ala	Val	Ser	Gly	Ser	Ser	Pro	Asp	Ser	Asp	Pro	Ala	Lys	Ala	Ala	Phe	Asn	Ser	....	-C

gIII 5'-	TGG	GAT	CCT	TAT	TCT	CAT	TTG	CTG	CAG	CAT	CCG	TAG	GGT	GGA	GGT	TCG	GCC	GAA	....	-3'
pIII N-	Trp	Asp	Pro	Tyr	Ser	His	Leu	Leu	Gln	His	Pro	Gln	Gly	Gly	Gly	Ser	Ala	Glu	....	-C

Figure 12. Engineered type 8-3 virus. (Top) Schematic representation of the type 8-3 engineered phage, #9s1. It contains gold-binding motifs (p8#9) fused on pVIII proteins

and anti-streptavidin motifs (p3s1) fused on pIII proteins. (Bottom) The DNA sequences of gVIII and gIII and the corresponding pVIII and pIII coat proteins are listed. The engineered genome and peptide in the virus are highlighted in gray. p8#9 motif contains eight amino acids and p3s1 motif contains 12 amino acids.

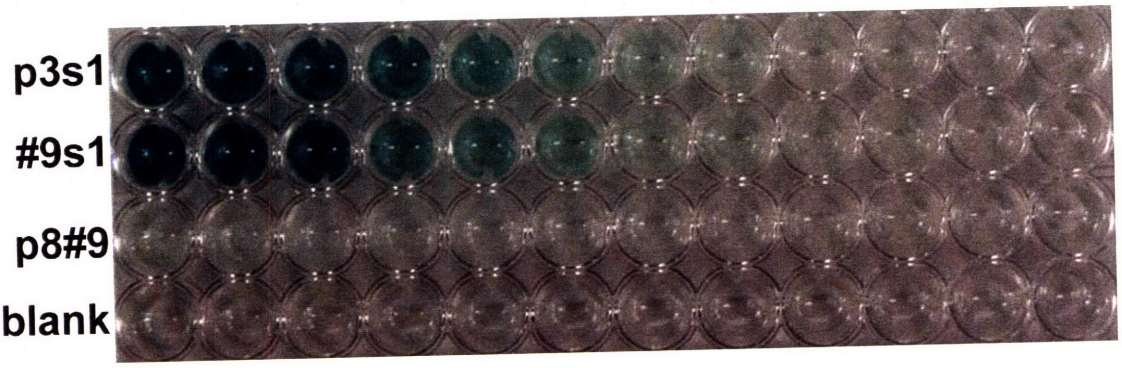

Figure 13. Enzyme-linked immunosorbent assay (ELISA) to verify the expression of anti-streptavidin peptide. ELISA plate result of the interactions between the s1 motif and the streptavidin-coated wells. The green color indicates positive interaction. The intensity of the green color represents the amount of the bound phage in the well. Serial dilutions (50%, 2-fold) of each phage clone were carried out in a row of ELISA plate wells.

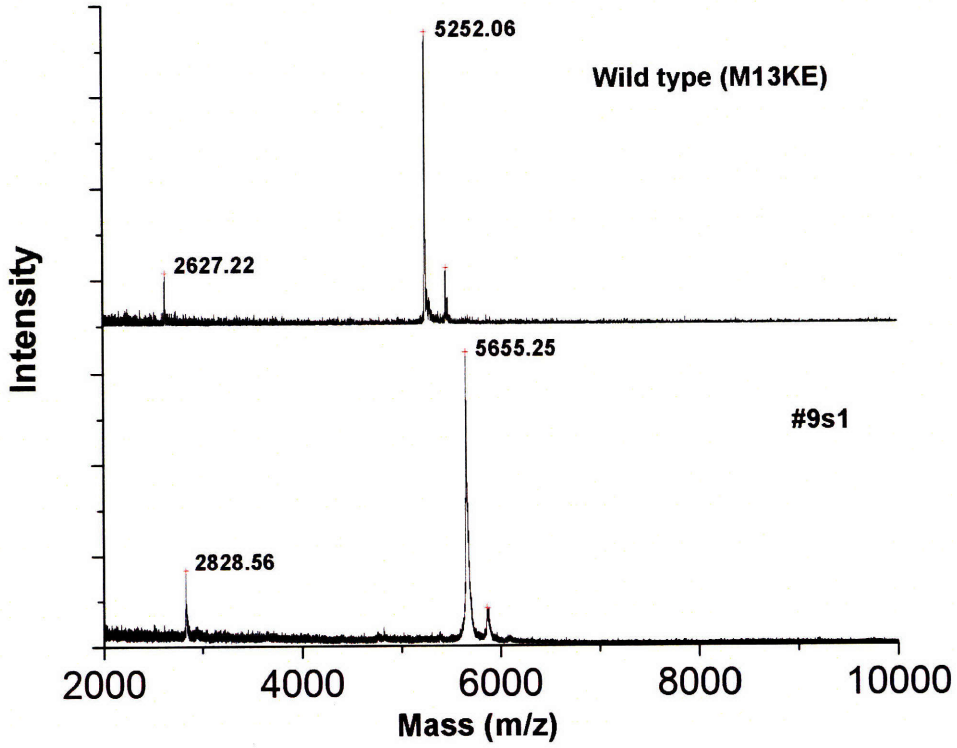

Figure 14. The mass spectra of wild-type (M13KE) and #9s1 clones. Experimental proofs confirmed the wild-type pVIII protein on M13KE clone and the display of p8#9 gold-binding motif on #9s1 clone.

Chapter III. Biological assembly of nano-materials and nano-structures

III.A. Summary

Biological systems possess inherent molecular recognition and self-assembly capability and are attractive templates for constructing complex material structures with molecular precision. The assembly of various nanoachitectures including nanoparticle arrays, hetero-nanoparticle architectures and nanowires utilizing highly engineered M13 bacteriophage as templates are reported.[20-23] The genome of M13 phage can be rationally engineered to produce viral particles with distinct substrate-specific peptides expressed on the filamentous capsid and the ends, providing a generic template for programmable assembly of complex nanostructures. Phage clones with gold binding motifs on the capsid and streptavidin-binding motifs at one end were created and used to assemble Au and CdSe nanocrytals into ordered one-dimensional arrays and more complex geometries. Initial studies showed such nanoparticle arrays could further function as templates to nucleate highly conductive nanowires providing a new avenue for addressing/interconnecting individual nanostructures.[24-26] In this chapter, type 8-3 engineered phage is demonstrated to serve as templates to assemble nanoarchitectures of various geometries and materials, such as Au and CdSe nanocrystal/hetero-nanocrystal arrays and Au nanowires.

III.B. Introduction

Biological molecules for nano-templating

One of the important issues in the future nano-world is the structural control of materials at the nano-scale. This has attracted a lot of attention to the fabrication of different architectures with various dimensions, ranging from zero-dimensional nanoparticles to three-dimensional nanonetworks.[27-32] To efficiently build complex nanostructures in the future, more knowledge and well-developed techniques are required to control the building blocks at the molecular level. And, these so-called building blocks usually have low dimensional structures. In the last decade, many approaches have been reported to fabricate one-dimensional metallic, semiconducting and magnetic nanowires. These approaches include, but not limit to, vapor-liquid-solid reaction[33, 34], electrochemical deposition[35, 36], photochemical reduction[37], surfactant-directed[38] and template-directed[39] syntheses. Although these techniques may produce good quality nanowires, few of them can make nanowires of controlled and monodispersed lengths. Recent efforts focused on the bottom-up assembly of functional nanosystems from nanoscale building blocks have led to substantial advances.[24, 25, 40, 41] However, the difficulties in precise placing and interconnecting individual building blocks[24-26, 42] have impeded further progress and thereby motivated significant efforts directed towards controlled assembly of nanoscale building blocks.[43-45] Biosystem is one of them. Biological systems are highly organized from molecular-scale building blocks such as nucleic acids and proteins with intricate hierarchical architecture and represent the unparalleled examples of bottom-up assembly.[46, 47] Biological molecules often possess highly specific and precise molecular recognition capability that can be programmed through genetic engineering[48-50] and can exert rational control over inorganic material nucleation, phase stabilization, assembly and pattern formation at molecular scale.[51-55] Integration of these unique capabilities of biomolecules with the design of new materials can offer many opportunities for nanofabrication including rational molecular design through genetics, spatial control on nanometer scale, and hierarchical assembly of two-dimensional (2D) or three-dimensional (3D) complex architectures.[56-60]

Biological templates for nanowires

Biological templates for fabricating nanomaterials have drawn a lot of attention due to the self-assembly and low-temperature synthesis process. To date, biological templates can be categorized into three main types: deoxyribonucleic acid (DNA), peptide and protein, and filamentous virus. The fabrication of nanowire using the biotemplate is based on either "buttom-up"[55, 61-63] or "top-down"[64-66] concept (Figure 1). In "bottom-up" method, the structural unit of the DNA or peptide is first modified to create a ligand to bind a precursor or attached with a preformed nanoparticle. Next, the modified structural unit is elongated in one dimension to form a wire-like structure. Finally, the wire-like biomaterial is used as the template to grow a material on it. As for the "top-down" method, amphiphilic peptides are used to make a micro- to nano-tubular structure, and then the material is nucleated inside the tube. After the nanowire forms inside the tube, the peptide scaffold is removed by dissolving them in a solvent or by heating it up. As for the filamentous virus being used as a template, both "bottom-up" and "top-down" methods have been reported.

However, in either of the biotemplating schemes, there are two important issues. One is to effectively modify the building block for templating a material, and the other is to control the dimensions of the template when propagating the building block. Each bio-template has its own advantages and disadvantages. Of these biological templates, the lengths of both DNA and filamentous virus can be genetically controlled, and peptide/protein is more stable than DNA. DNA only has four types of building blocks – nucleotides; and protein has twenty types of building blocks – amino acids. Although the diversity of protein is much more than that of DNA, the synthesis and construction of protein material are difficult. Fortunately, nature has developed controllable protein templates – viruses. Virus is a genetic product of the viral DNA, which assembles and fabricates virus progeny in its host. The coat proteins (or capsid) of a virus protect the viral genome and function to infect and transport viral DNA into the host. Viruses can be seen as the nature products combining all the advantages of the protein and DNA templates. Moreover, filamentous virus such as M13 bacteriophage has a high aspect ratio structure. This inherent property also makes the filamentous virus an interesting

template for making nanowires.

III.C. Experimental

III.C.1. Self-assembly of nanoparticle array

Materials. To demonstrate the specific templating effect of p8#9 motif, experiments were carried out with different clones, including p8#9 (positive motif), negative control wild type and p8#17 (a random motif selected from type 8 library). Each virus solution was amplified, purified, and diluted in water to ~10^9 pfu/μL. 5-nm gold colloidal suspension (5.0 x 10^{13} particles/mL, Ted Pella), streptavidin-coated 15-nm gold nanoparticle (Ted Pella), streptavidin-conjugated cadmium selenide (CdSe) quantum dots (Quantum Dot Corp.), and bovine serum albumin (BSA, Amersham Biosciences) were prepared.

Binding test. 10 μl of the phage solution was mixed with 100 μl of 5-nm gold colloidal suspension (without dilution). The mixture was incubated on ice for 1 hr.

Synthesis of hetro-particle nanoarray. #9s1 clone was first amplified to ~10^9 pfu/μL. 10μl of the phage solution was mixed with 5μl of 15-nm Au-streptavidin conjugates (or streptavidin-conjugated CdSe quantum dots) and 70 μL of TBST (tri-buffer saline (TBS) + 0.05[v/v] Tween-20 + 0.1% mL bovine serum albumin), and the mixture was agitated for about 1 hour, allowing s1 on the pIII proteins to bind to streptavidin-coated gold (or streptavidin-conjugated CdSe quantum dots). Then, 10 μL of the mixture solution was incubated with 100μL 5-nm colloidal Au to allow the second type of nanoparticle to bind to pVIII proteins.

III.C.2. Synthesis of gold nanowire using direct nucleation and electroless deposition

Materials. p8#9 clone was first amplified, purified and diluted to ~10^9 pfu/μL. $HAuCl_4$ (chloroauric acid), $NaBH_4$ (sodium borohydride) and NH_2OH (hydroxyl amine) was purchased from Sigma-Aldrich. 5-nm gold colloidal suspension was purchased from Ted Pella.

Direct nucleation for nanowire. To synthesize gold nanowires by the reduction reaction

from gold salt, 10 μL of the virus was first mixed with 100 μL chloroauric acid solution (HCl_4Au, 5 mM, pH = 5.5) at 0 °C. The gold precursor was reduced by the addition of iced-cold sodium borohydride solution (50 μl, 5 mM). The reaction was incubated on ice for 3 hours.

Electroless deposition for nanowire. This was achieved by electroless deposition of gold onto the existing Au nanoparticle arrays using the catalytic effect of gold surface to selectively reduce gold from $HAuCl_4$ solution at the presence of NH_2OH. 80 μL $HAuCl_4$ (0.3 mM) was added with 10 μL nanoparticle array obtained previously, and the mixture was then mixed with NH_2OH (40 mM) and incubated on ice.

III.C.3. Sample preparation for microscopy and electronic characterization

Materials. Silicon wafers with and without oxide layer (~100 nm) were purchased from University Wafer. TEM copper grids with carbon films were purchased from LADD Research. Uranyl acetate was purchased from EMS Corp.

Microscopy. 10 to 100 μL of sample was dispersed on the silicon wafer and incubated for 30 min. The sample was removed by filter paper and the wafer was briefly rinsed with water. Atomic force microscopy (AFM) images was taken by VEECO MultiMode V (Digital Instruments) operated under tapping mode to verify the connection of viral nanowires and electrodes. The TEM images were taken using JOEL 2010 high resolution transmission electron microscope (HR-TEM) operated at 200 kV. Uranyal acetate stained samples were prepared by floating on 50 μL uranyl acetate solution (~2%).

Electronic characterization. To measure the electrical properties of these nanowires, samples were dispersed on silicon substrates with oxide layers (SiO_2) containing large electrode patterns and further connected to the electrodes by focused ion beam (FIB) metal deposition or electron beam (EB) patterning. The current transported through the virus-based nanowire was measured by sweeping the voltage at room temperature using a probe station.

III.D. Results and Discussion

The viral capsid with expressed anti-Au motifs selected in **Chapter II** on pVIII proteins served as a template for organization of one dimensional (1D) Au nanocrystal array. To demonstrate the specific templating effect of p8#9 motifs, experiments were carried out with different clones, including p8#9(positive motif), negative controls wild type and p8#17 (a random motif selected from Type 8 library). After 2-3 minutes of incubation, the mixtures of control clones with the gold colloidal suspension and the blank control gold suspension remained clear (Figure 2). Transmission electron microscopy (TEM) studies on these samples showed that gold particles distributed randomly in the control sample (Figure 3a). Uranyl acetate stained samples showed clearly that Au nanoparticles were not templated by either wild type phage or p8#17 clones (Figure 3b and c). In the case of motif p8#9, a visible precipitate in the solution was observed, indicating that gold colloids formed aggregates. TEM studies showed that gold nanoparticles assembled into wire-like structures with diameters around 10 nm and lengths around 1 μm, which are consistent with the morphology of M13 virus (Figure 3d). Enlarged image revealed that gold nanoparticles were arranged into ordered 1D array on pVIII proteins along the viral axis (Figure 3 insert). One-dimensional metallic nanoparticle arrays may serve as the basis for plasmon structures that can selectively absorb or transmit specific electromagnetic radiation with high spectral sensitivity.[67]

With the successful modifications on both pIII and pVIII proteins, type 8-3 phage can serve as a template for assembly of nano-architectures with rich geometries and functionalities. #9s1 clones can further be utilized to assemble hetero-structures with gold particles forming 1D array on pVIII proteins and another streptavidin-coated material bound to pIII proteins. #9s1 clone was first mixed with 15-nm Au-streptavidin conjugates, allowing s1 on the pIII proteins to bind to streptavidin-coated gold. Then, the mixture solution was incubated with 5-nm colloidal Au to allow gold nanoparticles to bind to pVIII proteins. Resulting structures were examined with TEM. The images revealed that 5-nm gold particles formed a 1D array on pVIII proteins and the streptavidin-coated 15-nm gold particles bound to one end of the phage as the result of functionalities on pIII proteins (Figure 4a and b). This rational approach provides the

assembly of nanostructures based on genetic engineering of the viral system and can easily be extended to other materials/structures. For example, when streptavidin-coated Au was replaced with streptavidin-conjugated cadmium selenide (CdSe) quantum dots, hetero-nanoparticle arrays consisting of CdSe quantum dots (QD) bound to pIII proteins and gold nanoparticles arrays bound to pVIII proteins were obtained (Figure 4c). More than one phage could connect to the same streptavidin-coated nanoparticle and created more complex structures, such as a linear wire-dot-wire construct or a Y-shape structure (Figure 4d and e).

Moreover, the 1D metallic nanoparticle arrays on pVIII proteins could subsequently grow into continuous metallic nanowires. This was achieved by electroless deposition of gold onto the existing Au nanoparticle arrays using the catalytic effect of gold surface to selectively reduce gold from $HAuCl_4$ solution at the presence of NH_2OH.[68] The growth of the 1D nanoparticle arrays into continuous nanowires was verified by TEM studies, which revealed a progressive growth of the nanowires with increasing electroless deposition time. By controlling the electroless deposition time continuous Au nanowires can be achieved (Figure 5). Continuous nanowires obtained after 5 minutes of deposition have an average diameter of ~ 40 nm.

Gold nanowires was also obtained from direct nucleation from gold salt solution onto the pVIII proteins of the viruses. To synthesize gold nanowires by the reduction reaction from gold salt, virus sample (~ 10^9 pfu/μl) was first mixed with chloroauric acid solution and incubated on ice. The gold precursor was reduced by the addition of iced-cold sodium borohydride solution. The whole reaction was carried out on ice. All the samples showed visible precipitates after 1-hr incubation (Figure 6). TEM studies on these samples showed that the control sample without adding any virus only contained 100 nm gold nanoparticles (Figure 7a). The samples with negative control virus clones, wild-type and p8#17, showed mixtures of 100-nm and other smaller gold nanoparticles (Figure 7b and c). No nanowire was observed in these control samples. In the sample with p8#9, a large quantity of virus-based gold nanowires with uniform length was observed (Figure 7d). The gold nanowire was approximately 20 to 30 nm in width and 900 nm in length. The electron diffraction (ED) pattern of an individual nanowire showed

a combination of ring and spot patterns (Figure 8). This indicates that the nanowires were comprised of many single crystalline regions with random orientations on pVIII proteins. The scattering spots shown in the electron diffraction pattern correspond to various gold crystalline facets (111), (200), (220), (311), (222), (331) and others, which confirmed that the material synthesized on the bacteriophage surface was pure gold. Further analysis of ED patterns at individual segments did not show any specific alignment of the gold crystals along the viral nanowire (Figure 8).

To probe the mechanism of crystal growth on bacteriophage, ultraviolet-visible (UV-Vis) spectroscopy was used to monitor the formation of gold nanowires. Within ten minutes after the addition of the reduction agent, the UV-Vis spectrum showed a main transverse plasmon absorption peak of the gold nanoparticles at 521 nm (Figure 9). At this stage, segregated gold nanoparticles were formed on the bacteriopahge major coats and in the solution. After 3-hr reaction, the aggregation of gold particles was observed and the UV-Vis spectrum showed the characteristic curve of aggregated gold nanoparticles at the high wavelength range. On the other hand, the gold nanoparticles produced from the same reduction method and condition exhibited a transverse plasmon absorption peak around 521 nm, corresponding to 15-nm Au nanoparticle. From the high resolution TEM lattice images (Figure 9), some regions of the nanowire were comprised of 15-nm nanoparticles with well-defined particle shapes. This indicated that pVIII proteins also bound the gold nanoparticles that nucleating in the solution. The other parts of the nanowire did not have distinguishable 15-nm nanoparticles, indicating the coalescence and growth of gold randomly occurred on the pVIII proteins. These portions were mostly composed of polycrystals owing to the asymmetric growth and multiple nuclei forming within these regions. The gold nanoparticles were initially formed both on pVIII proteins and in solution during this synthesis. Both nucleation and physical adsorption were simultaneously occurred in the peptide-directed bio-mineralization process. Comparing the coverage of gold nanoparticles on type 8 virus with that on type 8+8 virus (engineered using phagemid system), type 8 virus showed better coverage due to the gold-binding motifs were fused on all pVIII proteins. As proved in **Chapter II**, the

recombinant pVIII proteins on a type 8+8 virus were only about 4%, resulting incomplete coverage of gold nanoparticles on the virus template (Figure 10).

To further investigate the potential of these biotemplated nanowires as electronic components in future nanoelectronic circuitry, electrical transport studies were performed on individual nanowires. Electron-beam (E-beam) lithography and focus ion beam (FIB) deposition were used to make electrical contacts to the nanowires, and the contacts were verified using AFM (Figure 11 and Figure 12). Two-terminal current-voltage (I-V) measurements were conducted at room temperature. For a continuous nanowire, the current-voltage curve showed a linear relation, indicating the ohmic contact behavior. Repeated measurements on the nanowire yielded reproducible I-V behaviors, indicating that the device was stable. A resistance of about 588 ohm is estimated for the device. These data give a resistivity ~ 1.8 X 10^{-6} Ω-m for the gold nanowire, which is about 100 times larger than the bulk gold (2.24X10^{-8} Ω-m). Diameter fluctuation, surface scattering and tunneling through different nanocrystal grain boundaries may contribute to this result. With increasing bias voltage the device failed when the current reached around 500 μA, which yielded a high failure current density about 10^{8} A/cm^{2}.

III.E. Conclusion

Type 8-3 engineered phage was demonstrated to serve as the template to assemble nanoarchitectures of various geometries and materials, including Au and CdSe nanocrystal/hetero-nanocrystal arrays and Au nanowires. These results suggest a generic assembly approach that can be extended to program the assembly of various material systems with nanometric precision: various substrate-specific motifs can be independently selected from type 8 and type 3 libraries and then genetically incorporated into M13 bacteriophage structures to produce highly decorative viral templates with rational controls (Figure 13). The type and amount of peptide motif displayed on pVIII proteins will directly affect the nucleation and binding result. The experimental results showed that using 100% peptide display on pVIII protein, which was the type 8 virus, gave the best coverage of particles to produce nanowires. Overall, this chapter demonstrates the great promise of bottom-up assembly for sophisticated electronic and optoelectronic systems from biotemplated materials and therefore opens up many exciting opportunities in nanoscale science and biotechnology.

III.F. Figures

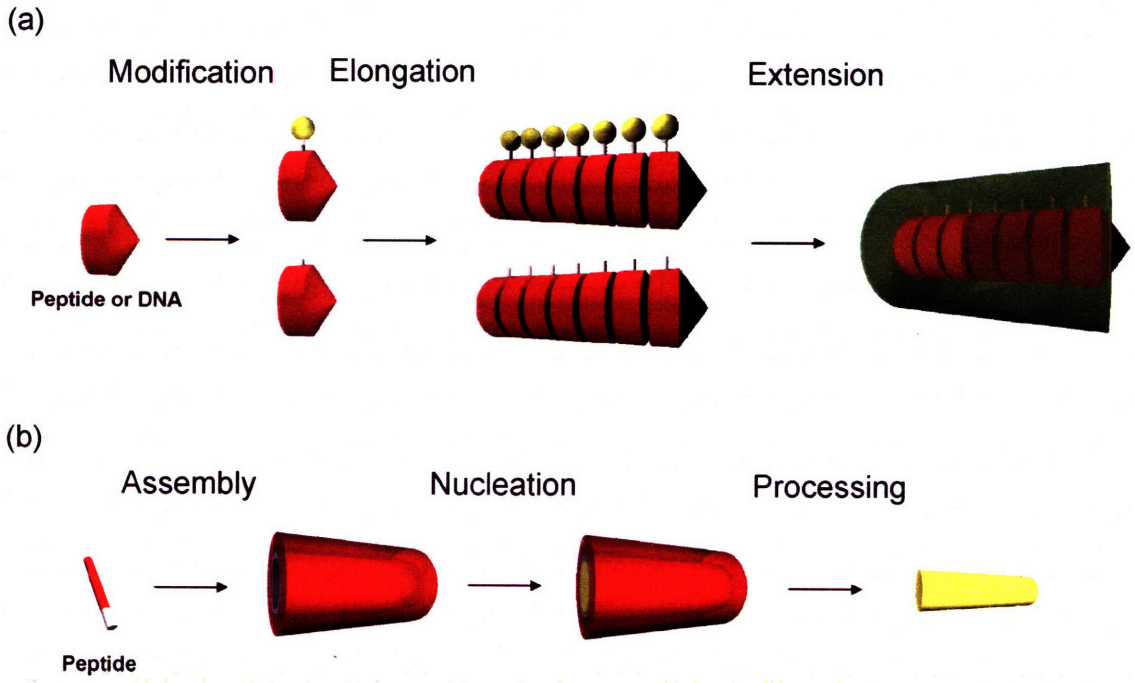

Figure 1. Self-assembly of biological templates. (a) Bottom-up: the construct unit is modified and polymerized into a long linear chain. Material is directly growing on the template. (b Top-down: amphiphilic molecules such as lipid or peptide are self-assembled into a hallowed scaffold, and an inorganic material is filled in and shaped by the scaffold. The biological template can be removed by heating or dissolved by solvents.

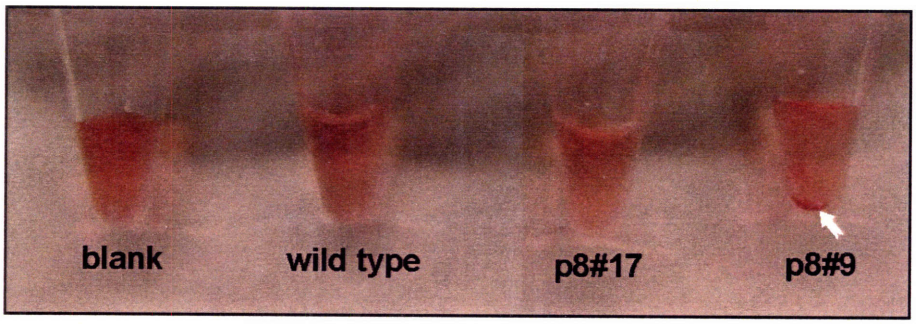

Figure 2. Gold-binding experiments. The photograph of different clones mixed with Au nanoparticles. Only sample p8#9 showed visible precipitate, highlighted by the arrow. All the other solutions remained clear.

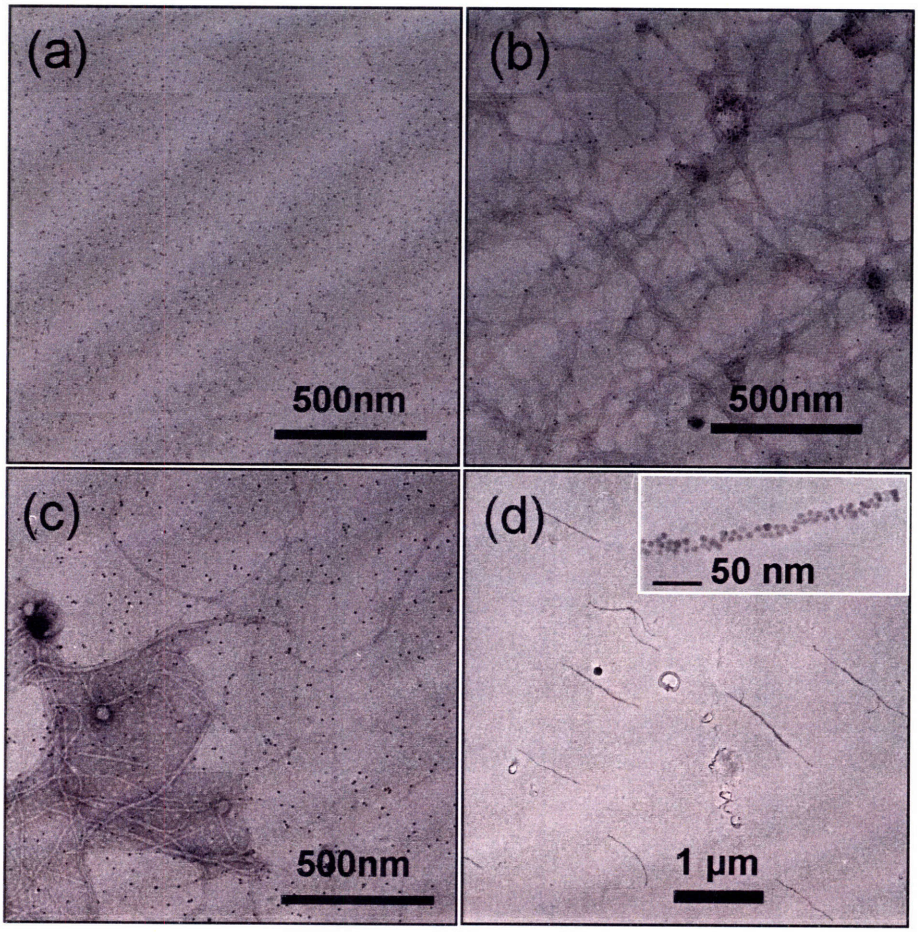

Figure 3. Corresponding TEM images of gold-binding experiments. (a) Au nanoparticles (blank control sample). (b) Wild-type phage mixed with Au nanoparticles (negative control sample), stained with 2% uranyl acetate. (c) Sample p8#17 mixed with Au nanoparticles (negative control sample), stained with 2% uranyl acetate. (d) Distinguishable wirelike structures in the mixture of sample p8#9 and Au particles. The inset shows Au particles self-assembled into 1D arrays on the virus.

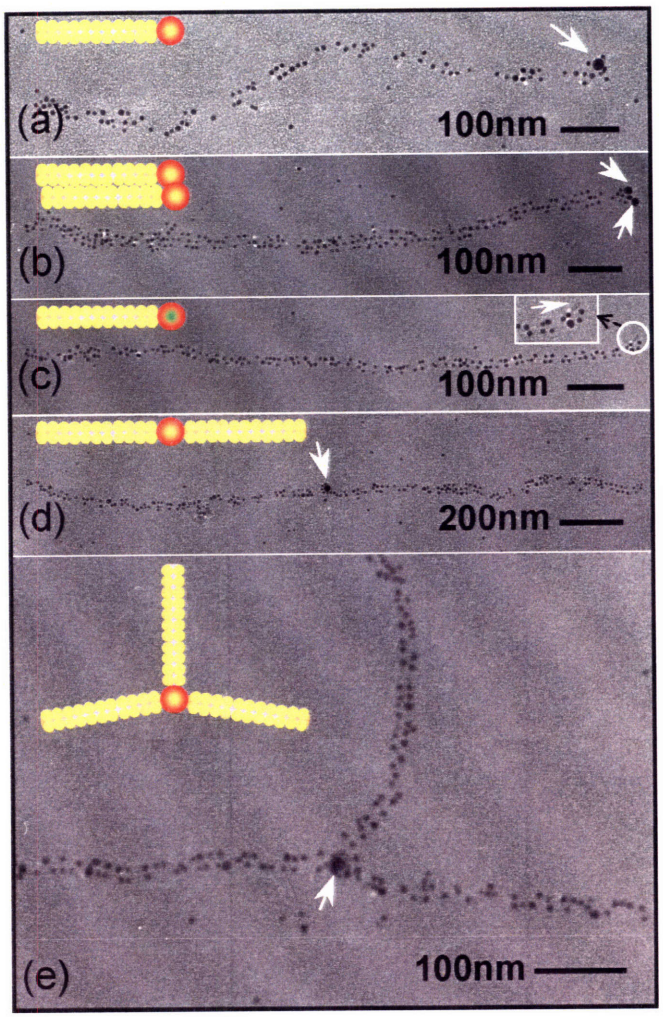

Figure 4. TEM images of various nanoarchitectures templated by clone #9s1. Gold nanoparticles (~ 5 nm) bind to pVIII proteins along the virus axis and form 1D arrays, while s1 motif on pIII protein simultaneously binds to streptavidin-coated nanoparticles. Arrows highlight the streptavidin-conjugated gold nanoparticles (~ 15 nm) and CdSe quantum dots bound on pIII proteins. The insets show the assembly schemes of observed structures. White represents the virus structure, yellow dots represent gold nanoparticles, the green dot represents a CdSe quantum dot, and red represents the streptavidin coating around gold or CdSe particles. (c, inset) The enlarged image of the CdSe quantum dot attached to the end of the virus.

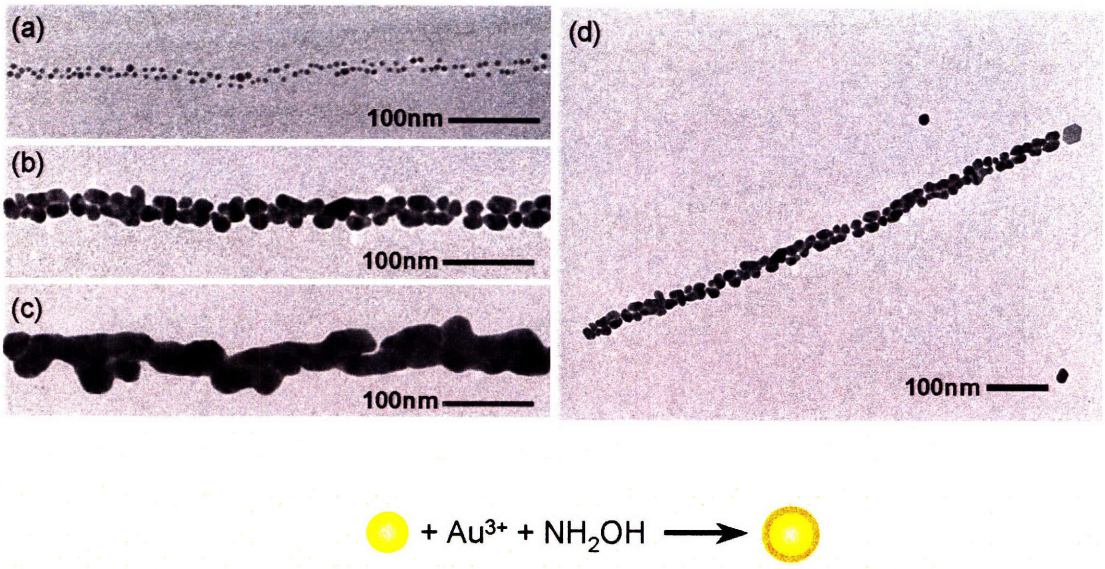

Figure 5. TEM images of the progressive growth of continuous gold nanowires templated by gold nanoparticle arrays on pVIII proteins. The growth of continuous gold nanowire (a) before electroless deposition, (b) 3-min deposition, and (c) 5-min deposition. (d) A full image of a gold nanowire. (Bottom) The reaction of electroless deposition of gold. The reduced gold metal is preferentially deposited onto the preformed gold particle.

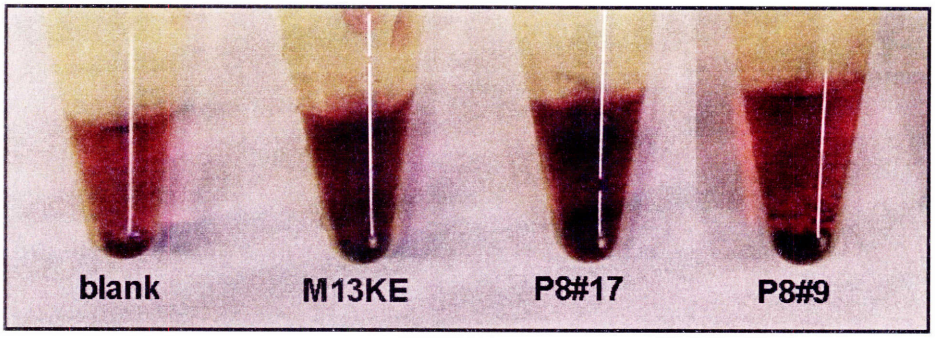

Figure 6. Gold nucleation experiments. The photograph of different clones mixed with chloroauric acid solutions (HCl_4Au) after adding sodium borohydride ($NaBH_4$, reduction agent). All the samples showed visible precipitates.

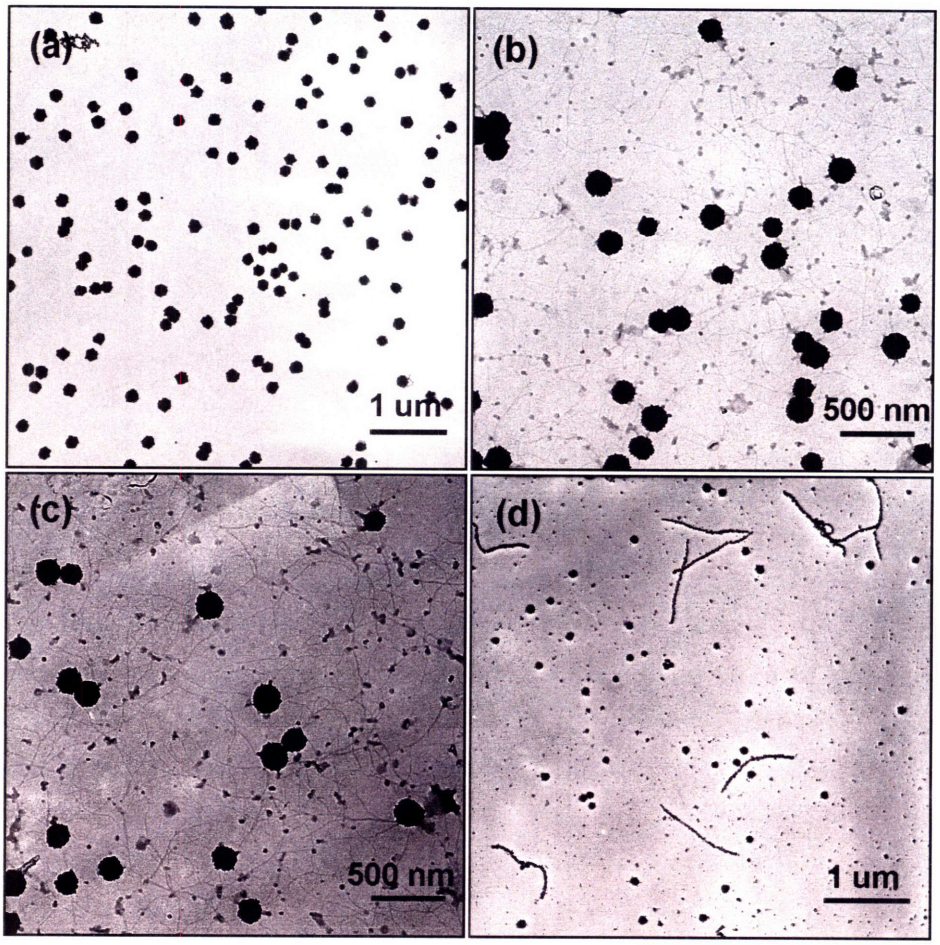

Figure 7. Corresponding TEM images of gold nucleation experiments. (a) Gold salt solution (5 mM chloroauric acid + 5 mM sodium borohydride). (blank control sample). (b) Wild type phage mixed with Au salt solution (negative control sample). Stained with 2% uranyl acetate. (c) Sample p8#17 mixed with Au salt solution (negative control sample). Stained with 2% uranyl acetate. (d) Distinguishable wire-like structures in the mixture of sample p8#9 and Au salt solution.

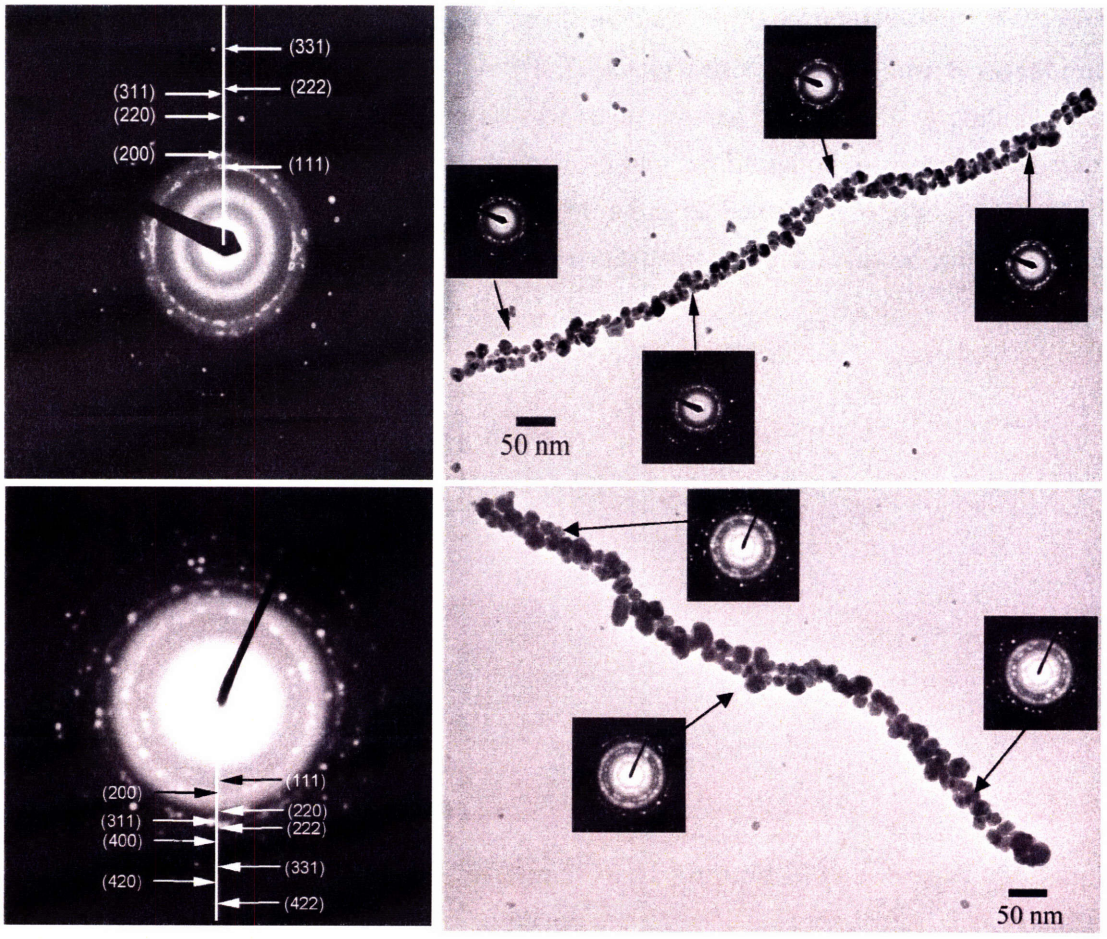

Figure 8. Electron diffraction (ED) patterns and TEM images of gold nucleation nanowires. (Left) Diffraction patterns of individual gold nanowires. The scattering spots corresponded to different gold crystalline facets. (Right) TEM images of viral gold nanowires. (Right insets) ED patterns of different regions on individual nanowires.

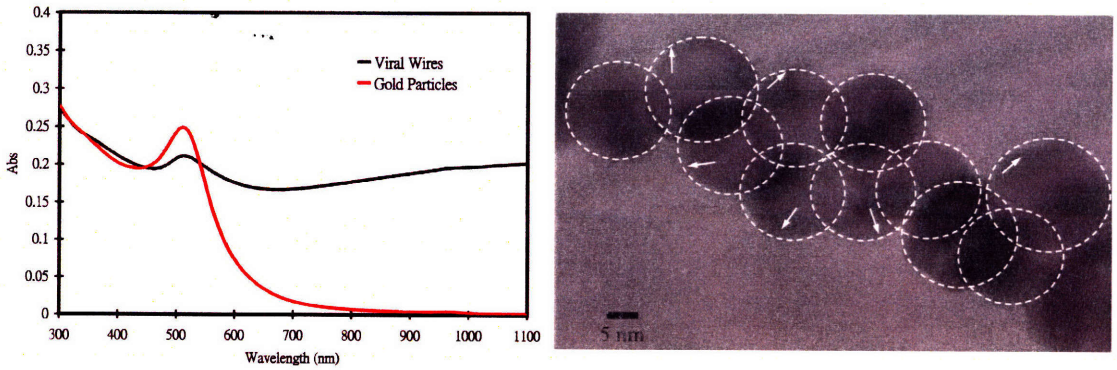

Figure 9. Ultraviolet-visible spectrum (UV-vis) and TEM image of gold nanopartilces nucleating on the virus. (Left) A transverse plasmon absorption peak corresponding to 15-nm gold nanoparticles was observed at 521 nm.Viral gold nanowire showed characteristic longitudinal plasmon absorption at the high wavelength range. (Right) TEM image confirmed discrete 15-nm gold nanoparticles bound to the virus, which was the proof of binding mechanism concurring with nucleation growth on the virus template.

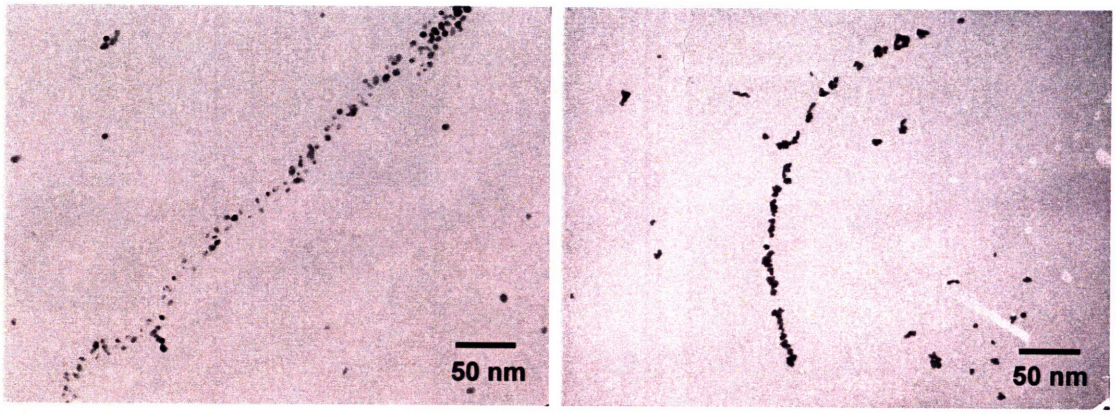

Figure 10. Type 8+8 gold-binding virus template. The virus template engineered using the phagemid system showed incomplete coverage of gold nanoparticles. The estimated amount of recombinant pVIII proteins for one M13 bacteriopahge was 4% (See Chapter II).

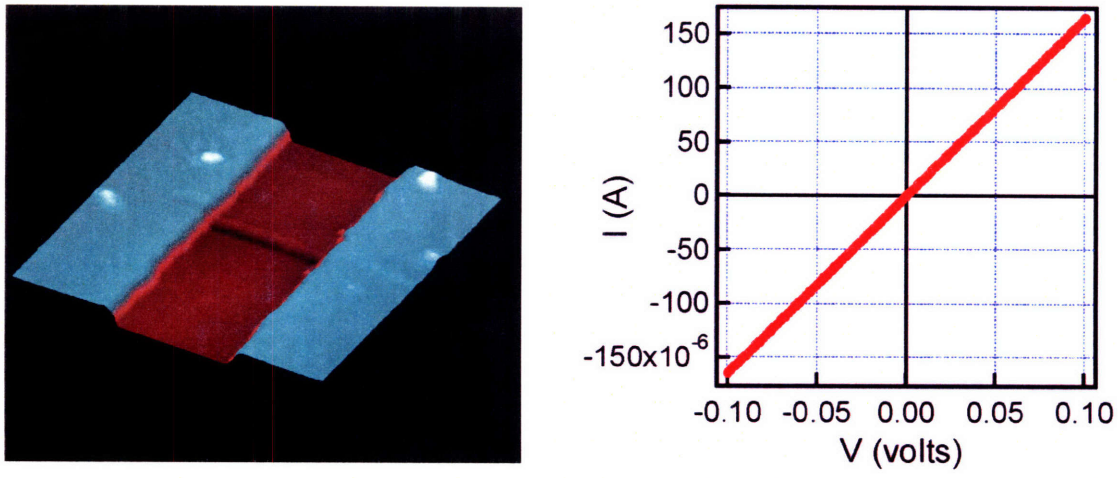

Figure 11. Atomic force microscopy (AFM) image and electrical property of

electroless deposited gold nanowire. (Left) Three-dimensional plot of an AFM image of a two-terminal device based on a single viral gold nanowire fabricated using electroless deposition. (Right) The two-terminal current-voltage (I-V) behavior of a nanowire measured at room temperature.

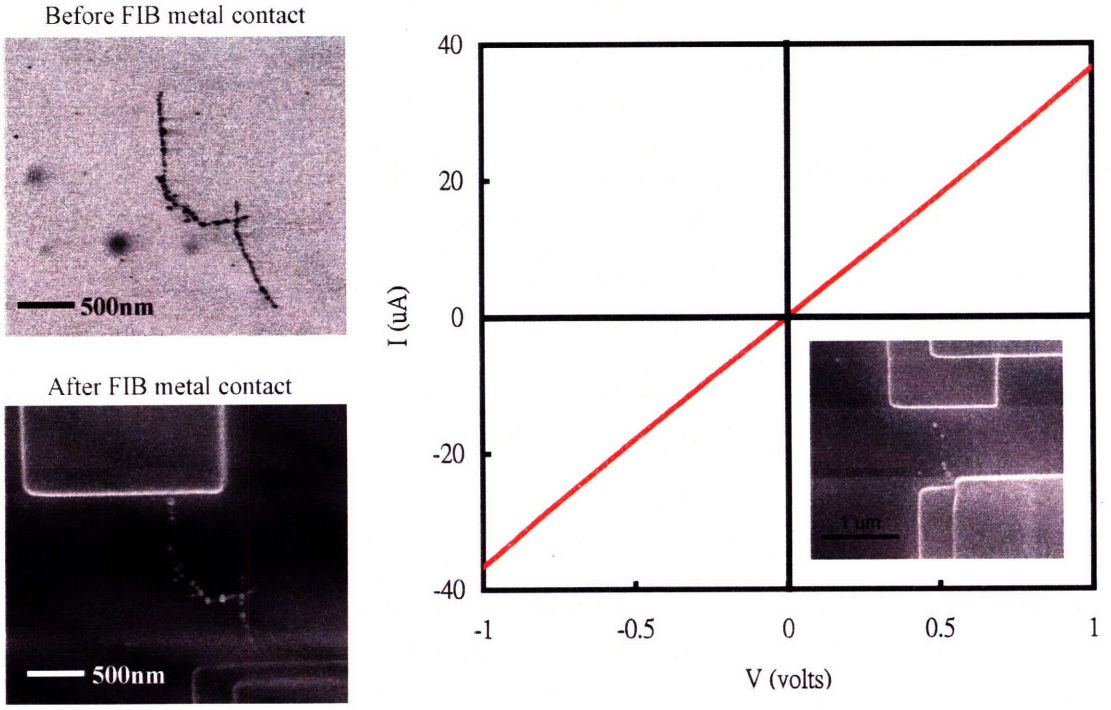

Figure 12. Scanning electron microscopy (SEM) images and electrical property of gold nucleation nanowire. (Left) SEM images of connected nanowires before and after depositing platinum contacts using focus ion beam (FIB). (Right) The I-V behavior of a virus-based gold nanowire showed linear relation and ohmic contact.

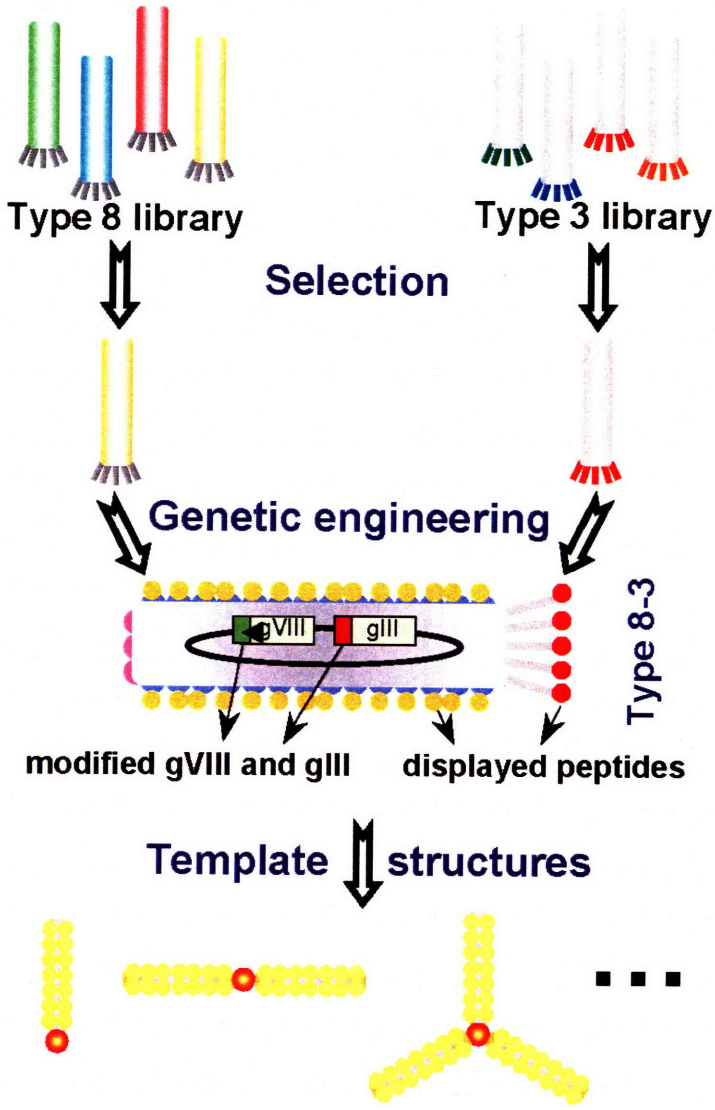

Figure 13. Scheme of engineering type 8-3 virus for templating various nano-sturctures. The binding motifs are selected from different types of libraries and fused into one virus. This multiple-engineered viral template can be used to create several types of nano-architectures.

Chapter IV. Virus-based biological sensor

IV.A. Summary

M13 bacteriophage is a genetically controllable toolkit for material designs to templating inorganic materials such metals and semiconducting materials. However, there is no research that reports to engineer bacteriophage for integrating enzyme with inorganic materials to construct useful devices. Phage display for fabricating devices such as enzymatic electrodes provides several advantages: 1) the orientation of the enzyme attaching to the electrode can be controlled; 2) the electron communication pathway can be precisely constructed; 3) hetero-functionalities to conjugate enzyme and nanomaterials can be easily altered through standard genetic modifications. The biological assembly process can ensure the alignment of expressed enzyme on the template and avoid the issues of inefficient random orientation of active molecule. The M13 bacteriophage template provides various engineering routes to tailor the electron communication channels because of the diverse functional groups and proteins presenting on the surface of the template. And, the most important feature is that M13 bacteriophage provides flexibilities and capabilities to be engineered and tuned easily by modifying the genome. In this chapter, the possibility of displaying and chemically conjugating enzyme on the filamentous bacteriophage that also can incorporate metals will be discussed.

IV. B. Introduction

Virus-based devices

Applications of biomolecules such as protein and DNA in devices have drawn a lot of attentions. One of the reasons is the precise displacement of materials and construction of rich structures that these biological templates can control at the nanometer scale. Other reasons are the ambient assembly/fabrication processes that are compatible to the integration of environmentally sensitive materials/molecules, such as enzymes. The last reason is that the virus template has more flexible engineering capabilities than DNAs or other protein molecules. Both functionalities and structures of virus such as M13 bacteriophage can be precisely controlled. As demonstrated in **Chapter III**, various nano-architectures could be built up using M13 virus, and the virus templated gold nanowires and nanoparticle arrays could be further utilized for electronic devices.

Biosensors

Biological templates, which possess predominant properties such as molecular recognitions, ease of engineering, and self-assembly, could be integrated with the enzyme immobilization techniques to produce enzymatic electrodes for biosensors. To construct an effective biosensor, an enzyme targeting to specific biomolecule needs to be immobilized onto a current collector. Generally, this could be done by surface functionalizations/modifications of conductive substrates and chemical conjugation of enzyme onto the substrates. However, structural and molecular tailoring on the surface is the key to direct the movement of electrons involved in the redox reaction of the enzyme. In general, a biologicial sensor can be realized to detect targeted molecules by mornitoring and interpreting the shuttling of the electrons or the electrochemical potential differences between the immobilized enzyme and the electrode.

Virus-based nanoelectrodes

M13 bacteriophage has a high aspect ratio structure and programmable functionalities, which can benefit the fabrication and performance of sensors. The high aspect ratio increases the density of enzyme that can be conjugated to the electrode surface, and the controllable functionalities can easily hybridize enzyme and conductive nanomaterials on the virus.

Glucose oxidase

Glucose oxidase (GOx) is a hydrogen peroxide-generating flavoprotein, catalyzing the oxidation of β-D-glucose to D-glucono-1,5-lactone (gluconic acid). The enzyme has been purified from *Aspergillus niger* and *Penicillium amagasakiense*. The structural similarities between the enzymes derived from the two fungus strains are about 70%. Glucose oxidase from *Penicillium amagasakiense* has a higher turnover rate and a better affinity to β-D-glucose than its counterpart from *Aspergillus niger*. Glucose oxidase is the most common enzyme used in biological sensor. Most recent researches for building biological sensors focused on developing electron relays with artificial electron acceptors or mediators used to shuttle electrons between the enzyme and the electrode.[69] The electrical communication between glucose oxidase and the electrode is mainly governed by the inert protein moiety of the enzyme. The performance of a biosensor is controlled by the impedance of electron relay, when electrons tunneling from the active site through the enzyme glucose oxidase to the electrode. In this thesis, glucose oxidase was chosen as the standard enzyme to be conjugated on the virus for making glucose sensors.

IV.C. Experimental

IV.C.1. Preparation of apo-glucose oxidase

Materials. *Aspergillus niger* glucose oxidase was purchased from ICN Biomedicals, Inc. Four types of sodium phosphage buffer were prepared as follows: 1) 25mM sodium phosphate (Mallinckrodt), pH=6.0 with 30% (w/v) glycerol; 2) 25mM sodium phosphate-H_2SO_4, pH=1.1 with 30% (w/v) glycerol; 3) 0.1M sodium phosphate, pH=1.7 with 30% (w/v) glycerol; 4) 0.1M sodium phosphate, pH=7.0. And, dextran-coated charcoal mixture made of 4ml of 0.4M sodium phosphate, pH=8.0, containing 20 mg of dextran (TCI America) and 600mg of activated charcoal (Darco® G-60, Sigma-Aldrich) was prepared. And, Sephadex G-25 (Amersham Bioscience) was packed in a titration column.

Procedure. 75 mg/ml solution of the glucose oxidase in 30% (w/v) glycerol in 25 mM sodium phosphate, pH = 6.0 was prepared. The exact enzyme concentration can be calculated from 450 nm using the millimolar extinction coefficient 14.1 $M^{-1}cm^{-1}$. The next step was acid-dissociation. Glucose oxidase solution 3 ml (or 6 ml) containing 0.225 g (or 0.450 g) of enzyme was stirred in a salt-ice bath, and ice-cold 30% (w/v) glycerol in 25 mM sodium phosphate-H_2SO_4, pH =1.1, was added until the whole solution reached pH = 1.7. This should require about an equal volume of reagent. The mixture was then incubated for 30 min at 0°C. The mixture was loaded onto a column of Sephadex G-25 equilibrated with 30% (w/v) glycerol 0.1 M sodium phosphate buffer, pH = 1.7, maintained at 4°C. The column was eluted with the same medium at a flow rate of 9 ml/min. The samples containing the protein were combined and were added with Dextran-coated charcoal. The elution of the apo-enzyme was monitored by its transmittance at 280 nm. The molar extinction coefficient of a 1% (w/v) solution at 280 nm is 13.8. FAD concentration was monitored at 450 nm with extinction coefficient of 11.3 $mM^{-1}cm^{-1}$. The pH of the collected solution was adjusted to 7.0 by slowly adding 1N NaOH. The collected solution was stirred for 1 hr at 4°C. The resulting solution was centrifuged (at 3400 rpm for 5 min) and filtered through a 0.45 μm filter. At this stage the apo-enzyme is stable to be stored at 4°C in a short-time. The solution was dialyzed against a 0.1 M sodium phosphate buffer, pH = 7.0. At this stage the apo-glucose oxidase

in lyophilized form was quite stable and might be maintained at 4°C for at least 18 months without loss of activity. The absorption at 280 nm of 1.71 was for a 1 mg/mL solution. The produced apo-glucose oxidase was further verified using MALDI mass spectrometry. The final concentration of apo-glucose was adjusted to 5 mg/mL.

IV.C.2. Chemical conjugation of glucose oxidase (GOx) onto virus-based nanowires

Materials. The co-enzyme of glucose oxidase, flavin adenine dinucleotide (FAD) was prepared in phosphate buffered saline (PBS, 0.1M, pH 7.0) to make 10 mM solution. The beta-D-glucose (ICN Biochemical Inc.) used for electrochemical test was dissolved in PBS to make a serial concentrations ranging from 5 mM to 100 mM. Glutaraldehyde (50%) purchased from Sigma-Aldrich was diluted in water to make 1% solution.

Immobilization of GOD. The M13 bacteriophage was anchored on the gold substrate and then mineralized with gold to form gold nanowire. 100 μL of FAD solution in PBS was incubated with the substrate for 10 min, followed with the addition of 10 μL glutaraldehyde (1% in water). The mixed solution was pipetted up and down and incubated for 30 min. After removing the solution, the substrate was rinsed with 1 mL PBS 5 times. The gold substrate was then incubated in 1 mL apo-glucose oxidase solution overnight.

Cyclic Voltammetry. The gold substrate grafted by GOx-conjugated virus nanowires was welded to the copper wire for connection to the potentiostat (Autolab, Model: PGSTAT 30). Silver/silver chloride electrode was used as the reference electrode. Platinum mesh was used as the counter electrode. The cyclic voltammetry was operated at 5 mV/s from -0.1V to 0.5V. The calibration line was plotted at 330 mV.

IV.C.3. Display of glucose oxidase on M13 bacteriophage

Materials. *Penicillium amagasakiense* fungus was purchased from American Type Culture Collection (ATTC# 28686). The sample was rehydrated with 880 μL sterilized

water and transferred to a falcon tube containing 6 mL sterilized water. The fungus was vortexed until the pellet was fully suspended. The rehydrated fungus was incubated at 25°C without shaking overnight. 12 g potato dextrose broth (PDB, from HiMedia Laboratories, Pvt. Ltd.) was dissolved in 500 mL Milli-Q® water and autoclaved. The designed primers were synthesized by Integrated DNA Technologies and diluted to 100 μM. Expand long template PCR buffered solutions and enzyme mix (Expand Long Template PCR System) were from Roche Applied Science. $Vent_R$® DNA polymerase was purchased from New England Biolabs. Deoxynucleotide solution mix (dNTP) was from Invitrogen.

Extracting ds-DNA of *Penicillium amagasakiense.* 60 mL PDB was inoculated with 50 μL rehydrated fungus solution in a culture flask. The fungus culture was shaked at 100 rpm at 25°C for 48 hrs. The culture was filtered with filter flask (0.2 μm pore size). The fungal cake was sandwiched by clean filter papers to remove the remaining water. The amplified fungi can be stored in 4°C for 6 months at this stage. To extract the DNA of the fungus, the fungal cake was dipped into liquid nitrogen and grinded using mortar and pestle. DNeasy® Plant Mini Kit (Qiagen) was used to complete the extraction and purification of the double strands fungal DNA (ds-DNA).

Cloning and mutagenesis of glucose oxidase gene. The ds-DNA of *Penicillium amagasakiense* extracted was used to clone the gene for glucose oxidase. Two cloning primers were designed to replicate the GOx gene in *Penicillium amagasakiense.* The sequence of GOx-273L was 5'- TTGCAATCCCGTTTACCTTC -3', and that of GOx-2158R was 5'- ACCGCGATTCATGACACCT -3'. The PCR reaction was carried out as follows:

H_2O	32.9 μL
dNTP (2.5 mM)	7 μL
GOx-273L (100 μM)	2 μL
GOx-2158R (100 μM)	2 μL
Fungal ds-DNA (~ 70 ng/μl)	0.1 μL
10X Expand long template buffer 1	5 μL
Expand long template enzyme mix (5 U/μl)	1 μL

, and the PCR cycling condition was

1 cycle	94°C	2 min
10 cycles	94°C	10 sec
	48.2°C	30 sec
	68°C	2 min
25 cycles	94°C	10 sec
	48.2°C	30 sec
	68°C	2 min + 20sec/cycle
1 cycle	68°C	7 min
1 cycle	4°C	forever

The cloned GOx gene was 1886 bases long and purified with 1% agarose gel electrophresis at 100V. Site-directed muntagenesis were used to create Sfi I restriction stie on each ends of this GOx gene. Two primers containing overhangs were designed for the muntagenesis PCR of the wild-type GOx gene sequence:

LPrimer_GOx_SfiI: 5'-CATGCGGCCCAGCCGGCCATGGCGGCAATGGTGTCTGT ATTTCTCAGCACTCTTCTTTTA-3' ;

and RPrimer_GOx_#9_SfiI: 5'- CCATTTTGGATGACTATGCCAAAAGTGCCGGAG GTGGATCAGCAGTGTCGGGGTCGTCGCCGGATTCGGATCCCGGCCAGGGAGG CCAGAATATG -3'

The details of mutagenesis PCR reaction is shown as follows

H_2O	35 μL
dNTP (2.5 mM)	3.5 μL
LPrimer_GOx_SfiI (100 μM)	1 μL
RPrimer_GOx_#9_SfiI (25 μM)	4 μL
1.8 kb GOx ds-DNA (~ 10 ng/μl)	0.5 μL
10X ThermoPol beaction buffer 1	5 μL
Vent® PCR Polymerase (2 U/μl)	1 μL

The mutagenesis PCR was carried out under the following conditions:

1 cycle	94°C	2 min
10 cycles	94°C	10 sec
	55°C	30 sec
	72°C	2 min
25 cycles	94°C	10 sec
	55°C	30 sec
	72°C	2 min + 20sec/cycle
1 cycle	72°C	7 min
1 cycle	4°C	forever

Sfi I restriction stie was created on each end of the mutant DNA containing p8#9 motif following the GOx gene sequence. The DNA product was confirmed by sequencing.

Engineering of phagemid with GOx. This mutant GOx gene and anti-phagemid vector (engineered by Dr. Beau Peelle) were then digested with Sfi I restriction enzyme under the following condition:

ds-DNA (~ 100ng/μl)	10 μL
H_2O	33.5 μL
10X NE Buffer 2	5 μL
100X BSA	0.5 μL
Sfi I (20U/μl)	1 μL

The digestion reaction was carried out at 50°C for 3 hours. After purifying the digested products, GOx gene was ligased into anti-phagemid vector, which contains two Sif I restriction sites in gene VIII. The ligation was carried out using T4 Ligase at 16°C overnight.

Amplification of GOx displayed M13 bacteriophage. The ligated DNA was cleaned up using QIA quick PCR purification kit and electroporated into XL-1 Blue electrocompetent cell at 1.7 kV. The transformed cell was grown in S.O.C. medium at 37°C for 20 min. Antibiotic screening was used to select successfully transformed cell,

which contained ampicillin-resistant gene in the electroporated phagemid/plasmid. The cells were stored in 50% glycerol at -80°C. The sequence of phagemid was confirmed by DNA sequencing. Helper phage with specific pVIII and pIII proteins would be used to infect the bacteria harboring the phagemid containing GOx gene, displaying glucose oxidases on the pVIII proteins of the amplified M13 bacteriophage. The amplification was carried out using regular procedures to amplify type 8+8 or type 8+8-3 virus.

Protein electrophoresis and enzyme assay. The protein electrophoresis analysis was carried out using 16% Tris-Glycine SDS-PAGE gel. To perform the enzyme assay, a mixture of 2'-azino-bis(3-ethylbenzthiazoline-6-sulphonic acid) (ABTS, 0.5mM) and horseradish peroxidase (HRP, 25 U/mL) was prepared. For each assay, 100 μL mixture was mixed with 100 μL of beta-D-glucose (1M) and 10 μL phage. 10 μL water instead of phage was used for the negative control, and active glucose oxidase solution was used for the positive control.

IV. D. Results and Discussion

To build a biosensor, sensing molecules and conductive materials need to be bridged and be able to communicate each other. The scheme was to display an anti-gold peptide in the pVIII protein of phage and covalently bond the N-terminus of pVIII protein to the enzyme. The anit-gold peptide was to create gold coating on the virus surface. The gold coating on the virus acted as an electron collector to direct the electrons out of the enzyme. The next goal was to pattern the viral electrode onto the substrate, by engineering the pIII protein to bind to the substrate. Before immobilizing glucose oxidase (GOx), the M13 bacteriophage was first conjugated with the co-enzyme, FAD, through the amine terminus on the pVIII protein. This step was to assure the placement of redox site in the enzyme would be close to the conductive nanoparticles grown on the virus. The apo-enzyme, apo-glucose oxidase, was then reconstituted onto this virus template. TEM images showed the apo-enzyme was immobilized onto the surface of the FAD-conjugated M13 virus (Figure 1).

The next step was to conjugate the enzyme onto the viral gold nanowire, which served as the electron relay between the enzyme and the current collector (substrate). Covalent coupling techniques were chosen to immobilize redox-enzymes onto pVIII proteins on the bacteriophage. For the first time, glucose oxidase was integrated into this viral nanowire system. After nucleating gold onto the pVIII proteins by the method described in **Chapter III**, the coenzyme of glucose oxidase, flavin adenine dinucleotide (FAD), was immobilized onto the virus through the free amine groups on pVIII proteins. Apo-glucose oxidase was therefore reconstituted onto the phage through the FAD. Individual engineered virus particle now could serve as an enzymatic nonoelectrode as schemed in Figure 2.

The type 8-3 virus was engineered with the anti-gold peptide motif, p8#9, on pVIII protein and the distinct anti-gold peptide (under the reduced from of pIII protein), p3-Au7C1r, on pIII protein. To avoid the aggregation of enzymatic nanoelectrodes and to test the activity of the enzyme reconstituted on the bateriophage surface, the virus was anchored onto a gold substrate as described in **Chapter III**, and then immobilization and

reconstitution of the enzymes were carried out on the viruses by using the described methods in this chapter. Atomic force microscopic (AFM) images showed filament and particle patterns, indicating the surface modifications by the hybrid structures of enzyme, gold nanoparticles and M13 virus (Figure 3). Cyclic voltammetry (CV) was measured using potentiostat to examine the built electron relay. The results showed that this virus-based electrode exhibited the oxidative peaks of glucose catalyzed by glucose oxidase at ~350 mV (vs SSCE). The measured currents and calibration line of the virus-based electrode operated at 330 mV was plotted in Figure 4. This amperometric glucose sensor operating at 330mV showed detectable currents when the surrounding glucose concentrations ranged from 5 mM to 100 mM. The current density of this virus-based electrode was approximately 0.1 mA/cm^2 at 50 mM glucose. The performance of an enzymatic virus electrode may be optimized by increasing the amounts of enzyme immobilized on the virus, changing the alignments of viral nanoelectrodes, or altering the electron relay structures between the enzyme and viral nanowire.

The incorporation of enzyme and biomineralization using a virus template also could be achieved by directly displaying a enzyme onto the pVIII protein of the virus. To date, *Penicillium amagasakiense* glucose oxidase was the only one successfully expressed in a prokaryotic host.[70] Since the bacteriophage is assembled in the bacterial cell, *Penicillium amagasakiense* glucose oxidase was chosen for the direct protein expression on the phage. The glucose oxidase genome was cloned from *Penicillium amagasakiense* using primers containing mutation sites to generate the Sfi I restriction sties on both ends of the GOx gene. This gene was then ligased into the anti-phagemid vector containing two Sfi I restriction sites in the gene VIII, which was later transformed into XL-1 Blue electrocompetent cells. The display of glucose oxidase on the virus was confirmed using SDS-PAGE protein electrophoresis (Figure 5). The enzyme displayed on the virus was reconstituted with FAD and tested for its activity using the enzyme assay. The active glucose oxidase will oxidize beta-D-glucose and water to generate gluconic acid and hydrogen peroxide. With the presence of hydrogen peroxide, horseradish peroxidase (HRP) will oxidize the substrate, ABTS, to turn the solution from colorless to green color. The enzyme assays were carried out with a serial dilution of GOx expressed

bacteriophage. However, the enzyme showed no activity up to this point. A denature and renature process was carried out to re-fold the enzyme. The GOx engineered bacteriophage was denatured with 8 M urea for 10 min and then diluted with PBS containing FAD 30-fold to re-nature it[71, 72]. The sample was then dialyzed using 12,000-14,000 MWCO membrane in PBS and concentrated after the dialysis. The enzyme assay still showed negative result. Further investigations are required to improve the enzyme expression and reactivation.

IV. E. Conclusion

The incorporation of these two techniques, the growing of conductive material and the immobilization of enzyme on the pVIII protein in bacteriophage, could be used to build electron relays between enzymes and viral nanowires. This enzymatic virus nanoelectrode potentially functions as an electrode for bio-energy generation or bio-sensor. The most attractive characteristics of using M13 bacteriophage as the template is that the enzyme could be directly displayed onto the virus. The viral template hence serves for two purposes: one is to serve as the biominerization scaffold to bind inorganic materials, and the other is to serve as the platform to grow/express biological reactors, such as enzymes. Although the preliminary results did not show active enzymes to be directly displayed on the bacteriophages, a feasible novel device design was proposed and demonstrated. Future researches on the direct display of enzyme will help to realize the engineering scheme described in this chapter.

IV. F. Figures

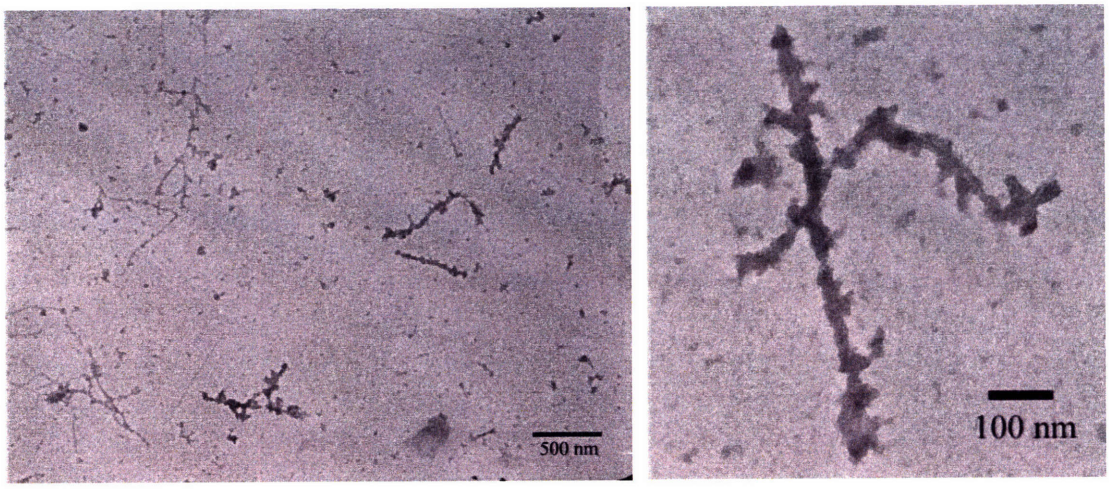

Figure 1. TEM images of glucose oxidase coated virus nanowires. Co-enzyme flavin adenine dinucleotide (FAD) was chemically linked to the virus and apo-glucose oxidase was then reconstituted onto the virus.

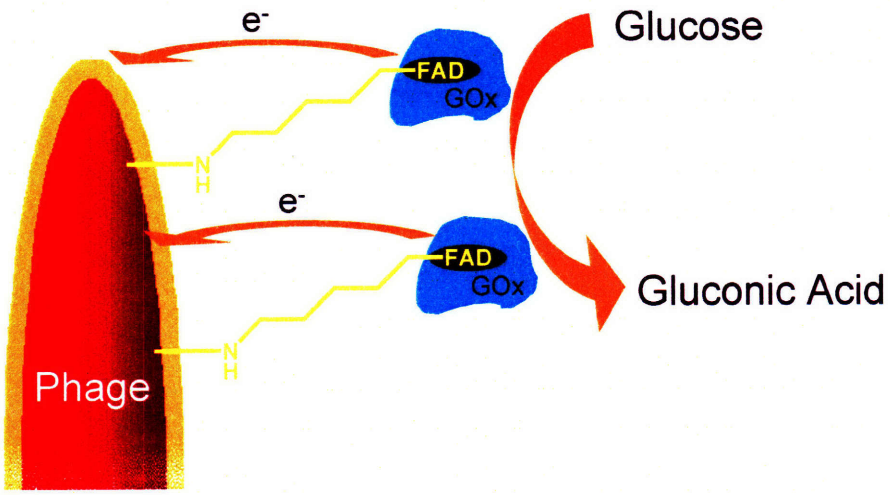

Figure 2. Schematic representation of glucose oxidase conjugated M13 bacteriophage. The glucose oxidase (GOx) was reconstituted onto the flavin adenine dinucleotide (FAD) to ensure the orientation of enzyme. FAD was used to bridge GOx and the virus.

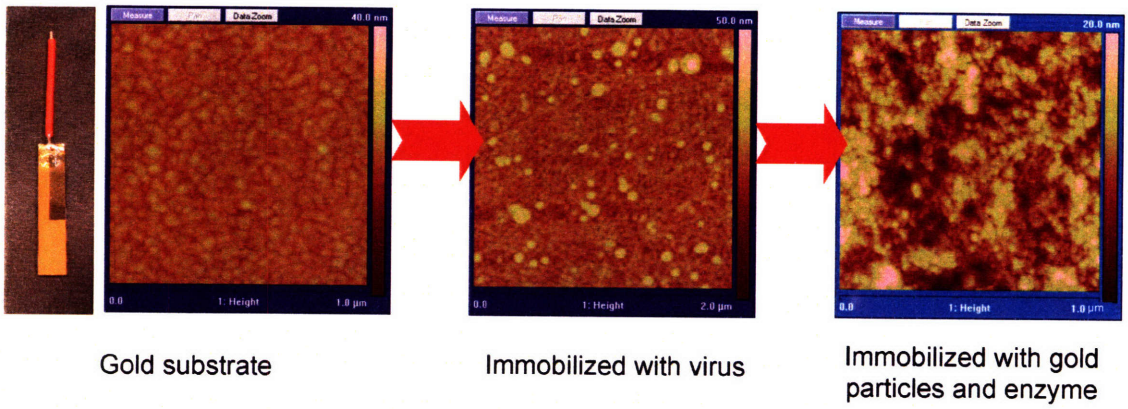

Figure 3. Enzymatic glucose oxidase electrode. A wired gold substrate was immobilized with gold-binding virus. After conjugating the virus with flavin adenine dinucleotide, the apo-enzyme was reconstituted on the surface.

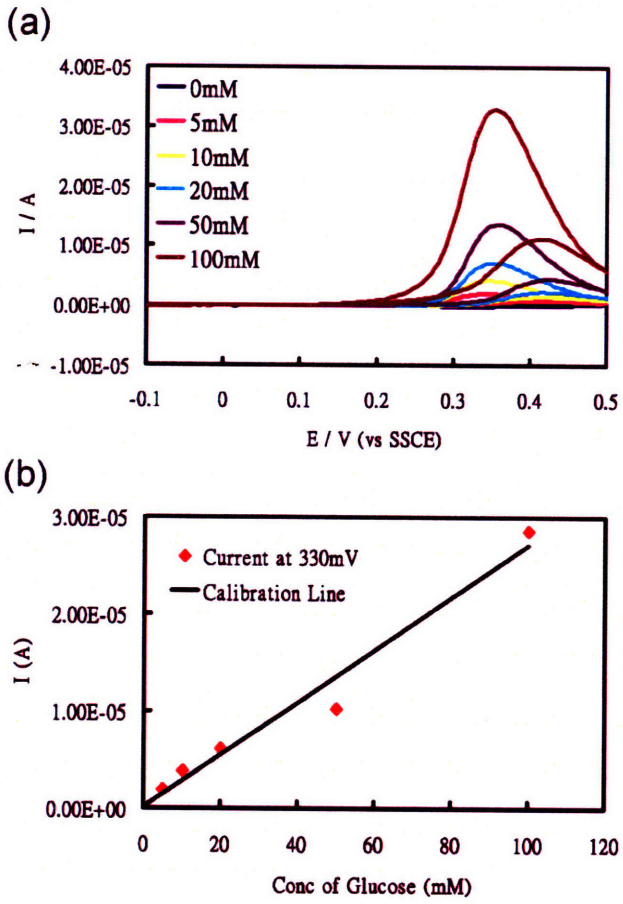

Figure 4. Electrical properties of glucose oxidase electrode. (a) Cyclic voltammetry of of modified electrode was recorded in 0.1 M phosphate buffer (pH = 7.0) and at potential scan rate 50 mV/s. (b) the calibration plot at 330 mV (vs SSCE) indicated that this

modified electrode could serve as an amperometric glucose sensor for monitoring the range of glucose concentration from 5 mM to 100 mM.

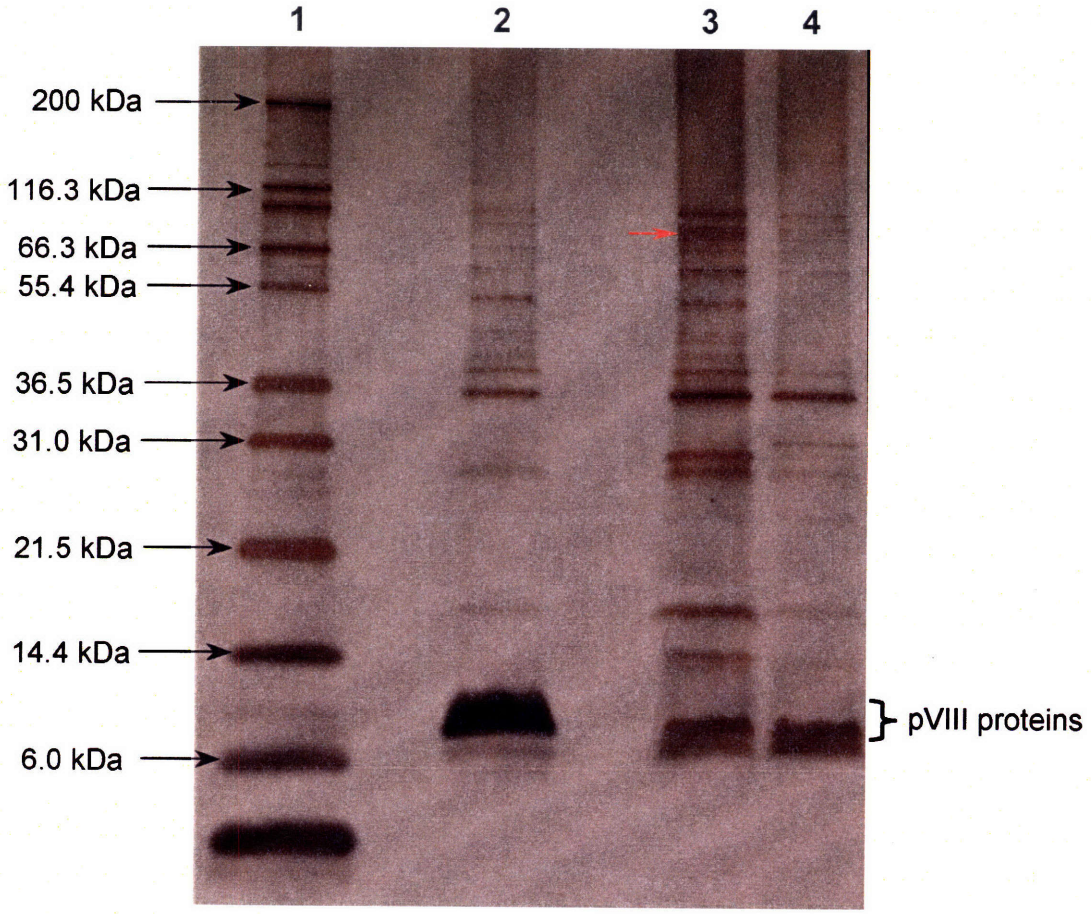

Figure 5. SDS-PAGE electrophoresis of glucose oxidase expressed virus. Lane 1 was a protein standard (Mark 12^{TM}). Lane 2 was p3-Au7C1r amplified in normal E. Coli ER2738 culture. Lane 3 was p3-Au7C1r amplified in the phagemid engineered E.coli (anti-phagemid vectro containing glucose oxidase gene) with isopropyl β-D-thiogalactoside (IPTG), and lane 4 (negative control) was that without IPTG. The phagemid contains the gene to produce glucose oxidase (GOx), and the assembly and production of GOx was triggered by IPTG. The band of displayed GOx (~ 72 kDa) on M13 virus was highlighted by the red arrow.

Chapter V. Micro-fabrication of virus-based functional fiber

V.A. Summary

Despite the increasing need for material multifunctionality in optical and semiconducting fibers, anti-microbial textiles, molecular filtration membranes, and other applications, the production of functionalized fibers has posed a challenge in materials science and engineering. In this chapter, the design and synthesis of fibers with genetically controllable and functionalized surfaces using M13 filamentous viruses are discussed. This work applies genetic engineering, chemical conjugation, and biotemplating methods to produce continuous fibers of centimeter-scale length and micrometer-scale diameter from nanoscale virus scaffolds. In addition, we find the virus fibers to be mechanically comparable to synthetic homopolymer fibers. The tunable functionalities and mechanical properties of the virus fibers show the promise of these high aspect ratio structures as useful materials for various applications including detection, catalysis, energy storage, and power generation.

V.B. Introduction

Issues in developing functional fibers

Increasing demand for tuning the molecular dimensions, structures, and functionalities in nanoscience has driven the search for materials with precisely controllable properties. Fibers are currently used in energy and electronic applications to obtain high energy density, energy capacity, and transportation efficiency, which may all be further improved by using nanostructured materials.[73-76] Synthetic polymers are commonly used as fiber materials;[77, 78] however, since it is difficult to produce varied functionalities on a single fiber surface, synthetic polymer-based fibers often lack functional versatility. Surface modifications of synthetic fibers usually require multistep chemical modifications and/or expensive enzyme treatments.[78-81] In addition, due to the lack of control over molecular structures and conformations, mixing incompatible functionalities in a material often leads to disorganized structures at the molecular level or to micro- to macroscopic phase separation, resulting in unintended or defective functionalities in the fiber surface.

Consequently, biological macromolecules such as DNA, proteins, and microorganisms (e.g., virus and fungi) have become key materials design components due to the inherent nanoscale control of molecular functionalities and structures.[82-86] In nature, functionalities and hierarchical structures of fibrous proteins are precisely controlled by DNA and widely used to make strong and functional fibers such as spider silk[87-89] and collagen.[90] However, these natural proteins are already highly evolved for specific functions, and it is difficult to engineer new design parameters into them. By adopting and combining the principles of fabrication found both in nature and in laboratories, the building blocks with desired functionality and structural hierarchy at the nanometer level can be designed and further these building blocks can be assembled into continuous and mechanically robust fibers.

Fibers made of filamentous virus

The ease of modifying M13 makes this virus an attractive platform for the growth and assembly of a variety of materials. At sufficiently high concentrations, M13 viruses behave as lyotropic liquid crystalline mesogens and self-organize to form micrometer-scale long-range order in aqueous solutions.[91, 92] The liquid crystalline property of M13 is driven by its high aspect ratio and anisotropic polarity. Inspired by the synthesis routes and properties of natural fibers,[93] viral liquid crystalline solutions were used to fabricate virus-based fibers. Here, the goal was to fabricate genetically functionalized fibers by spinning engineered M13 viruses.

V.C. Experimental

V.C.1. Wet-spun virus fibers

Materials and equipment. M13 bacteriophage was amplified, purified and concentrated to 10^{13} pfu/μL. The crosslinking agent (glutaraldehyde, 50%) was purchase from Sigma-Aldrich. The spinning speed is controlled by Pump 22 Multiple Syringe Pump (Harvard Apparatus). The 33 gauge needles were purchased from Hamilton Co.

Wet-spinning procedure. A concentrated virus solution (~ 470 mg/mL in Milli-Q® water, 1.7 x 10^{13} pfu/μL) was spun vertically through the needle into a glutaraldehyde solution by a syringe pump at a constant speed of 0.025 mL/hr, producing approximately 13 cm of virus fiber per μL of viral suspension. After incubating in glutaraldehyde for 2 hrs, virus fibers were rinsed with Milli-Q® water. These fibers were then vertically pulled out of the water by forceps and dried in air.

V.C.2. Chemical conjugation of nanoparticles onto virus

Materials. Qdot® 705 ITK™ amino quantum dots were purchased from Invitrogen Corp. 1-Ethyl-3-(-(3-Dimethylaminopropyl) carbodiimide Hydrochloride (EDC) was from BD BioSciences.

Chemical conjugation. To conjugate quantum dots to M13 viruses, 5 μL EDC (200 mM) was added to 200 μL virus solution (~ 5.5 x 10^{11} plaque forming unit or pfu/μL in Milli-Q® water), which was mixed with 5 μL quantum dot (QD) solution (8.25 μM). The mixture was vortexed and incubated at room temperature for 1.5 hrs. After adding 40 μL PEG/NaCl solution (20% (w/v) polyethylene glycol-8000, 2.5 M NaCl), the mixture was centrifuged at 10,000 rpm for 10 mins. Unbound QDs in the supernatant were removed, and the virus pellet was re-suspended in 10 μL Milli-Q® water.

V.C.3. Biomineralization of functional virus fibers

Materials. Virus fiber spun in 2.5% crosslinking solution. $HAuCl_4$ (chloroauric acid) and $NaBH_4$ (sodium borohydride) were purchased from Sigma-Aldrich.

Biomineralization. To test the gold mineralization capability of fibers, the wet fiber was immersed in a 300 μL chloroauric acid solution (5 mM, pH 7.5) and incubated on ice for 10 min. A 150 μL sample of ice-cold sodium borohydride solution (5 mM) was then added to reduce the gold. After 12 hrs, the fiber was manually removed from the solution, rinsed with Milli-Q® water, and dried in air.

V.C.4. Instrumental analysis on virus fibers

Microscopy and energy dispersive X-Ray characterization. Polarized optical and fluorescence microscopy images were obtained using an optical microscope (Olympus IX51). SEM images were analyzed with FEI/Philips XL30 Field Emission Gun Environmental Scanning Electron Microscopy (FEG-ESEM), operated at 10 kV with an electron backscattering detector. Energy dispersive X-ray (EDX) images were collected at a resolution of 256 x 200 pixels with 256 frames.

Uniaxial tension test. Under dry conditions, the ends of each fiber were secured between two stainless steel shims coated with cyanoacrylate, and the uniaxial tension tests were performed using 8848 Micro Tester (Instron Corp.) at ambient temperature, humidity, and pressure. Strain was recorded as crosshead displacement measured via a digital optical encoder within the load train.

Bending stiffness test. The fibers were mounted as end-clamped cantilevers and fixed at one end with cyanoacrylate at the edges of glass slides. A scanning probe microscope (3D-Molecular Force Probe, Asylum Research) was used to acquire the force-displacement response of the fibers via deflection of silicon nitride cantilevers (OMCL-AC160TS, Olympus Corp.). The optical lever sensitivity of the silicon nitride cantilevers was 41.64 ~ 47.35 nm/V and the spring constants k calculated from the thermal vibration

spectrum were 59.25 ~ 71.36 N/m. Bending stiffness measured at different force application points can be interpreted to obtain the Young's modulus E of the virus fiber and the x' using the nonlinear relation:

$$\frac{P}{d} = \frac{3EI}{(x + x')^3} \qquad (1)$$

where I is the moment of inertia of the cylindrical fibers. In Equation (1), d is the free-end displacement of a cantilevered fiber when it is subjected to a force P, x is the distance from the application point to the reference point, x' is the distance from the reference point to the support, and the moment of inertia I equals to $D^4/64$ for a cylindrical fiber of diameter D.

Error analysis. The dimensions of the fiber and the resolution of the uniaxial tensile apparatus were the dominant sources of error in the mechanical properties measured here. The resolution of the uniaxial tensile apparatus is 0.1 μm in displacement and 10 nN in force. The suspended length of the fiber was measured using a digital caliper with an error of 0.1%, and the fiber diameter was measured using optical microscopy with an error of 5%. For scanning probe microscope (SPM) bending experiments, the SPM system calibration had 3% error for both optical lever sensitivity and cantilever spring constant k. The linear fit of the uniaxial stress-strain response with an error of 1% and the nonlinear fit of the SPM stiffness-position response with an error of 3% were calculated using Microcal Origin®. For each experimental variable, five specimens were tested via uniaxial tension or via nanoscale bending test.

Thermal gravimetric analysis. Thermal gravimetric analyses were acquired using GTA7 Thermogravimetric Analyzer (Perkin Elmer). TGA samples were preheated to 100°C and held for 5 min. After cooling down to 40°C at 20°C/min, samples were heated from 40°C to 600°C at 5°C/min.

V.C.5. DNA extraction

Materials. Premixed solution of Phenol : Chloroform : Isoamyl Alcohol (25:24:1) and water-saturated ether were prepared. Phenol was purchased from Fluka, chloroform, isoamyl alcohol and ether were purchased from Sigma-Aldrich. Four sequencing primers designed to PCR inserted peptides on pVIII were synthesized by Integrated DNA Technologies. 1164Lprimer was 5'-TGTACTTTGTTTCGCGCTTG-3', 1339Rprimer was 5'-AACGGCTACAGAGGCTTTGA-3', #9g8Rprimer was 5'-CGAATCCGGCGA CGA-3', and KEg8Rprimer was 5'-CGGGATCGTCACCCTCAG-3'. Deoxynucleotide solution mix (dNTP), polymerase, and PCR reaction buffer were from New England Biolabs.

Phenol Extraction. A piece of viral fiber (abou 5 - 10 mm) was mixed with 50 μL phenol solution (premixed with chloroform and isoamyl alcohol). The sample was heated up to 90°C for 2 min and then cooled down to room temperature. 50 μL of water was added and the sample was vortexed for 5 min. The sample was centrifuged at 6,000 rpm for 5 min. The upper aqueous layer was transferred to a fresh sample tube. The aqueous solution was added with 50 μL water-saturated ether, vortexed, and centrifuged at 6,000 rpm for 4 min. The upper layer (ether) was discarded. The ether cleaning step was repeated three times. The final extract was vacuumed for 10 to 20 seconds to vaporize remaining ether.

PCR of extracted DNA in the fiber. The PCR condition was described as follows:

H_2O	43 μL
DNA extract	5 μL
1164Lprimer (100 μM)	20 μL
Rprimer (100 μM)	20 μL
dNTP (10 mM)	1 μL
10X Polymerase Buffer	10 μL
Taq® Polymerase (5 U/μl)	1 μL

And, the cycling condition was:

1 cycle	94°C	2 min
20 cycles	94°C	15 sec
	49°C	15 sec
	72°C	45 sec
1 cycle	72°C	5 min
1 cycle	4°C	forever

Electrophoresis. The PCR products was purified and quantified using 2% Agarose gel electrophoresis containing ethidium bromide running at 90V. 25 bp DNA Ladder (Invitrogen) was used as the standard.

V.D. Results and Discussion

Two synthetic routes to fabricate virus-based functional fibers were demonstrated: i) biotemplating the viruses with desired functionality before spinning the viruses into fibers; ii) spinning evolutionally selected and genetically modified viruses into fibers or outer sheaths of fibers for subsequent biotemplating.

For the former case, amine-terminated cadmium selenide quantum dots (QD) were chemically conjugated to M13 virus templates via the carboxylic acid side groups displayed on the pVIII proteins. A continuous fiber of micrometer-scale diameter (micro-fiber) was created through a wet-spinning process where a concentrated QD-conjugated virus solution was spun vertically into 2.5% glutaraldehyde solution at a constant rate. The virus fibers containing QDs emitted red light under exposure to ultra-violet light (Figure 1a and b). This demonstrated that conjugated quantum dots could be retained in virus fibers after the wet-spinning and washing processes. These quantum dot/fiber assemblies might serve as optical devices and advanced sensors.[94] To adjust the optical performance of a virus fiber, increasing the displayed copies of carboxylic acid side groups on pVIII proteins may result in relatively higher quantity of QDs to be conjugated to the virus. To demonstrate this surface tunability, a genetically engineered glutamate-rich virus, named E4, was used for QD conjugation. This virus contains four glutamates (Glu) and one aspartate (Asp) in the outer six amino acids at the N-terminus of the pVIII protein. Compared with the wild-type M13KE virus, E4 has two additional glutamates in the outer part of each pVIII protein and therefore exhibits increased conjugation of amine-terminated QDs (Figure 1c). This experiment demonstrated that genetic engineering is essential to improve or tune the bio-templating properties.

For the latter fabrication route, the capability of surface-functionalized M13 virus to make self-supported or composite functional fibers for subsequent biotemplating of gold was demonstrated. The peptide sequence Val-Ser-Gly-Ser-Ser-Pro-Asp-Ser (VSGSSPDS), termed p8#9, was selected from screening a type 8 bacteriophage library on gold substrates (see Chapter II). Genetically modified M13 virus containing p8#9 peptides has been shown to act as a template for growing gold nanowires and gold nano-

particle arrays in Chapter III. Through genetic engineering, bacteriophage building blocks provide flexibility in designing and modifying the fiber surface (Figure 2).

Continuous micro-fibers were produced using the same wet-spinning process described above. After the virus fibers were rinsed with water to remove unreacted glutaraldehyde, gold nanoparticles were directly nucleated from aqueous Au^{3+} solutions upon reduction via sodium borohydride ($NaBH_4$), resulting in nanoparticles which bound specifically to the engineered virus fibers at room temperature (Figure 3). The fiber surface and the distribution of biotemplated gold on the virus fibers were analyzed using scanning electron microscopy (SEM) and energy dispersive X-ray imaging (EDX). The homogeneous coating of gold nanoparticles on the genetically functionalized p8#9 fibers indicated the correct presentation of functionalities on the virus fiber surface (Figure 4a).

To demonstrate specificity of this gold-binding on genetically engineered M13 virus fibers, fibers were also spun from a wild-type clone, M13KE, which does not contain the gold-binding functionality. These control fibers contained discrete and scattered gold islands on the fiber surfaces after the identical processing for the p8#9 fibers (Figure 4b). Although the surface roughness of virus fibers provides high surface tension, which may be expected to facilitate non-specific binding of gold particles onto the fiber, the M13KE fiber itself still exhibited low gold-binding affinity. This resulted in a low density of gold on the M13KE fiber surface.

The ability of Kevlar® fibers to bind gold was also explored. These synthetic homopolymer fibers showed a negligible amount of gold deposition (Figure 4c). Absence of binding affinity to gold and the smooth surface of these synthetic fibers resulted in poor adhesion of gold particles. To create multifunctional fibers having high mechanical strength and capability of surface mineralization, a core-sheath structure was achieved, using Kevlar® as the core material and the engineered virus as the sheath. A Kevlar® fiber was dipped into a minimally crosslinked gold-binding virus suspension containing 0.05% glutaraldehyde. Both Kevlar® and the virus contain functional groups in their chemical structures that can participate in secondary forces, such as hydrogen bonding and hydrophobic interactions, resulting in adhesion between Kevlar® and the virus. This

virus-coated Kevlar® fiber was then transferred to a 2.5% glutaraldehyde solution to continue the crosslinking reaction. After coating with this gold-binding virus, gold nanoparticles were templated directly onto the composite fiber (Figure 4d).

Although agents such as glutaraldehyde will crosslink the amine groups at the N-termini of pVIII proteins, no disruption of surface functionality of the M13 viruses in these fibers was observed. This demonstrates the capability of the genetically engineered nanometric virus scaffold to mineralize inorganic materials at ambient temperature and to retain the desired functionality when assembled as micro-fibers. Such micrometer-sized fibers containing nanoparticles may be used in catalytic filtration, battery electrodes, and photovoltaic devices.[73, 95, 96]

The reproducible dimensions and structures of these centimeter-long fibers enabled us to study the mechanical properties of virus fibers for the first time. Although reports discussing the mechanics of protein-based natural fibers have been reported,[97, 98] the mechanical properties of virus-based fibers have not yet been considered. To evaluate the practical applications of such functional fibers, the elastic modulus, yield and ultimate tensile strength, failure stress and strain, and strain-rate sensitivity of the virus fibers were measured. To verify the effects of the virus crosslinking density on the fiber mechanical properties, virus fibers were synthesized in various concentrations of glutaraldehyde ranging from 0% to 10% (v/v). The estimated spinning rate was 5.3 cm min^{-1} for all concentrations tested. A change in the liquid crystalline phase during fiber spinning was expected to directly affect the mechanical properties of the virus fibers due to the orientation of the viral particles. Thus, all the virus fibers were spun from nematic liquid crystalline solutions to avoid variation resulting from different liquid crystalline phases.

No fiber was formed in the absence of crosslinking agent; the fibers spun into 0.1% and 0.5% glutaraldehyde were diffuse and semitransparent; and the fibers spun into crosslinking agent of ≥ 1% were solid and opaque (Figure 5). The diameters of the fibers varied from 10 to 50 μm depending on the spinning rate, the %-glutaraldehyde, and elongation ratio ($\frac{L_f - L_i}{L_i} \times \%$, where L_i is the initial length of fiber spun from the

spinneret in the wet state and L_f is the final length of fiber in the dry state). All the fibers could be pulled out of the solution by forceps, indicating sufficient strength for mechanical processing such as drawing and weaving.

Uniaxial tensile tests were conducted to examine the mechanical properties of these virus fibers in the dry state (Figure 6). On average, engineering stress-strain responses of pure virus fibers indicated a Young's elastic modulus E of ~ 3 GPa, an ultimate tensile strength σ_u of ~ 33 MPa, and an ultimate tensile strain ε_{uts} of ~ 1.3%. Overall, E of the pure virus fiber was similar to that of Nylon 6,6 (E = 1 – 3 GPa) and glassy homopolymers such as polystyrene (E = 2 – 4 GPa). Fiber ultimate tensile strength σ_u was comparable to that of atactic polystyrene and poly(tetrafluorethylene) (σ_u = 15 – 50 MPa). The normalized tensile strength (σ_u/E) of the virus fibers (0.005 – 0.030) was bounded by that of Nylon 6,6 (0.02 – 0.06) and polystyrene (0.002 – 0.02), indicating that the mechanical strength of virus fiber is similar to common synthetic (and glassy) homopolymers (Figure 7).

Mechanical data were analyzed statistically using one-way ANOVA (analysis of variance). When varying the crosslinker concentrations in the processing, statistically significant changes occurred in stiffness as quantified by E ($F(4,20) = 2.919$; $F(x,y)$ is the measurement of difference between individual distributions, where x is the degrees of freedom for the between group, and y is the degrees of freedom for the within group, probability $p < 0.047$) and effective ductility as quantified by ε_{uts} ($F(4,20) = 4.966$, $p < 0.006$); however, changes in σ_u as a function of %-glutaraldehyde were not statistically significant ($F(4,20) = 0.9765$, $p < 0.44$) (Figure 8). It is important to note that the variation of measured mechanical properties is attributed to both the resolution of the uniaxial tensile apparatus and the imprecise elongation of virus fibers during the drying process, the latter of which affects the extent of fiber crystallinity, as discussed below.

The extent of elongation in the wet state and the crosslinking density of a virus fiber will determine the %-crystallinity in the fiber and its mechanical properties. Virus fibers fabricated from < 1% glutaraldehyde can be elongated 5 – 20% before drying in air. The maximum E was observed for the lowest crosslinker concentration of 0.5%

glutaraldehyde. This is because the crosslinking density of the virus fiber determines the degrees of freedom of virus orientation during the processing preceding drying. The effects of virus orientation on fiber crystallinity were observed using polarized optical microscopy (POM) (Figure 9). The crystallinity of the virus fibers with low crosslinking density can be easily increased by elongating the wet fibers. This reorients the virus particles and promotes secondary interactions among viruses. In other words, low crosslinking density gives the fibers sufficiently high degrees of freedom for reorientation of the virus particles upon extension in the wet state. Conversely, for the fibers with high crosslinking density, the virus particles have limited degrees of freedom, resulting in a lower degree of crystallinity even upon elongation of the virus fiber in the wet state.

An independent set of samples was tested under uniaxial tension and bending to examine the effects of virus orientation on fiber mechanical properties. In this experiment, oriented fibers were elongated at least 15% in the wet state and analyzed to measure E in the dry state. In tension, we observed that E of the oriented virus fiber (3.13 ± 1.88 GPa) increased significantly compared to the unoriented fiber (0.68 ± 0.39 GPa) and that the σ_u of the oriented fiber (35.05 ± 25.53 MPa) also increased significantly with respect to the unoriented counterpart (6.02 ± 5.40 MPa). The bending stiffness (force P normalized by free end displacement d) of the same set of samples was also measured using a scanning probe microscope (SPM) at different force application points (x+x') along the cantilevered virus fiber (Figure 10). The elastic moduli E acquired via this method were 0.98 ± 0.74 GPa and 3.15 ± 1.54 GPa for non-oriented and oriented virus fibers, respectively, which agreed well with that measured via uniaxial tension. We therefore conclude that the crosslinker is only needed to process the virus fibers via spinning but not necessary to enhance the mechanical properties of virus fibers. In the case of virus fibers with low chemical crosslinking densities, both the mechanical strength and stiffness is attributed to the secondary inter-viral interactions such as hydrogen bonds and ionic interactions, and the mechanical properties can be enhanced through fiber elongation that promotes crystallinity via environmentally benign processing.

To evaluate the extent of viscoelasticity in the virus fibers, uniaxial tensile tests were conducted at three different displacement rates: 10^{-2}, 10^{-3} and 10^{-4} mm sec^{-1},

corresponding to strain rates $\dot{\varepsilon}$ of 10^{-1} to 10^{-3} sec^{-1} (Figure 11).A slight increase in E ($F(2,12) = 4.974$, $p < 0.027$) and decrease in ε_{uts} ($F(2,12) = 27.78$, $p < 0.0001$) were observed as a function of $\dot{\varepsilon}$. For a 100-fold increase in strain rate, E increased only by 1.5-fold. This indicates that the virus fibers are well approximated as linearly elastic materials. In addition, no statistically significant change in σ_u ($F(2,12) = 0.8042$, $p < 0.47$) was observed over this strain rate range. Neither necking nor significant plastic deformation prior to fracture was observed under uniaxial tension (Figure **6**), and the fracture surfaces appeared globally brittle (flat and normal to the loading axis) under optical microscopy (Figure 11). However, scanning electron microscopy images showed locally ductile fracture features (< 1 μm in length and < 20 nm in width) across the whole fracture surface of the virus fiber (Figure 11). The fracture surface was perpendicular to the loading axis and was microscopically rough because of this localized pullout of virus materials. Thus, the mechanical failure of these virus fibers appears macroscopically brittle and microscopically ductile, consistent with the hydrostatic stress-sensitive failure surface of brittle polymers.

After nucleation of gold nanoparticles on the virus fibers, E decreased to 0.2 – 1.5 GPa, due most likely to the chemical and physical deterioration caused by the reducing agent and the formation of gold inside the fibers. This deterioration may be avoided by employing a milder reduction reaction for gold, such as hydrogen reduction. On the other hand, the composite fiber with a core-sheath structure maintained structural integrity upon gold nucleation: E of Kevlar® fibers before virus functionalization was ~ 35 GPa, and remained unchanged after gold was mineralized onto the composite fibers (~ 33 GPa). This indicates that viruses can serve as a functional template to alter the functionality of Kevlar® fibers without any chemical or mechanical deterioration of the overall fiber mechanical properties.

Thermal gravimetric analysis (TGA) showed that both non-coated and gold-coated virus fibers exhibit thermal stability up to 190°C (< 5% weight loss) in nitrogen. Substantial degradation initiated at ~ 260°C. Residual char was > 30 wt% for the uncoated virus fiber and > 60 wt% for the gold-coated fiber (Figure 12). Therefore, the amount of gold coated on a virus fiber was ~ 30 wt% with respect to that of the uncoated

virus fibers. Both non-coated and gold-coated virus fibers were more stable in air than in nitrogen at the high temperature range between 300°C and 500°C, where the thermal degradation was delayed in the presence of oxygen (Figure 12). This is due to the interaction of oxygen with nitrogen and phosphor atoms, which exist in the viral DNA as well as in the coated proteins and may act as flame retardants in the virus.

The viral DNA stored in the virus fiber exhibited long-term stability at room temperature. The DNA could be extracted using phenol extraction as described in the experimental session, and its integrity was verified using PCR, Agarose electrophoresis, and DNA sequencing. Four primers were designed for PCR and sequencing. 1164Lprimer and 1339Rprimer, targeting gene VIII for 176 bp cloned DNA, were universal primers for any type of M13 bacteriophage. #9Rprimer was designed for targeting the M13 virus containing p8#9 gene in the gene VIII, producing 233 bp DNA. KERprimer was used to target virus with the wild-type gene VIII, producing 225 bp cloned DNA. The targeted DNA was varied from 176 to 233 base pairs depending on the type of virus used to spin the fiber and the primer added during the PCR. The virus fiber showed excellent preservation of the viral DNA. All the virus fibers used in the DNA integrity test were left on bench at environmental temperature for more than 6 months. Agarose gel and DNA sequencing results showed that the DNA extracted from the virus fiber remained its integrity (Figure 13). The virus fiber could be used as a long-term storage device for preserving DNA information at environmental temperature without fridge or serving as a encryption material.

V.E. Conclusion

This work provides a new conceptual scheme for fiber design and fabrication through genetic modification of a biotemplate (Figure 14). Using an engineered virus to continuously produce functional materials or coatings for synthetic fibers could simplify current surface modification processes such as multistep chemical or enzymatic treatments. The potential of the M13 virus to serve as a powerful toolkit for designing a specific functional fiber material from standard techniques including biopanning, bacteriophage amplification, and genome modification was demonstrated in this chapter. The virus fibers exhibit mechanical toughness and strength comparable to synthetic polymer fibers, indicating that this filamentous virus can be integrated into current fibril and woven mesh manufacturing systems. The genetic manipulation of diverse functionalities on the virus fiber surfaces offers a convenient and powerful basis for conjugating organic or inorganic materials for a variety of applications such as the creation of anti-microbial, catalytic, optical, medical, and electronic materials.

V.F. Figures

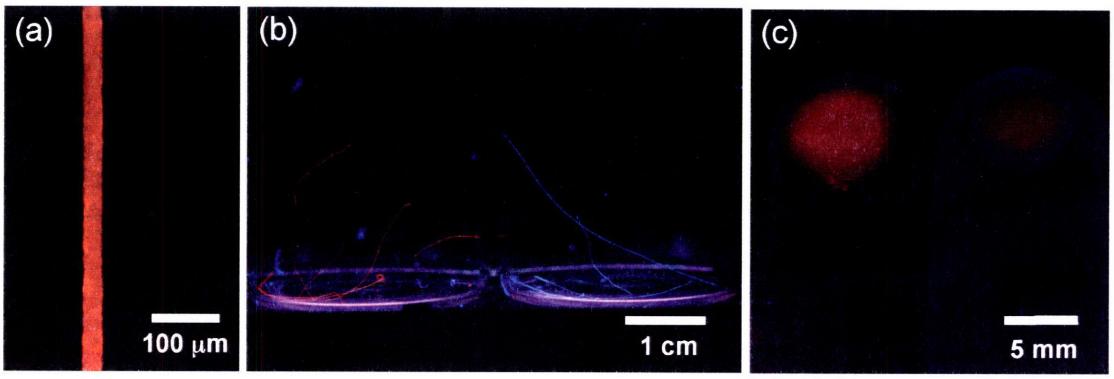

Figure 1. Images of chemically engineered functional fibers. (a) Fluorescence microscopy image of E4 virus (a genetically engineered glutamate (Glu)-rich virus) fiber conjugated with QDs excited by using UV light. (b) Under exposure to UV light, virus fibers conjugated with QDs emitted red light (left) and nonconjugated virus fibers emitted blue light (right). (c) The E4 virus (left) showed a relatively higher intensity of light emission than the wild-type M13KE virus (right) after QD conjugation and purification.

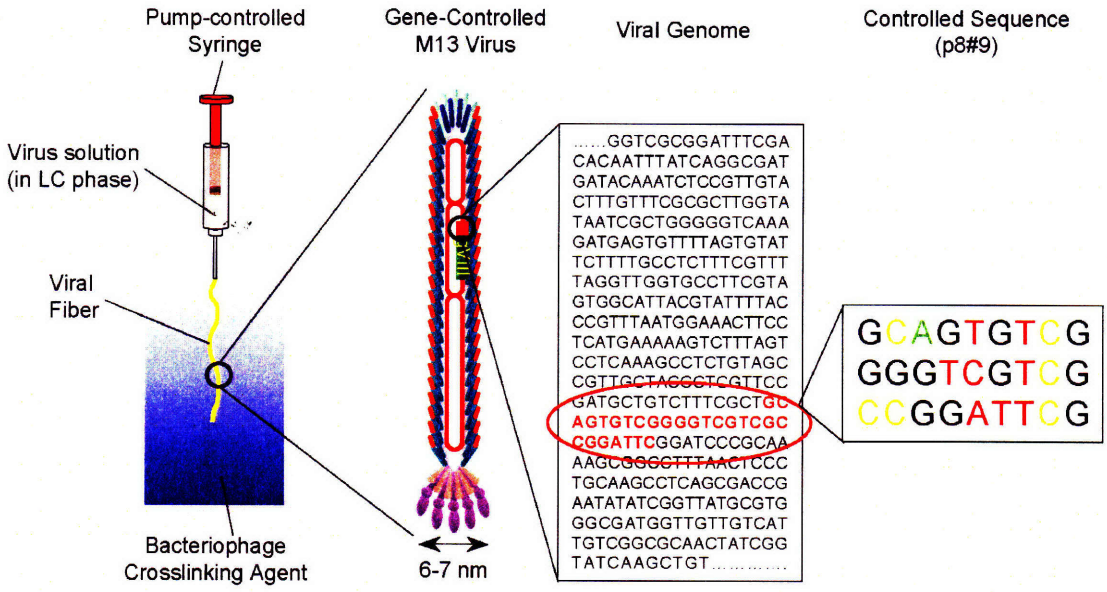

Figure 2. Schematic design of genetically engineered functional fibers. Schematic illustration of an inserted DNA sequence displaying specific peptides (orange) along the M13 virus that is spun into a fiber with the desired surface functionality.

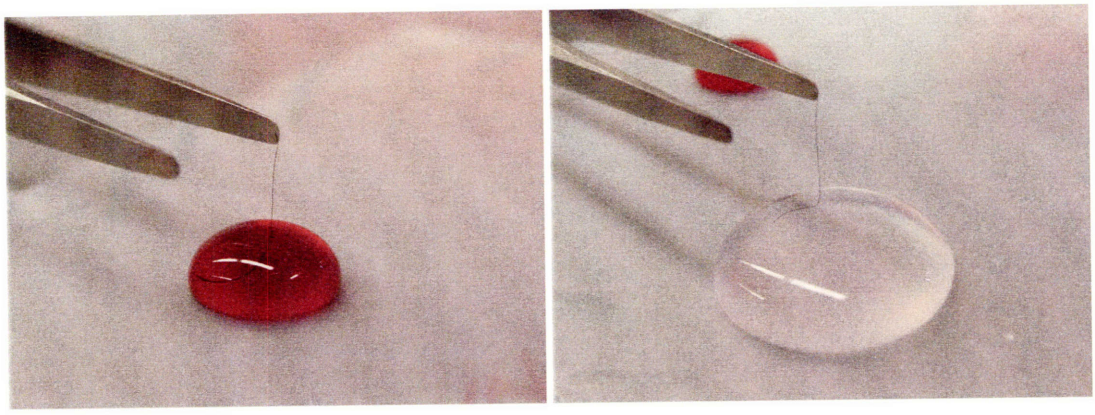

Figure 3. Gold nucleation on virus fiber. (Left) A virus fiber was immersed in gold precursor solution and added with the reduction agent to nucleate gold nanoparticles on the fiber. (Right) The gold-coated virus fiber was rinsed with water to remove unbound gold nanoparticles.

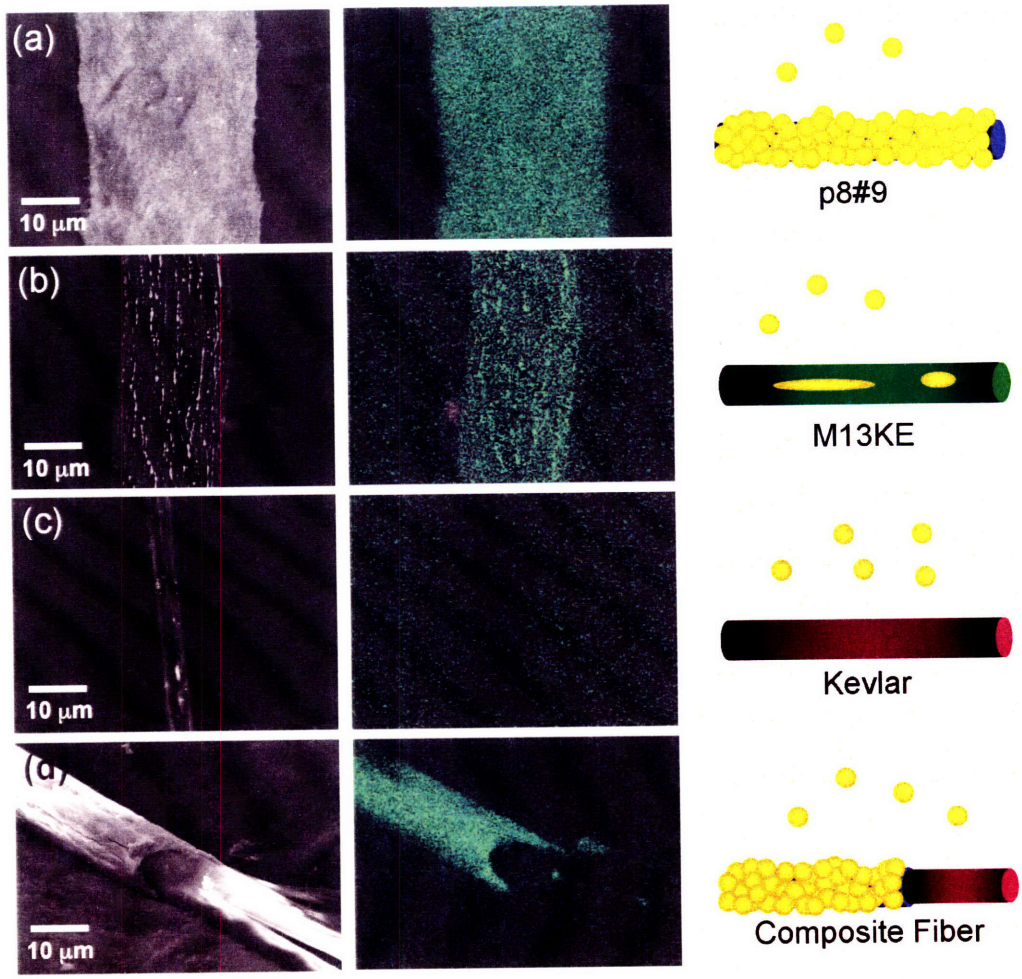

Figure 4. Effects of genetic engineering on mineralization. SEM and EDX images, and schematic representations of different types of fibers after gold mineralization. (a) Dense gold nanoparticles are homogeneously mineralized on a fiber comprising viruses (p8#9) selected to bind gold nanoparticles. (b) The M13KE fiber contains no specific gold-binding affinity and exhibits a small amount of random binding to gold particles. (c) The Kevlar fiber exhibits limited, if any, gold-particle attachment. (d) Nucleation of gold nanoparticles is only observed on the portion of a Kevlar fiber coated with p8#9 viruses.

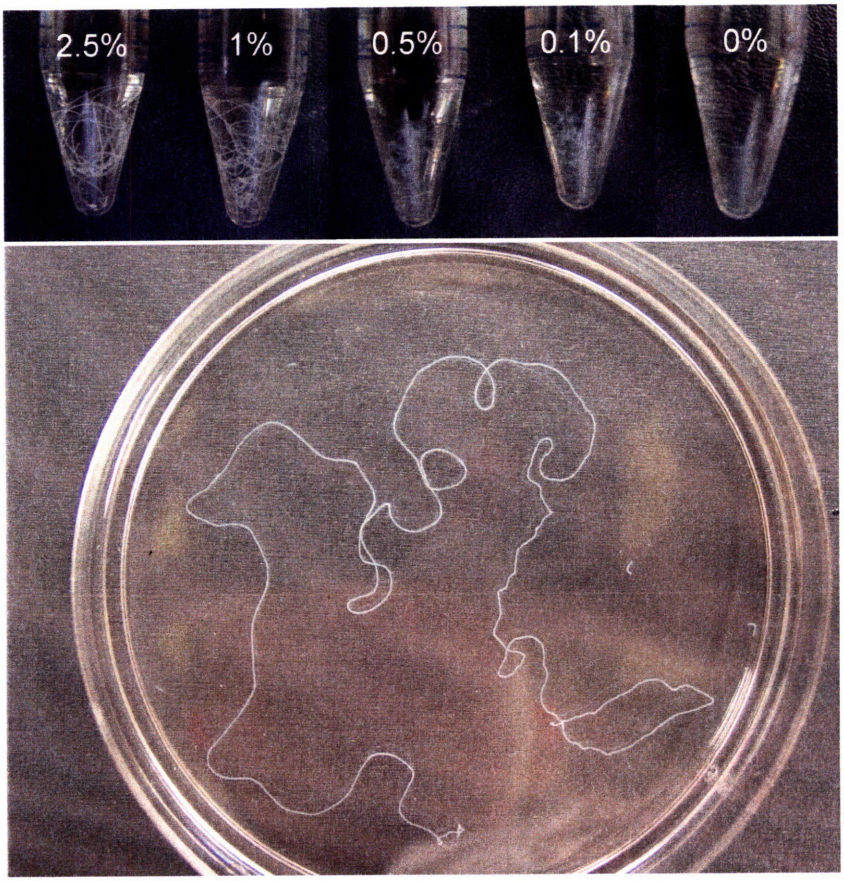

Figure 5. Images of virus fibers. (Top) Virus fibers fabricated in various glutaraldehyde solutions ranged from 0% to 2.5%, indicated as vol%. (Bottom) A continuous virus fiber (longer than 30 cm) fabricated in 2.5% glutaraldehyde in a petri dish.

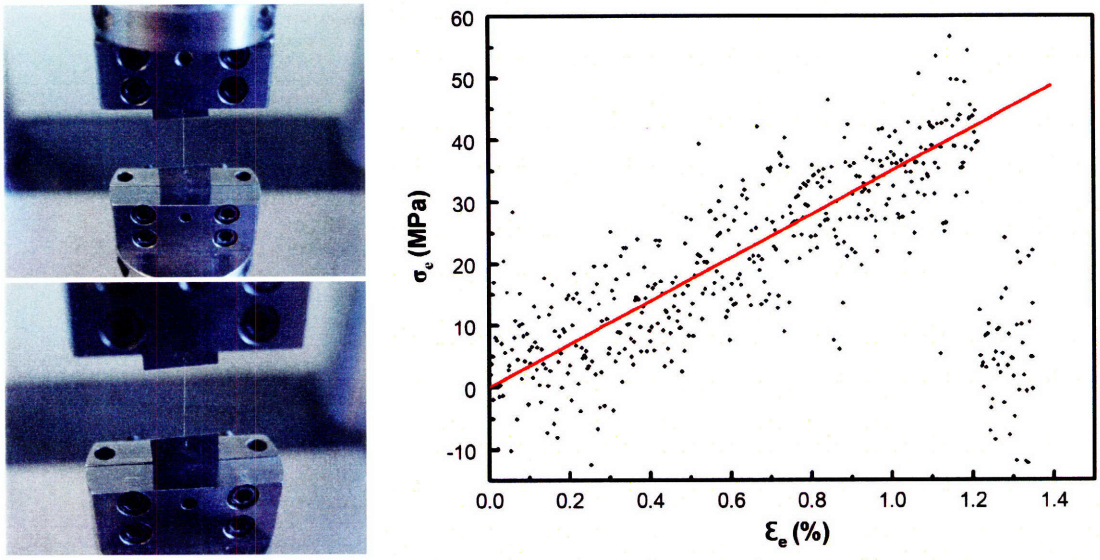

Figure 6. Uniaxial tension test. (Left) A virus fiber sandwiched by stainless shims was mounted on the tensile tester before and after fracturing. Data was only collected when the fracture occurred between the two mounting stainless shims. (Right) Representative engineering stress–strain response of virus fibers. No plastic deformation was observed until the fiber fractured.

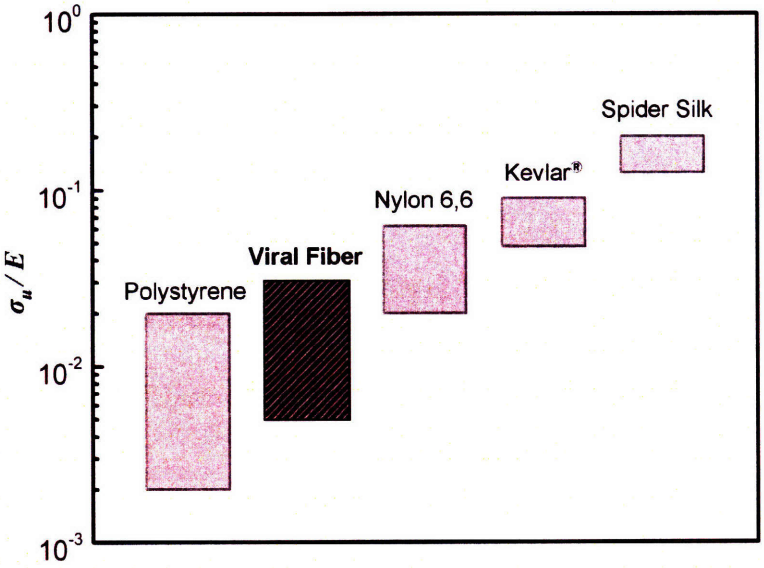

Figure 7. Bar-chart of normalized tensile strength (σ_u/E) for selected natural and synthetic polymers. The normalized tensile strength of the virus fibers was bounded by that of Nylon 6,6 and polystyrene, indicating that the mechanical strength of virus fiber is similar to common synthetic homopolymers.

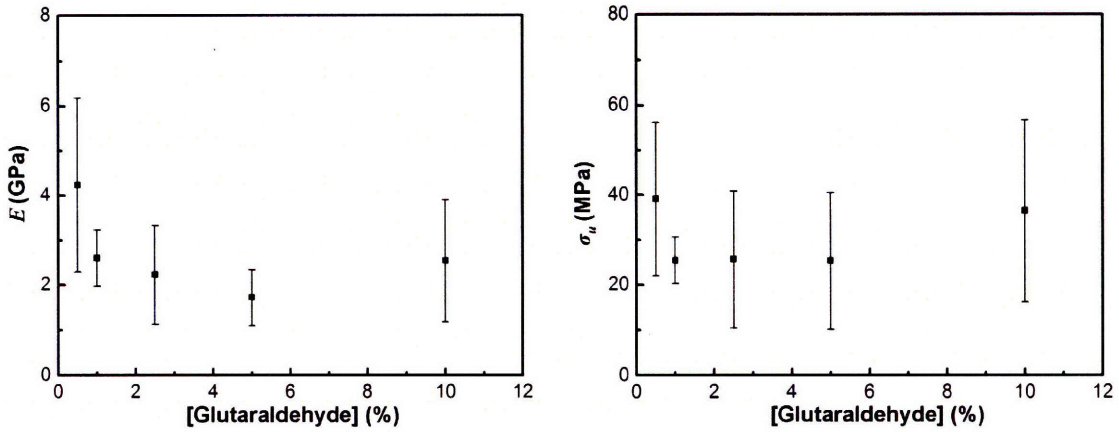

Figure 8. Mechanical properties of virus fibers. (Left) Effects of glutaraldehyde concentration on the Young's modulus E shows a local minimum around 5% glutaraldehyde. (Right) The variation of ultimate tensile strength σ_u with glutaraldehyde concentration.

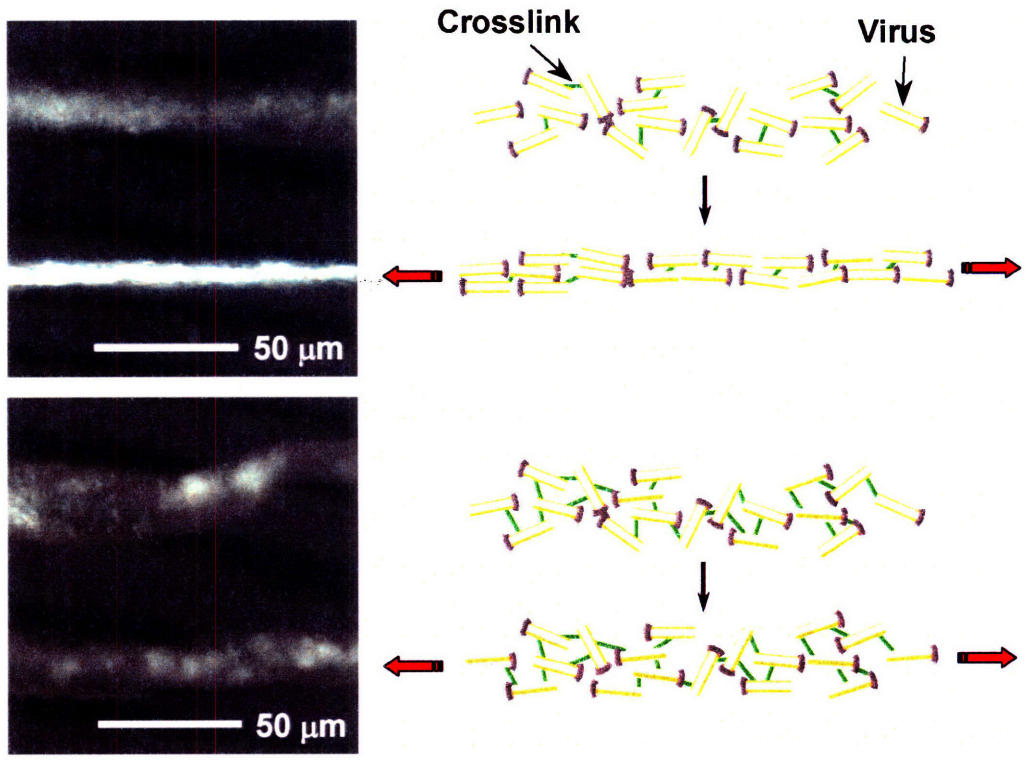

Figure 9. Elongation of the virus fiber. Polarized optical microscopy (POM) images of virus fibers (left) and schematic graphs of virus assemblies (right), where rods represent individual virus particles constrained by crosslinks (in green). The virus fibers fabricated from 0.5% (top) and 5% (bottom) glutaraldehyde solutions before stretching and after manual elongation while drying.

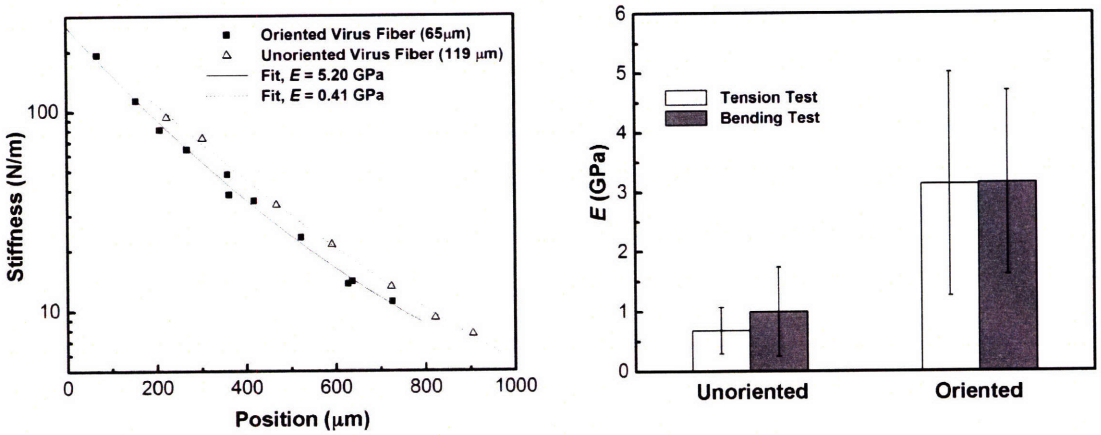

Figure 10. Comparison of bending and tension tests. (Left) Relationships of fiber bending stiffness (P/d) to force application position ($x+x'$) from vertical bending tests on an oriented fiber (D = 65 μm) and an unoriented fiber (D = 119 μm) made from 0.5% glutaraldehyde solution. (Right) Comparison of E for unoriented and oriented virus fibers consisting of 0.5% glutaraldehyde solution under uniaxial tension test and cantilevered bending test.

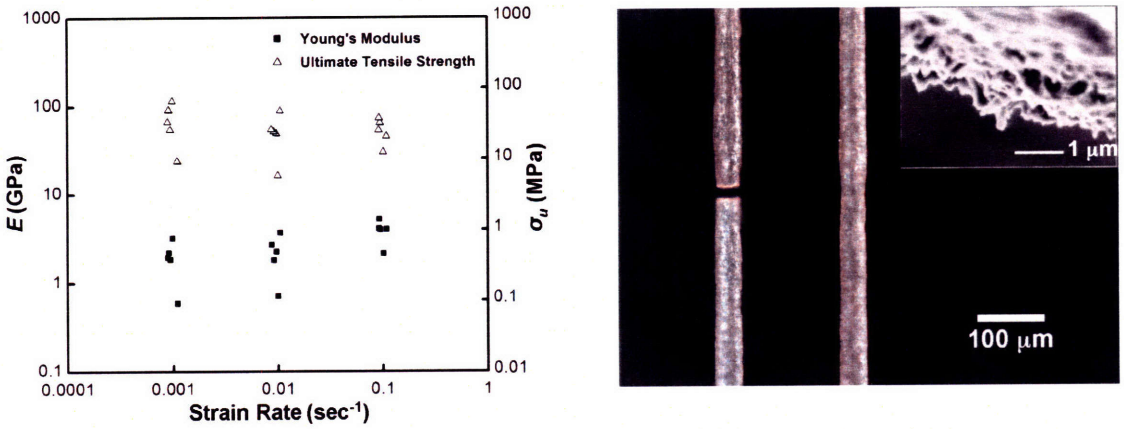

Figure 11. Viscoelastic behavior of virus fibers. (Left) Young's modulus E and ultimate tensile strength σ_u as a function of strain rate. (Right) Polarized optical microscopy images of virus fiber before and after fracture; and scanning electron microscopy image (inset) of fracture surface.

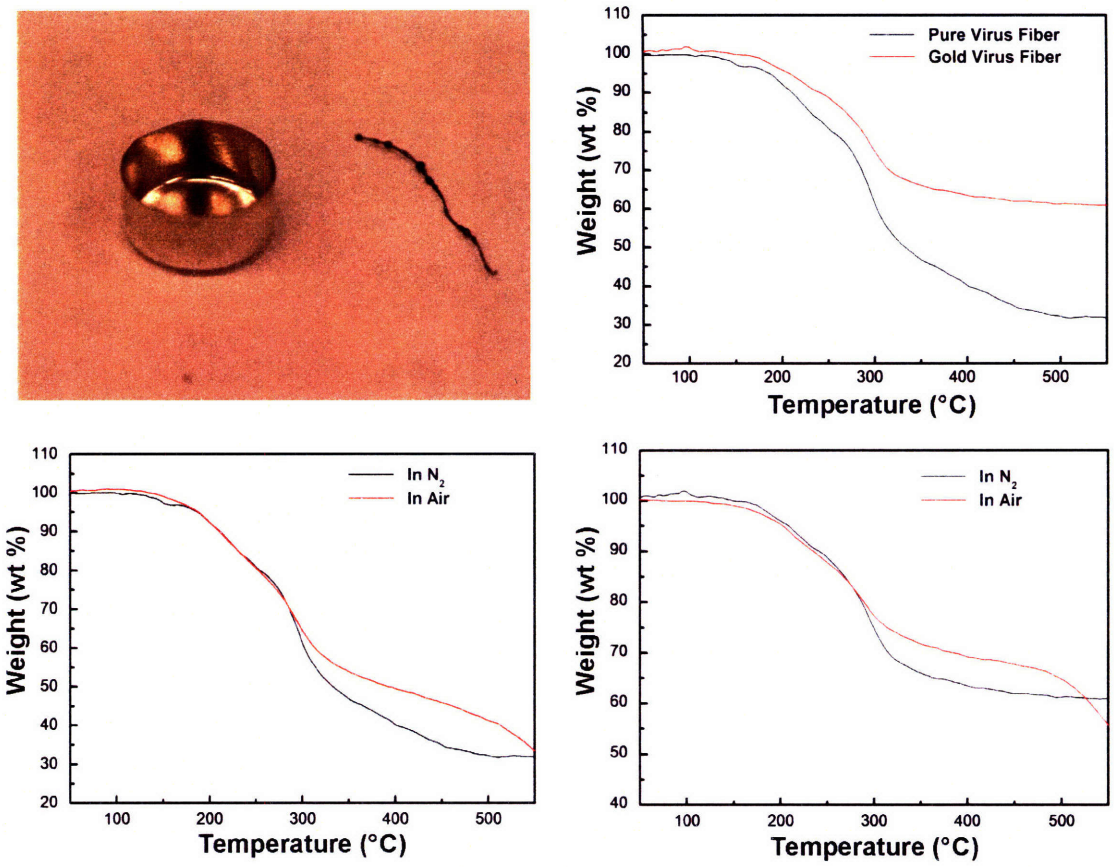

Figure 12. Thermal degradation of virus fiber. Thermal gravimetric analysis responses of pure and gold-coated virus fibers made from 2.5% glutaraldehyde solution. (Upper left) Picture of virus fiber after heated up to 600 °C in air. (Upper right) Comparison of pure and gold-coated virus fibers in nitrogen. (Bottom) Comparison of thermal degradations in nitrogen and in air for pure (bottom left) and gold-coated (bottom right) virus fibers.

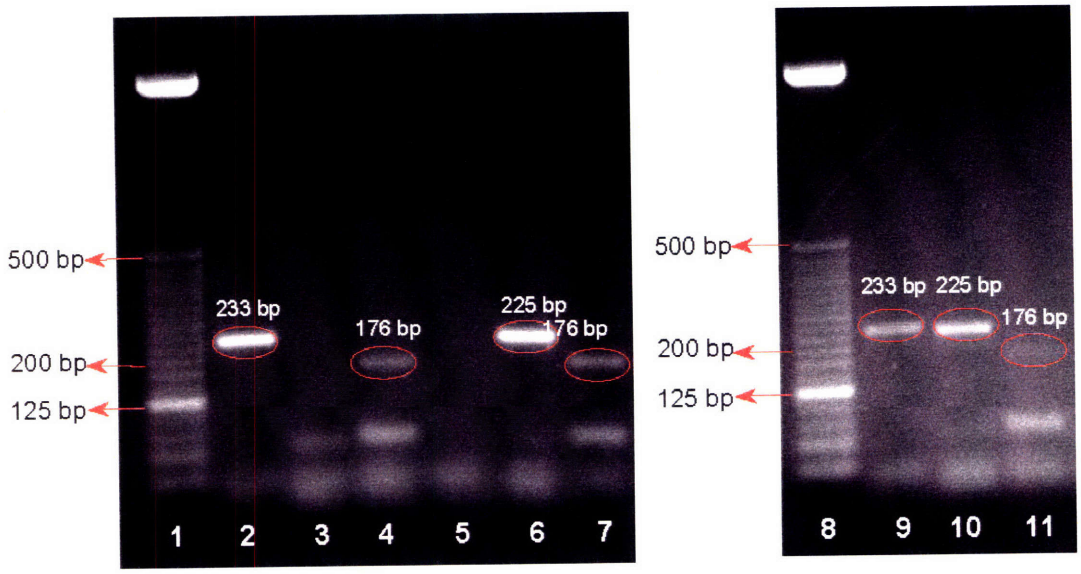

Figure 13. Genetic information stored in virus fibers. Each virus fiber could have its own genetic information based on the DNA stored in it. Lane 1 and 8 were 25 bp DNA ladder. Lanes 2 to 4 were the PCR products of p8#9 virus fiber; lanes 5 to 7 were the products of M13KE virus fiber; and lanes 9 to 11 were products of the virus fiber spun from a mixture of p8#9 and M13KE clones. All samples were cloned using the same universal primer, 1164Lprimer. 1339Rprimer was used for the samples loaded in lane 4, 7, and 11. #9Rprimer was used for the samples loaded in lane 2, 5, and 9. KERprimer was used for the samples loaded in lane 3, 6, 10. From the electrophoresis results, each types of virus fibers could be easily differentiated.

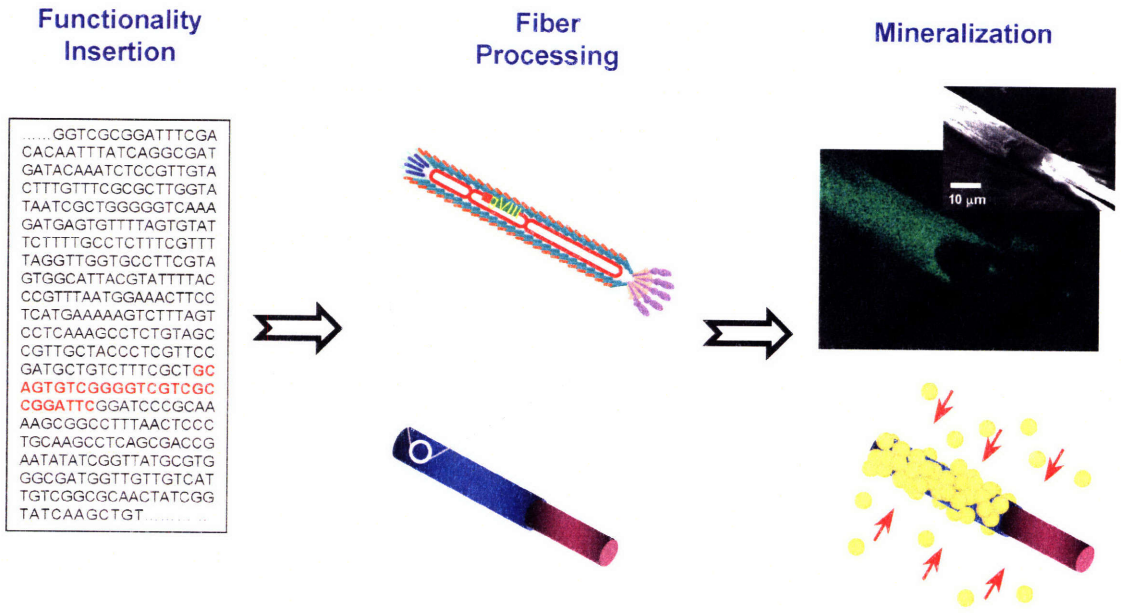

Figure 14. Genetically tunable functional fiber. Functionality-tunable fibers made from M13 virus are mechanically comparable to synthetic homopolymer fibers. The desired functionality can be programmed by manipulating the virus genome. The tunable functionalities and mechanical properties of the virus fibers show the promise of various applications.

Chapter VI. Energy applications of virus-based materials

VI.A. Summary

The conformation of the filamentous virus is a structure of interest for creating high surface density materials. All the chemical or catalytic reactions happen at the interfaces or surfaces of materials. The kinetic barrier of a chemical reaction is inversely proportional to the surface density. In this chapter, the M13 viruses served as filamentous templates to form uniform nanowires, comprised of densely packed nanoparticles. The electrochemical reaction of such nanostructure was studied to prove the concept mentioned above. The electrochemically active materials synthesized using the viral template showed relatively high reversible reactivities when compared to the active materials made without the viral templates. This virus also provides flexible designing capabilities to create hybrid nanomaterials, which may greatly improve the material performances.

VI. B. Introduction

Energy crisis

Energy crisis is an inevitable issue. Global energy consumption is projected to increase by 54% over the next 25 years. In the United States, total energy consumption increases more rapidly than domestic energy supply through 2025. Net imports of energy are predicted to increase from 27% in 2003 to 38% in 2025 (Figure 1). The decline of total domestic petroleum supply will speed up the increase of net imported energy. Improvement of current energy supply system and development of new energy sources are world-wide trends. In the human energy history, most of the energetic power generated by human beings has brought a lot of containments and by-products which have greatly changed the global environment. For example, the combustion of fossil fuels in combustors to generate power emits carbon oxides (CO_x), sulfur oxides (SO_x) and nitrogen oxides (NOx), which cause green house effect, acid rain and air pollution. Unlike the combustions, electrical power is the one which is clean and zero-emitting. However, the processes to create electrical power may not be clean nor be efficient. Coal-fired power plants, the main power plants using coal to generate electricity, emit enormous polluted air as the combustors and are not efficient. Electricity generated by nuclear fuel is efficient, but it generates radioactive waste which causes proliferation of biological mutations and therefore requires long-term high level waste storage. Only few energy sources to generate electricity such as solar, wind and hydroelectricity are classified as "renewable energy", "green energy", or "zero-emission energy". However, these green energy sources are limited and not designed for portable usages in autos or mobile electronics. Hence, electrochemical cells (or batteries) are designed to accommodate the purpose of portable uses. Unlike the traditional combustors converting fuels into heat and further converting heat into electricity, electrochemical cells directly transform fuels into electricity. This mechanism greatly increases the efficiency of energy usage and minimizes the loss of energy transformation, which makes electrochemical cell an efficient power source. However, electrochemical cells may still cause environmental pollutions. Primary batteries (e.g. zinc-carbon battery, alkaline-manganese battery) require recycle system to avoid potential pollution to soil. Although secondary batteries

such lead-acid battery (LAB), nickel-metal hydride battery (Ni-MH), and lithium battery can be applied to cycle usages, the utilization of secondary batteries is still limited by serving life, toxic contents and low capacity. The desire for clean and permanent energy still urges scientists and engineers to exploit new power sources.

Fuel cell

In addition to the energy crisis and pollution issue, miniaturization of electronic devices has become the need of the day owing to biological and medical applications such as biosensors, pacemakers, and hearing aids. However, the development of small power cells for these micro-devices is relatively slow. Although a lot of portable power sources such as lithium ion batteries are available and wildly used in electronic devices, the capability of these secondary batteries being used as implant power sources is restricted to the external application because of the limited discharge time and the possible leakage of toxic reactants stored in the electrodes. To fit in the strict requirements of medical applications, a long-term power source using non-toxic fuels is the ideal choice. In this category, fuel cells are the best of choices. Fuel cell can use non-toxic reactants as fuels such as hydrogen and its byproducts are just pure water; therefore, fuel cell has been classified as a "green energy". It keeps generating energy as long as the reactants (or fuels) are continuously delivered into the cells. To date, the micro fuel cell made by microelectromechanical system (MEMS) technology has been reported, but its application to implanted electronic devices is still limited by the choice and storage of fuels and the high working temperature.

Bio-fuel cell

Deriving from the concept of fuel cell, bio-fuel cells use the biomoleucles (such as glucose)[99] in physiological environment as fuels and operate at physiological temperature. It uses renewable fuel sources which are generated or recovered by biological metabolisms and therefore provides electrical power eternally. Bio-fuel cell is an ideal

power source to integrate artificial circuits or devices into metabolism cycles without producing any harmful by-products. Redox-enzymes used in a bio-fuel cell can oxidize or reduce specific biomolecules. A combination of oxidative enzyme on an anode, reductive enzyme on a cathode, and electrolyte results in an electrochemical potential difference between the anode and the cathode. Thus, a bio-fuel cell can generate electrical power at physiological conditions. A schematic mechanism is depicted in (Figure 2). In this example, glucose oxidase (GOx) is used as oxidative enzyme on the anode, and laccase or cytochrome c/cytochrome oxidase (Cyt c/ Cox) is used as reductive enzyme on the cathode. These bioelectrocatalytic electrodes oxidize glucose and reduce oxygen to generate electricity. This power generation mechanism makes bio-fuel cell the best power source for implanted devices. However, the practical application of bio-fuel cell to implanted devices is still far to reach because of the lack of researches and techniques to build efficient electron relays between enzymes and electron collectors. To date, the best operation voltage and power density that have been reported to be suffice to drive silicon integrated circuits are 0.78 V and 268 $\mu W \cdot cm^{-2}$, but this bio-fuel cell lost 10% of its power per day.[100] Efficient electron relay, long-term enzyme stability, and high power density are the key issues in improving the performance of bio-fuel cells.[101, 102] To fabricate efficient enzymatic electrodes, it requires techniques to tailor molecular structures at nanometric scale.

Surface density

To improve the power density of electrochemical cell, surface-volume ratios of electrode materials is a main factor. In a solid state chemical reaction, the reaction rate is determined by the interfacial surfaces among the reactants. The more the surface area is, the less the kinetic limitation of reaction is. In terms of a tubular material, the higher the aspect ratio (ratio of the length to the width) of this material is, the more the specific surface area (ratio of surface area to volume) is (Figure 3). Therefore, nanomaterials, such as nanotubes and nanowires, are very useful in promoting the efficiency of energy usage. A material comprised of nanowires not only provides a high surface density but also has structural stability, which can result from the structural supports of these

nanowires themselves. Nanomaterials can store or generate energy more efficiently than other materials of micro-scale structures. In other words, introducing well-tailored nanomaterials into a electrochemical cell can greatly improve its power density.

VI.C. Preliminary Experimental

VI.C.1 Biomineralization of cobalt oxide on virus

Materials. E4 virus contains tetra-glutamate preceded with an alanine on the N-terminus of pVIII proteins was engineered by Dr. Soo-Kwan Lee. Cobalt chloride ($CoCl_2 \cdot 6H_2O$) was purchased from Afla Aesar. $NaBH_4$ (sodium borohydride) was purchased from Sigma-Aldrich.

Biomineralization of cobalt oxide nanowire. 100 μL of E4 virus (~ 10^9 pfu/ μL) were incubated in 1 mL aqueous cobalt chloride solution (1 mM) for 30 min at room temperature to promote cobalt ion binding. Following reduction with 1 mL $NaBH_4$ (5 mM) and spontaneous oxidation in water, monodisperse and crystalline cobalt oxide (Co_3O_4) nanowire were produced.

VI.C.2 Electrochemical analysis of cobalt oxide nanowires

Materials. Cobalt oxide nanowires made in VI.C.1., Super P™ (MMM Carbon), poly(vinylidene fluoride)-hexafluoropropylene (PVDF-HFP), Swagelok™ design cells, and separator Celgard™ 2400 were prepared.

Galvanostatic measurement. For electrochemical evaluation of the cobalt oxide nanowires, cathode material was the mixture of 3.29 mg of the virus-based nanowires, Super P™ (MMM Carbon) carbon black, and poly(vinylidene fluoride)-hexafluoropropylene (PVDF-HFP) binder in a mass ratio of 74 : 15 : 11. The cathode material was spread on copper foil, and Li metal foil was used as the anodic electrode. The cathode and anode electrodes sandwiched a separator film of Celgard™ 2400 were assembled into Swagelok™ design cell. The whole cell was saturated with the electrolyte, 1M $LiPF_6$ in ethylene carbonate and dimethyl carbonate (1:1 by volume). Galvanostatic cycle was performed between 3.0 V and 0.01 V using a MACCOR automated tester.

VI.C.3 Synthesis of iron phosphate virus fiber

Materials. M13 bacteriophage was amplified, purified and concentrated to 10^{13} pfu/μL. The crosslinking agent (glutaraldehyde, 50%) was purchase from Sigma-Aldrich. Iron phosphate powder (~1 μm) was a gift from Nonglak Moothong in Prof. Yet-Ming Chiang's group at M.I.T.

Fabrication of iron phosphate virus fiber. A mixture of bacteriophage suspension, Super P™ carbon black, and iron phosphage in a mass ratio 75 : 20 : 5 was loaded into the 1 mL syringe with gauge 31 needle. The spinning process was the same as described in **Chapter V**. To test the electrochemical properties, the spun virus fiber was deposited on an aluminum foil and assembled in a Swagelok™ design cell with a Li metal foil as the anodic electrode and Celgard™ 2400 as the separator.

VI. D. Results and Discussion

Transition metallic ions are known to be chelated by electronegative atoms such as nitrogen and oxygen in the ligands of molecules. Examples include, but not limits to, ethylenediaminetetraacetic acid (EDTA), heme, and nickel (II) nitrilotriacetic acid (NTA)....etc. The introduction of carboxylate ligands onto a surface theoretically will enhance the number of metallic ions bound to the surface. Therefore, the goal was set to create a peptide motif containing rich carboxylic groups on pVIII proteins to facilitate the nucleation process on the filamentous virus by seeding metallic ions on the virus. One of the successful engineering on the M13 bacteriopahge was the E4 clone. Tetra-glutamate motif containing four successive glutamates (EEEE), termed E4, was fused to the N-terminus of each copy of pVIII protein. The E4 virus was incubated with cobalt ions, followed by reducing the cobalt ion with $NaBH_4$. The mineralized cobalt metal was further oxidized in aqueous solution. The high resolution TEM (HR-TEM) electron diffraction pattern and lattice spacing (Figure 4) confirmed that the crystal structure on the virus template was Co_3O_4. Figure 4 inset showed that the measured lattice spacing corresponds to the planes of Co_3O_4. Because pVIII proteins were genetically engineered with high population of carboxylic groups and thousands of cobalt ions bound to the viral surface could be reduced simultaneously, homogeneous and high crystalline nanoparticles were densely grown on this viral template. Compared to the Au nanoparticles grown in **Chapter III**, the crystal and grain structures of of the Co_3O_4 nanoparticles had totally different morphology, indicating different growing mechanisms. In this case, the growth of Co_3O_4 nanoparticle on E4 virus was dominated by nucleation process. Contrary to E4 virus, the wild type virus M13KE expressing no peptide insert or the solution without virus formed irregular and large precipitates of Co/Co_3O_4 mixtures, indicating the specificity of peptide binding/nucleating process.

The viral Co_3O_4 nanowires had a large surface area of 141.7 m^2/g as measured by the Brunauer-Emmett-Teller (BET) method. The mass ratio of Co_3O_4 and virus was 0.837 : 0.163 and the volume ratio of the virus compared to the Co_3O_4 was estimated to be 1.7 %. Voltage/capacity curves for the Co_3O_4 nanowires/Li half cell showed typical lithiation/delithiation behaviors of Co_3O_4 materials. The larger first-insertion capacity

compared to that in subsequent delithiation was characteristic of this material, and was mainly due to irreversible reactions occurring upon initial lithiation. The estimated lithiated state of $Li_xCo_3O_4$ was $Li_{1.47}Co_3O_4$. Reversible capacity (Figure 5) ranging from 600 to 750 mAh/g was observed. The lithiation/delithiation capacity stabilized at 600 mAh/g over 20 cycles. The virus mediated the growth of uniform sized cobalt oxide nanomaterials, maintained the structural integrity, and imparted dense materials packing provided electrochemical advantages. Samples synthesized without the virus templates exhibited rapidly fading capacity (Figure 5), which was most likely attributable to large particle size, incomplete oxidation of cobalt, and inhomogeneous structure and composition.

In the cycle use of the electrochemically active material, the lost of its capacity is mostly attributed to the formation of non-conductive inert layers occurring in the oxidation process. Therefore, introducing conductive metals into the active materials will facilitate the electron dispersion and improve the capacity during the charging/discharging cycles. However, depending on the types of electrolyte used in the electrochemical cell, conductive metals will also lower the overpotentials required to decompose the electrolytes. Fortunately, the electrolyte ($LiPF_6$, ethylene carbonate and dimethyl carbonate) used here has relatively higher overpotential compared with the operating/charging voltages performed by the viral Co_3O_4 nanowires/Li cell.

Due to the advantages could be brought by intruding conductive metals, a type 8+8 phage containing gold binding motif (p3-Au12) and tetra-glutamate (E4) motif was designed and produced using the methods described in the **Chapter II**. This virus was named AuE4. The incubation of the AuE4 clones with 5 nm gold colloid suspension (as described in **Chapter III**) also resulted in one dimensional arrays of Au nanoparticles. Different clones such as wild type and E4 virus which do not have gold binding motif, could not lead to the attachment of gold nanoparticles along the length of virus. After removing unbound excess gold nanoparticles by centrifugation, Co_3O_4 was nucleated and grown via the tetra-glutamate functionality, producing hybrid nanostructures of 5-nm Au nanoparticles spatially interspersed within Co_3O_4 wires (Figure 6). The crystal structure of Co_3O_4 was confirmed by electron diffraction, and inductively coupled plasma mass

spectrometry (ICPMS) analysis indicated that Au nanoparticles were associated in Co_3O_4 in a weight ratio of 2.4 : 97.6. The result, again, demonstrated the capability of viral template for producing hybrid nanoarchitectures through genetic engineering.

The electrochemical property of the hybrid Au-Co_3O_4 nanowire was evaluated using galvanostatic cycling and cyclic voltammetry. The nanowires (~3.41 mg) were deposited on the Cu substrate for the assembly of the electrochemical cell. Galvanostatic measurement showed that the hybrid composite generated higher initial and reversible lithiation capacity than the pure Co_3O_4 nanowires when tested at the same current rate (Figure 7). The higher lithiation capacity might result either from the formation of Li-Au intermetallic compound[103] or the conductive effects of Au nanoparticles on the reaction of Li with Co_3O_4. However, the theoretical capacity of Au is approximately 408.2 to 136.1 mAh/g for the formation of Li_xAu (x = 1 to 3), which suggests a negligible contribution to the lithiation capacity when considering the Au : Co_3O_4 ratio (2.4 : 97.6) as obtained above. Besides, when compared with the viral Co_3O_4 nanowire, the cyclic voltammogram of hybrid Au-Co_3O_4 nanowire (Figure 8) showed no significant new redox peaks that could be associated with the lithiation of Au.[103] This was the evidence to improve the electronic conductivity upon the reduction of Co_3O_4 nanoparticles. The incorporation of gold nanoparticles increased the lithiation rate (reduction) of Co_3O_4 as indicated by the enhanced reduction peak seen by cyclic voltammetry in Figure 8, and the specific capacity of the hybrid Au-Co_3O_4 nanowire was estimated to be ~ 30 % better than that of the Co_3O_4 nanowire (Figure 7).

The spinning of virus fiber can be designed into a roll-to-roll fabrication process and the virus fiber can be continuously spun and produced. By integrating electrochemical active materials with the virus, continuous fiber-based electrode was fabricated. The virus-based electrode made by this process was flexible and could be complied upon various substrate structures such as rod or film (Figure 9a and b). A prototype of fibril electrode containing iron phosphate was spun and coiled upon an aluminum rod and tested for electrochemical properties (Figure 9d and e). Galvanostatic measurement was performed to test the lithiation capacity. The capacity was less than 10% of its theoretical capacity, and this might be due to the microphase separations of

iron phosphate, carbon black, and engineered virus. The material compositions to spin fibril electrode were not best tuned yet. More investigations are needed to optimize the processing condition and electrochemical performance.

IV. E. Conclusion

The cobalt oxide nanowires templated by M13 virus at room temperature demonstrated comparable properties to nanoparticles fabricated at high temperature (above 500°C). The high aspect ratio structure of the M13 virus was proved to provide advantages of creating high surface density of materials through homogenous nucleation and stabilizing nanomaterials for electrochemical reaction. Fiber-based battery can be designed using virus as the templating materials in the future (Figure 10). In addition, the viral template was demonstrated to be a genetically tunable platform for creating hetero-functionalities or hybrid materials. While more investigations on the effects of Au in Co_3O_4 are required to reveal the exact electrochemical mechanism, the experimental results has showed that a small amount of Au nanoparticles dispersed within Co_3O_4 to produce a hybrid material markedly improved the electrochemical performance. Such hybrid nanostructue showing the promise of improving electrochemical properties makes the tunable M13 bacteriophage a unique template for the convenience of designing other potential hetero-materials.

IV. F. Figures

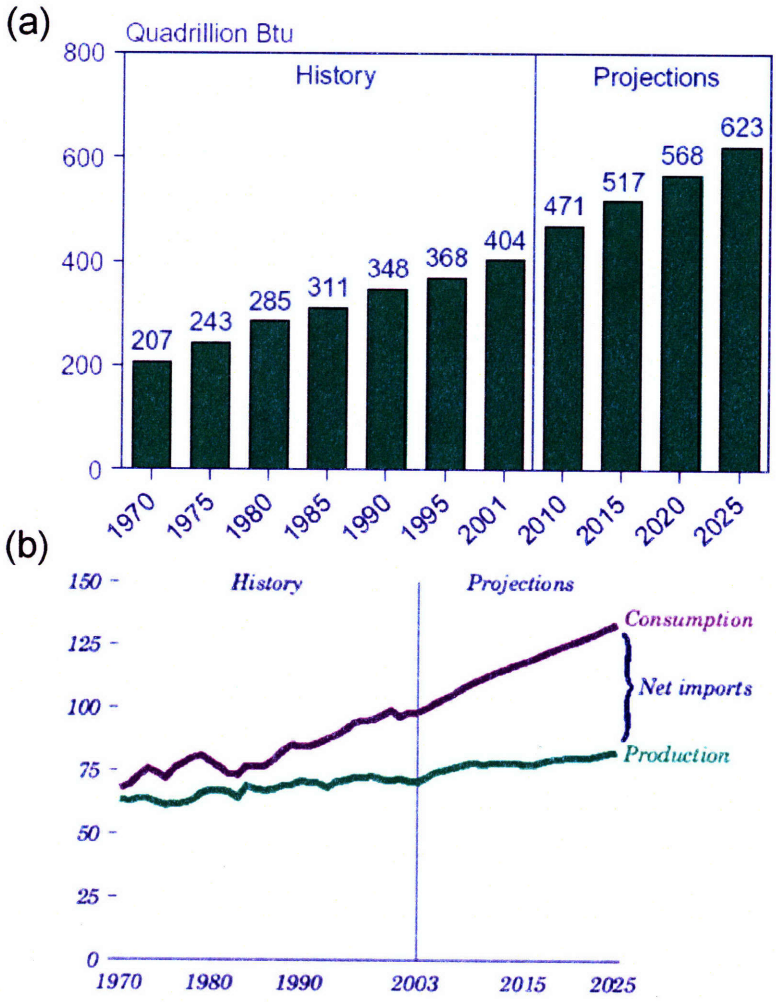

Figure 1 The trend of increasing energy consumption. (a) World marketed energy consumption, 1970-2025. (b) Total energy consumption and production (quadrillion Btu) in the US, 1970-2025 (Graph Source: Energy Information Administration, International Energy Outlook 2004 and Annual Energy Outlook 2005).

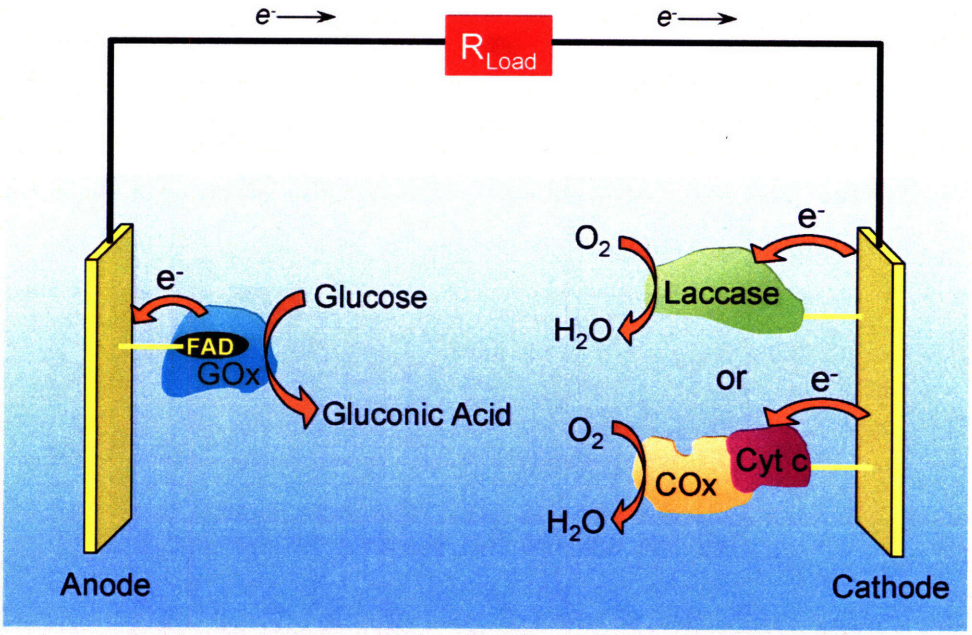

Figure 2 A schematic representation of bio-fuel cell. In this bio-fuel cell, glucose oxidase is used as the anode to oxidize glucose into gluconic acid and release electrons. Reductive enzymes such laccase and cytochrome c/cytochrome oxidase complex can be used as the cathode to reduce oxygen into water and complete the electrochemical cycle.

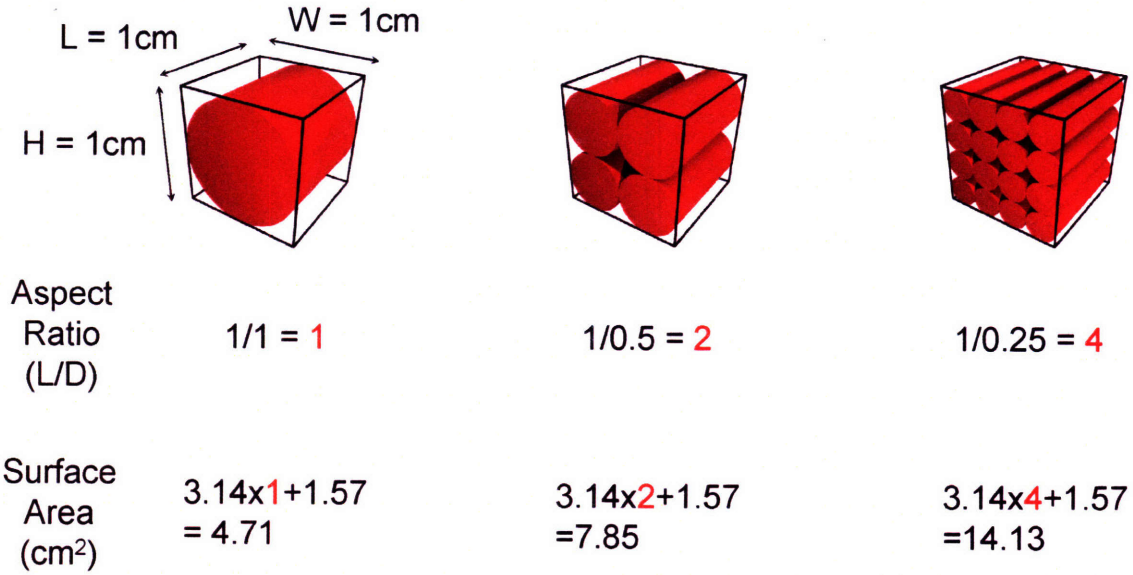

Figure 3 Comparison of aspect ratio to surface area for tubular structures. Surface density is the key parameter to affect the performance and life span of an energy material. The higher the surface density, the better the overall performance.

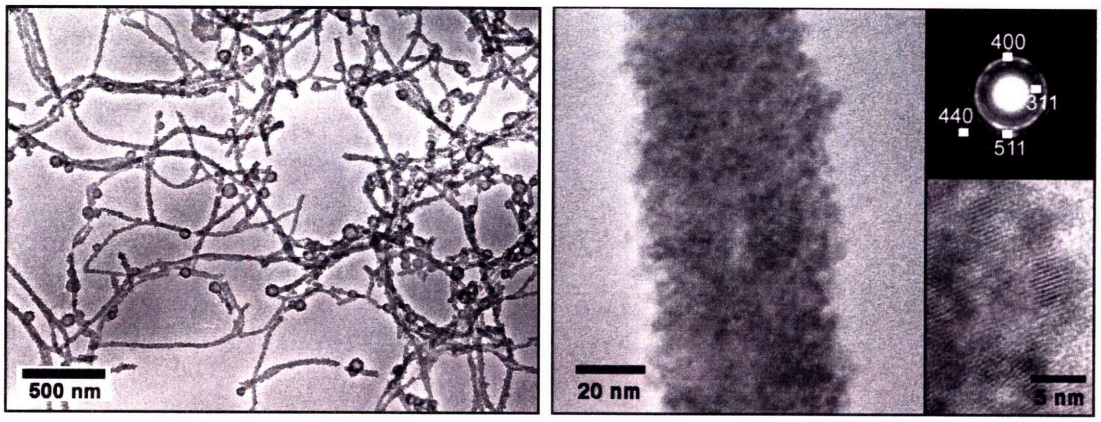

Figure 4. TEM images of virus templated Co_3O_4 nanowires. (Left and right) High-resolution TEM images of Co_3O_4 viral nanowires. Electron diffraction pattern (inset, upper right) confirmed that the crystal structure was Co_3O_4. The measured lattice spacing corresponded to the planes of Co_3O_4. Magnified image (inset, lower right) shows the lattice fringe of Co_3O_4 nanocrystals along the major coat pVIII proteins of a virus.

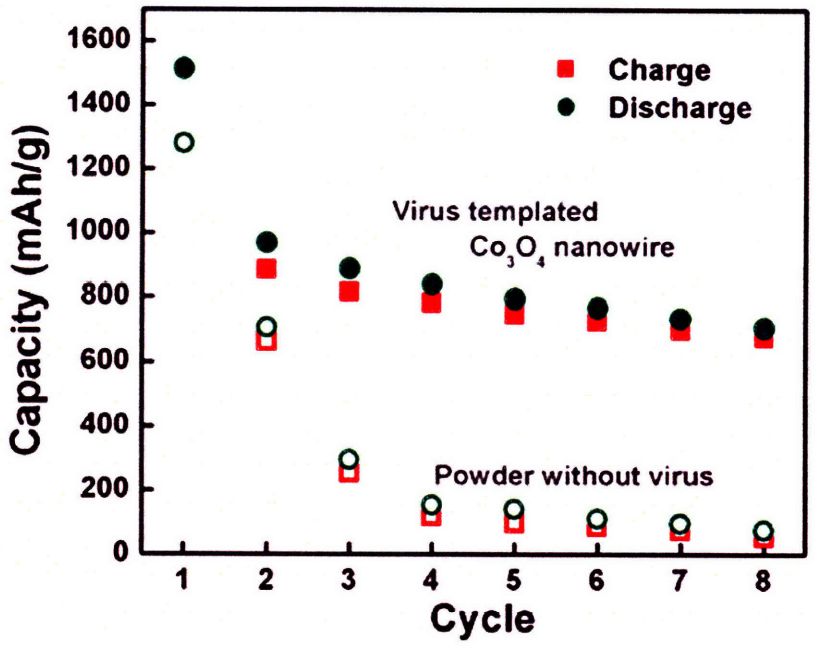

Figure 5. Specific capacity versus cycle number. The capacity was calculated based on the mass of Co_3O_4 only. The data of virus templated nanowires and the powder that was fabricated without viruses under the same condition was compared.

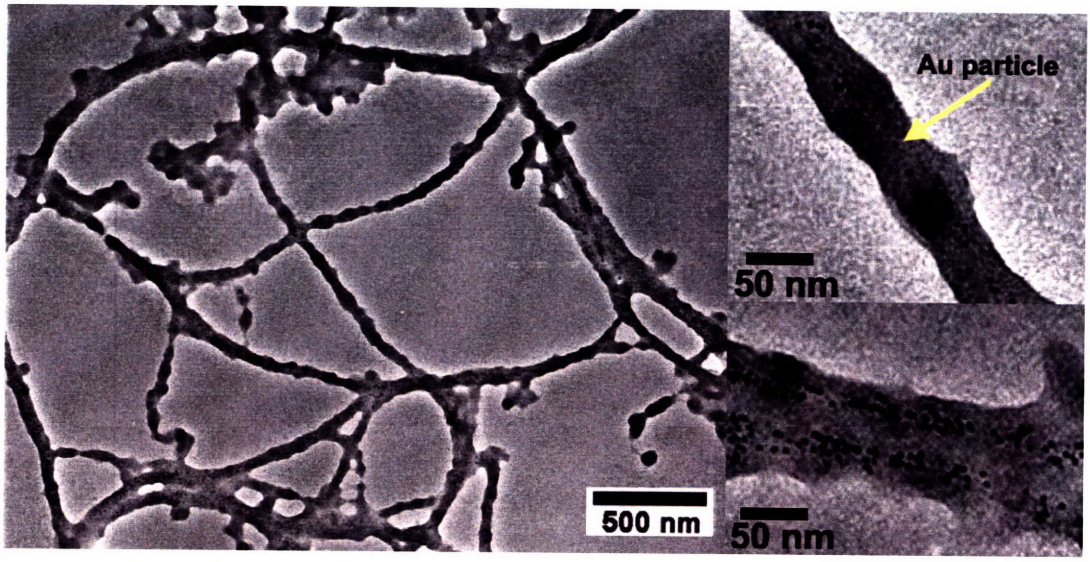

Figure 6. TEM image of hybrid nanowires of Au nanoparticles/Co_3O_4. The gold nanoparticles assembled in the hybrid nanowires were located at the center of the Co_3O_4 nanowires. The nanoparticles dispersed in the cobalt oxide materials could improve the electrical performance of the active materials.

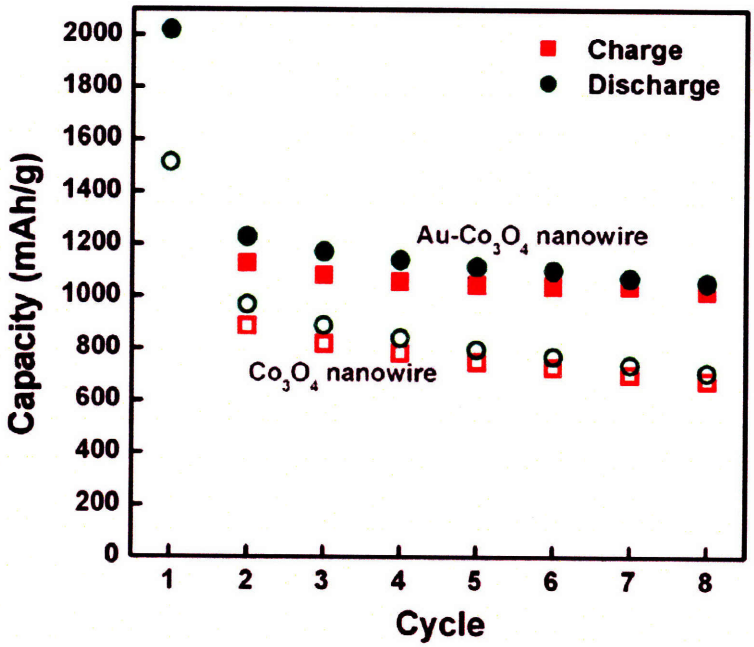

Figure 7. Specific capacity of hybrid Au-Co_3O_4 nanowires. Half cell with Li electrode was cycled at a rate of C/26.5. Virus mass was subtracted and the mass of active materials such as Co_3O_4 and Au was counted. The capacity of virus-directing Co_3O_4 nanowires without Au nanoparticles was compared with that of hybrid Au-Co_3O_4 nanowires.

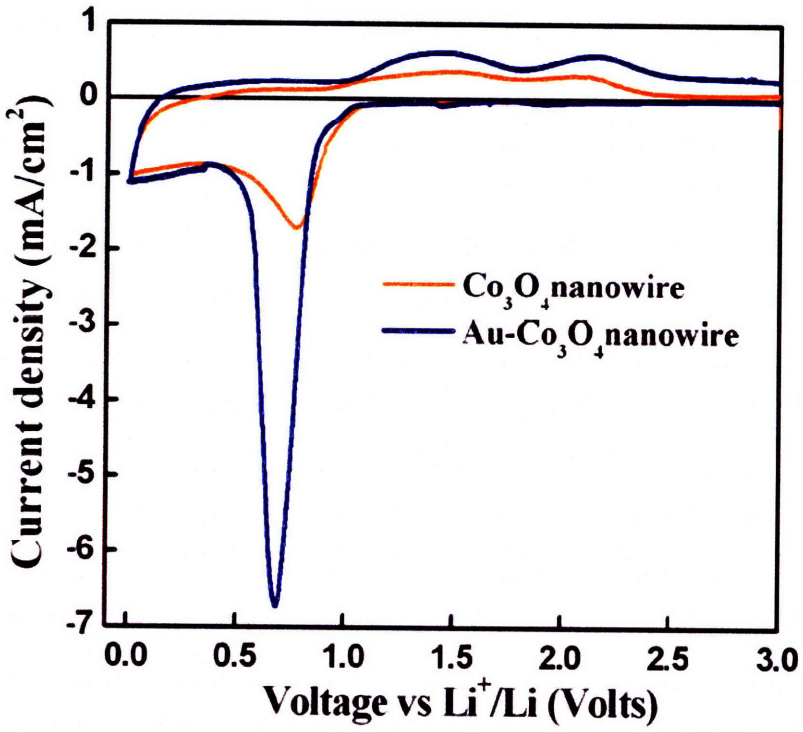

Figure 8. Cyclic voltammograms of hybrid Au-Co_3O_4 and Co_3O_4 nanowires. Approximately same quantities of active materials were compared. The cyclic voltammetry was performed at a scanning rate of 0.3 mV/s. The electrochemical performance was greatly improved when the gold nanoparticle was introduced.

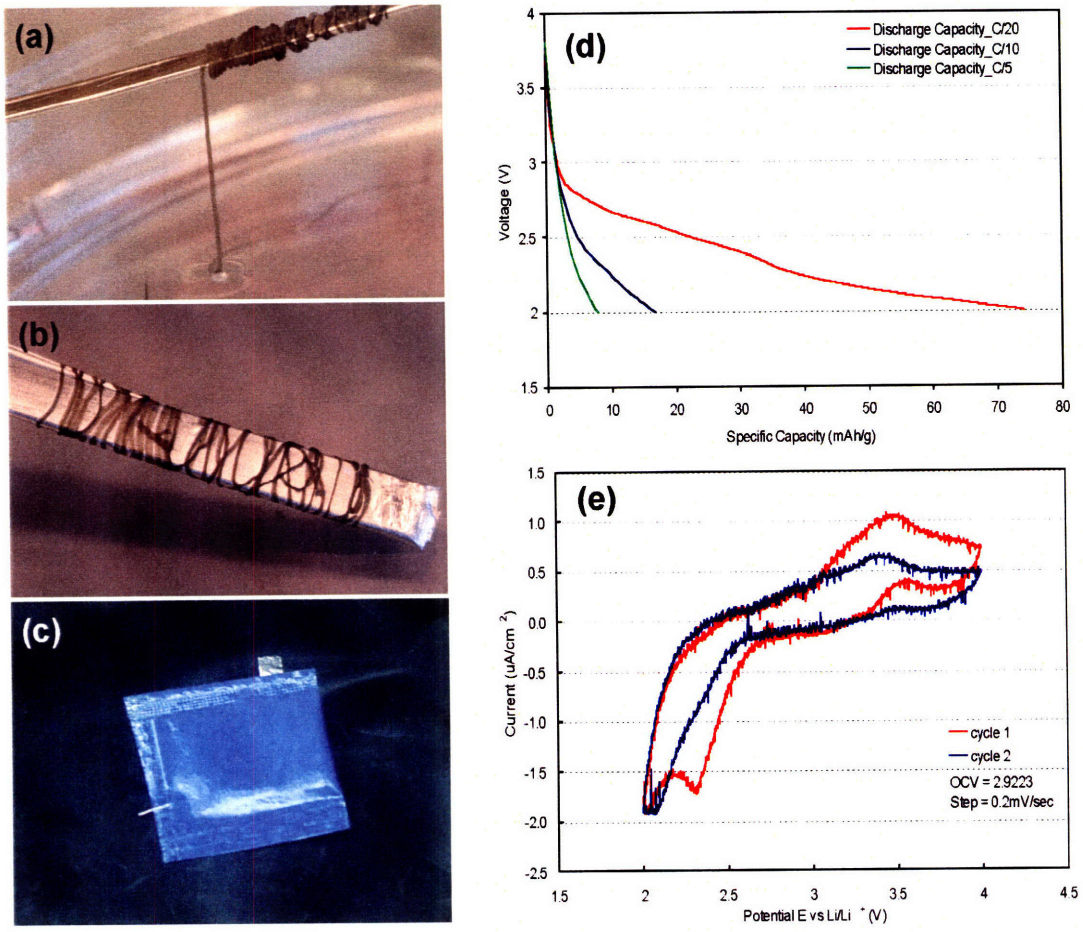

Figure 9 Fiber based lithium battery. (a, b) Virus based fibers containing iron phosphate particles were spun and wrapped on an aluminum current collector. (c) A half-cell was assembled with a lithium foil for electrical property measurements. (d) Specific capacities of the virus based fiber discharged at three different rates. (e) Cyclic voltammetry of $FePO_4$ virus fiber in the range of 2 to 4 V.

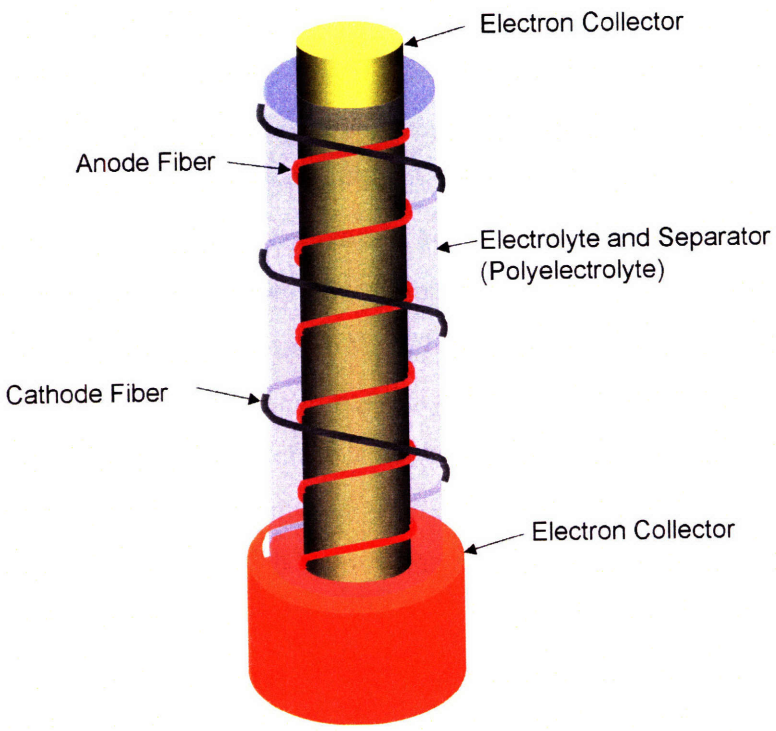

Figure 10. Schematic design of uniaxial fiber-based battery. The center and outermost layer are the current collectors. A layer of polyelectrolyte is coated between the anodic and cathodic fibers.

Remarks

The research presented here has expanded the applications of natural templates for material syntheses and structural fabrications from nanometer scale to micrometer scale. However, a lot still remains to be discovered and explored. The future studies should focus on: 1) revealing the binding and growing mechanisms of materials synthesized by the protein/peptide scaffolds; 2) developing new types of libraries based on the engineering portions on the biological templates; 3) expanding the capabilities to perform molecular expressions on the biological templates from small and single entities (e.g. peptide) to large and multiple objects (e.g. enzyme). Continued efforts are needed to establish complete techniques to fully control over the building blocks and manipulate individual components at the molecular level. Undoubtedly, the fundamental studies of peptide/protein materials and the driving forces of engineering applications eventually need to be integrated to exploit the potentials of natural materials and to benefit the world.

Reference

1. Cha, J. N.; Stucky, G. D.; Morse, D. E.; Deming, T. J. *Nature* **2000,** 403, (6767), 289-292.
2. Weaver, J. C.; Pietrasanta, L. I.; Hedin, N.; Chmelka, B. F.; Hansma, P. K.; Morse, D. E. *Journal of Structural Biology* **2003,** 144, (3), 271-281.
3. Smith, B. L.; Schaffer, T. E.; Viani, M.; Thompson, J. B.; Frederick, N. A.; Kindt, J.; Belcher, A.; Stucky, G. D.; Morse, D. E.; Hansma, P. K. *Nature* **1999,** 399, (6738), 761-763.
4. Belcher, A. M.; Wu, X. H.; Christensen, R. J.; Hansma, P. K.; Stucky, G. D.; Morse, D. E. *Nature* **1996,** 381, (6577), 56-58.
5. Fritz, M.; Belcher, A. M.; Radmacher, M.; Walters, D. A.; Hansma, P. K.; Stucky, G. D.; Morse, D. E.; Mann, S. *Nature* **1994,** 371, (6492), 49-51.
6. Komeili, A.; Vali, H.; Beveridge, T. J.; Newman, D. K. *Proceedings of the National Academy of Sciences of the United States of America* **2004,** 101, (11), 3839-3844.
7. Komeili, A.; Li, Z.; Newman, D. K.; Jensen, G. J. *Science* **2006,** 311, (5758), 242-245.
8. Marvin, D. A.; Hale, R. D.; Nave, C.; Citterich, M. H. *Journal of Molecular Biology* **1994,** 235, (1), 260-286.
9. Marvin, D. A. *International Journal of Biological Macromolecules* **1990,** 12, (2), 125-138.
10. Holliger, P.; Riechmann, L.; Williams, R. L. *Journal of Molecular Biology* **1999,** 288, (4), 649-657.
11. Holliger, P.; Riechmann, L. *Structure* **1997,** 5, (2), 265-275.
12. Armstrong, N.; Adey, N. B.; McConnell, S. J.; Kay, B. K. *Phage Display of Peptides and Proteins* **1996**, 35-53.
13. Belien, T.; Hertveldt, K.; Van den Brande, K.; Robben, J.; Van Campenhout, S.; Volckaert, G. *Journal of Biotechnology* **2005,** 115, (3), 249-260.
14. Corey, D. R.; Shiau, A. K.; Yang, Q.; Janowski, B. A.; Craik, C. S. *Gene* **1993,** 128, (1), 129-134.
15. Sarikaya, M.; Tamerler, C.; Jen, A. K. Y.; Schulten, K.; Baneyx, F. *Nature Materials* **2003,** 2, (9), 577-585.
16. Brown, S. *Nature Biotechnology* **1997,** 15, (3), 269-272.
17. Matsuura, T.; Miyai, K.; Trakulnaleamsai, S.; Yomo, T.; Shima, Y.; Miki, S.; Yamamoto, K.; Urabe, I. *Nature Biotechnology* **1999,** 17, (1), 58-61.
18. Petrenko, V. A.; Smith, G. P.; Gong, X.; Quinn, T. *Protein Engineering* **1996,** 9, (9), 797-801.

19. Lee, S.-W.; Lee, S. K.; Belcher, A. M. *Advanced Materials (Weinheim, Germany)* **2003,** 15, (9), 689-692.

20. Fowler, C. E.; Shenton, W.; Stubbs, G.; Mann, S. *Advanced Materials (Weinheim, Germany)* **2001,** 13, (16), 1266-1269.

21. Flynn, C. E.; Lee, S.-W.; Peelle, B. R.; Belcher, A. M. *Acta Materialia* **2003,** 51, (19), 5867-5880.

22. Schlick, T. L.; Ding, Z.; Kovacs, E. W.; Francis, M. B. *Journal of the American Chemical Society* **2005,** 127, (11), 3718-3723.

23. Huang, Y.; Chiang, C.-Y.; Lee, S. K.; Gao, Y.; Hu, E. L.; De Yoreo, J.; Belcher, A. M. *Nano Letters* **2005,** 5, (7), 1429-1434.

24. Liang, W.; Shores, M. P.; Bockrath, M.; Long, J. R.; Park, H. *Nature (London, United Kingdom)* **2002,** 417, (6890), 725-729.

25. Klein, D. L.; Roth, R.; Lim, A. K. L.; Alivisatos, A. P.; McEuen, P. L. *Nature (London)* **1997,** 389, (6652), 699-701.

26. Deshmukh, M. M.; Prieto, A. L.; Gu, Q.; Park, H. *Nano Letters* **2003,** 3, (10), 1383-1385.

27. Brust, M.; Walker, M.; Bethell, D.; Schiffrin, D. J.; Whyman, R. *Journal of the Chemical Society-Chemical Communications* **1994**, (7), 801-802.

28. Mirkin, C. A. *Inorganic Chemistry* **2000,** 39, (11), 2258-2272.

29. Tan, Y. W.; Li, Y. F.; Zhu, D. B. *Langmuir* **2002,** 18, (8), 3392-3395.

30. Matsui, S.; Kaito, T.; Fujita, J.; Komuro, M.; Kanda, K.; Haruyama, Y. *Journal of Vacuum Science & Technology B* **2000,** 18, (6), 3181-3184.

31. Mayer, C. R.; Neveu, S.; Cabuil, V. *Advanced Materials* **2002,** 14, (8), 595-597.

32. Sun, H. B.; Nakamura, A.; Shoji, S.; Duan, X. M.; Kawata, S. *Advanced Materials* **2003,** 15, (23), 2011-2014.

33. Westwater, J.; Gosain, D. P.; Tomiya, S.; Usui, S.; Ruda, H. *Journal of Vacuum Science & Technology B* **1997,** 15, (3), 554-557.

34. Morales, A. M.; Lieber, C. M. *Science* **1998,** 279, (5348), 208-211.

35. Whitney, T. M.; Jiang, J. S.; Searson, P. C.; Chien, C. L. *Science* **1993,** 261, (5126), 1316-1319.

36. Xu, D. S.; Xu, Y. J.; Chen, D. P.; Guo, G. L.; Gui, L. L.; Tang, Y. Q. *Advanced Materials* **2000,** 12, (7), 520-+.

37. Zhao, W. B.; Zhu, J. J.; Chen, H. Y. *Journal of Crystal Growth* **2003,** 258, (1-2), 176-180.

38. Sun, Y. G.; Gates, B.; Mayers, B.; Xia, Y. N. *Nano Letters* **2002,** 2, (2), 165-168.

39. Wong, T. C.; Li, C. P.; Zhang, R. Q.; Lee, S. T. *Applied Physics Letters* **2004,** 84, (3), 407-409.

40. Huang, Y.; Duan, X.; Cui, Y.; Lauhon, L. J.; Kim, K.-H.; Lieber, C. M. *Science (Washington, DC, United States)* **2001,** 294, (5545), 1313-1317.

41. Tans, S. J.; Verschueren, A. R. M.; Dekker, C. *Nature (London)* **1998,** 393, (6680), 49-52.

42. Keren, K.; Berman, R. S.; Buchstab, E.; Sivan, U.; Braun, E. *Science (Washington, DC, United States)* **2003,** 302, (5649), 1380-1382.

43. Yang, P.; Kim, F. *ChemPhysChem* **2002,** 3, (6), 503-506.

44. Huang, Y.; Duan, X.; Wei, Q.; Lieber, C. M. *Science (Washington, DC, United States)* **2001,** 291, (5504), 630-633.

45. Alivisatos, A. P. *Science (Washington, D. C.)* **2000,** 289, (5480), 736-737.

46. Seeman, N. C.; Belcher, A. M. *Proceedings of the National Academy of Sciences of the United States of America* **2002,** 99, (9, Suppl. 2), 6451-6455.

47. Sarikaya, M.; Tamerler, C.; Jen, A. K. Y.; Schulten, K.; Baneyx, F. *Nature Materials* **2003,** 2, (9), 577-585.

48. Brown, S. *Proc Natl Acad Sci U S A FIELD Full Journal Title:Proceedings of the National Academy of Sciences of the United States of America* **1992,** 89, (18), 8651-5.

49. Whaley, S. R.; English, D. S.; Hu, E. L.; Barbara, P. F.; Belcher, A. M. *Nature (London)* **2000,** 405, (6787), 665-668.

50. Nam, K. T.; Peelle, B. R.; Lee, S.-W.; Belcher, A. M. *Nano Letters* **2004,** 4, (1), 23-27.

51. Douglas, T.; Young, M. *Nature (London)* **1998,** 393, (6681), 152-155.

52. Mao, C.; Solis, D. J.; Reiss, B. D.; Kottmann, S. T.; Sweeney, R. Y.; Hayhurst, A.; Georgiou, G.; Iverson, B.; Belcher, A. M. *Science (Washington, DC, United States)* **2004,** 303, (5655), 213-217.

53. Hartgerink, J. D.; Beniash, E.; Stupp, S. I. *Science (Washington, DC, United States)* **2001,** 294, (5547), 1684-1688.

54. Reches, M.; Gazit, E. *Science (Washington, DC, United States)* **2003,** 300, (5619), 625-627.

55. Weizmann, Y.; Patolsky, F.; Popov, I.; Willner, I. *Nano Letters* **2004,** 4, (5), 787-792.

56. Yan, H.; Park, S. H.; Finkelstein, G.; Reif, J. H.; LaBean, T. H. *Science (Washington, DC, United States)* **2003,** 301, (5641), 1882-1884.

57. Li, Z.; Chung, S.-W.; Nam, J.-M.; Ginger, D. S.; Mirkin, C. A. *Angewandte Chemie, International Edition* **2003,** 42, (20), 2306-2309.

58. Dujardin, E.; Peet, C.; Stubbs, G.; Culver, J. N.; Mann, S. *Nano Letters* **2003,** 3, (3), 413-417.

59. Hall, S. R.; Shenton, W.; Engelhardt, H.; Mann, S. *ChemPhysChem* **2001,** 2, (3), 184-186.

60. Lee, S.-W.; Mao, C.; Flynn, C. E.; Belcher, A. M. *Science (Washington, DC, United States)* **2002,** 296, (5569), 892-895.

61. Eichen, Y.; Braun, E.; Sivan, U.; Ben-Yoseph, G. *Acta Polymerica* **1998,** 49, (10-11), 663-670.

62. Braun, E.; Eichen, Y.; Sivan, U.; Ben-Yoseph, G. *Nature* **1998,** 391, (6669), 775-778.

63. Scheibel, T.; Parthasarathy, R.; Sawicki, G.; Lin, X. M.; Jaeger, H.; Lindquist, S. L. *Proceedings of the National Academy of Sciences of the United States of America* **2003,** 100, (8), 4527-4532.

64. Reches, M.; Gazit, E. *Nano Letters* **2004,** 4, (4), 581-585.

65. Reches, M.; Gazit, E. *Science* **2003,** 300, (5619), 625-627.

66. Hendler, N.; Sidelman, N.; Reches, M.; Gazit, E.; Rosenberg, Y.; Richter, S. *Advanced Materials* **2007,** 19, (11), 1485-+.

67. Brongersma, M. L.; Hartman, J. W.; Atwater, H. A. *Physical Review B: Condensed Matter and Materials Physics* **2000,** 62, (24), R16356-R16359.

68. Brown, K. R.; Natan, M. J. *Langmuir* **1998,** 14, (4), 726-728.

69. Xiao, Y.; Patolsky, F.; Katz, E.; Hainfeld, J. F.; Willner, I. *Science* **2003,** 299, (5614), 1877-1881.

70. Witt, S.; Singh, M.; Kalisz, H. M. *Applied and Environmental Microbiology* **1998,** 64, (4), 1405-1411.

71. Gouda, M. D.; Thakur, M. S.; Karanth, N. G. *Applied Biochemistry and Biotechnology* **2002,** 102, 471-480.

72. Shin, J. S.; Ryu, S. H.; Lee, C.; Yu, M. H. *Journal of Biochemistry and Molecular Biology* **2006,** 39, (1), 55-60.

73. Gu, Y.; Chen, D.; Jiao, X. *Journal of Physical Chemistry B* **2005,** 109, (38), 17901-17906.

74. Gvishi, R.; Narang, U.; Ruland, G.; Kumar, D. N.; Prasad, P. N. *Applied Organometallic Chemistry* **1997,** 11, (2), 107-127.

75. Dresselhaus, M. S.; Dresselhaus, G. *Journal of Electroceramics* **1997,** 1, (3), 273-286.

76. Nazar, L. F.; Goward, G.; Leroux, F.; Duncan, M.; Huang, H.; Kerr, T.; Gaubicher, J. *International Journal of Inorganic Materials* **2001,** 3, (3), 191-200.

77. Li, D.; Xia, Y. *Advanced Materials (Weinheim, Germany)* **2004,** 16, (14), 1151-1170.

78. Ma, M.; Mao, Y.; Gupta, M.; Gleason, K. K.; Rutledge, G. C. *Macromolecules* **2005,** 38, (23), 9742-9748.

79. Wei, Q. F.; Mather, R. R.; Wang, X. Q.; Fotheringham, A. F. *Journal of Materials Science* **2005,** 40, (20), 5387-5392.

80. Gubitz, G. M.; Paulo, A. C. *Current Opinion in Biotechnology* **2003,** 14, (6), 577-582.

81. Deitzel, J. M.; Kosik, W.; McKnight, S. H.; Beck Tan, N. C.; DeSimone, J. M.; Crette, S. *Polymer* **2001,** 43, (3), 1025-1029.

82. Rothemund, P. W. K. *Nature (London, United Kingdom)* **2006,** 440, (7082), 297-302.

83. Hartgerink, J. D.; Beniash, E.; Stupp, S. I. *Science (Washington, DC, United States)* **2001,** 294, (5547), 1684-1688.

84. Flynn, C. E.; Lee, S.-W.; Peelle, B. R.; Belcher, A. M. *Acta Materialia* **2003,** 51, (19), 5867-5880.

85. Li, Z.; Chung, S.-W.; Nam, J.-M.; Ginger, D. S.; Mirkin, C. A. *Angewandte Chemie, International Edition* **2003,** 42, (20), 2306-2309.

86. Brutchey, R. L.; Yoo, E. S.; Morse, D. E. *Journal of the American Chemical Society* **2006,** 128, (31), 10288-10294.

87. Guerette, P. A.; Ginzinger, D. G.; Weber, B. H. F.; Gosline, J. M. *Science (Washington, D. C.)* **1996,** 272, (5258), 112-15.

88. Lazaris, A.; Arcidiacono, S.; Huang, Y.; Zhou, J.-F.; Duguay, F.; Chretien, N.; Welsh, E. A.; Soares, J. W.; Karatzas, C. N. *Science (Washington, DC, United States)* **2002,** 295, (5554), 472-476.

89. Sofia, S.; McCarthy, M. B.; Gronowicz, G.; Kaplan, D. L. *Journal of Biomedical Materials Research* **2000,** 54, (1), 139-148.

90. Fantner, G. E.; Hassenkam, T.; Kindt, J. H.; Weaver, J. C.; Birkedal, H.; Pechenik, L.; Cutroni, J. A.; Cidade, G. A. G.; Stucky, G. D.; Morse, D. E.; Hansma, P. K. *Nature Materials* **2005,** 4, (8), 612-616.

91. Dogic, Z.; Fraden, S. *Physical Review Letters* **1997,** 78, (12), 2417-2420.

92. Lee, S.-W.; Lee, S. K.; Belcher, A. M. *Advanced Materials (Weinheim, Germany)* **2003,** 15, (9), 689-692.

93. Kerkam, K.; Viney, C.; Kaplan, D.; Lombardi, S. *Nature (London, United Kingdom)* **1991,** 349, (6310), 596-8.

94. Meissner, K. E.; Holton, C.; Spillman, W. B. *Physica E: Low-Dimensional Systems & Nanostructures (Amsterdam, Netherlands)* **2005,** 26, (1-4), 377-381.

95. Nam, K. T.; Kim, D.-W.; Yoo, P. J.; Chiang, C.-Y.; Meethong, N.; Hammond, P. T.; Chiang, Y.-M.; Belcher, A. M. *Science (Washington, DC, United States)* **2006,** 312, (5775), 885-888.

96. Kemell, M.; Pore, V.; Ritala, M.; Leskelae, M.; Linden, M. *Journal of the American Chemical Society* **2005,** 127, (41), 14178-14179.

97. Altman, G. H.; Diaz, F.; Jakuba, C.; Calabro, T.; Horan, R. L.; Chen, J.; Lu, H.; Richmond, J.; Kaplan, D. L. *Biomaterials* **2002,** 24, (3), 401-416.

98. Feughelman, M. *Journal of Applied Polymer Science* **2002,** 83, (3), 489-507.

99. Chen, T.; Barton, S. C.; Binyamin, G.; Gao, Z. Q.; Zhang, Y. C.; Kim, H. H.; Heller, A. *Journal of the American Chemical Society* **2001,** 123, (35), 8630-8631.

100. Mano, N.; Mao, F.; Shin, W.; Chen, T.; Heller, A. *Chemical Communications* **2003**, (4), 518-519.

101. Mano, N.; Mao, F.; Heller, A. *Journal of Electroanalytical Chemistry* **2005,** 574, (2), 347-357.

102. Mano, N.; Mao, F.; Heller, A. *Chembiochem* **2004,** 5, (12), 1703-1705.

103. Mui, S. C.; Trapa, P. E.; Huang, B.; Soo, P. P.; Lozow, M. I.; Wang, T. C.; Cohen, R. E.; Mansour, A. N.; Mukerjee, S.; Mayes, A. M.; Sadoway, D. R. *Journal of the Electrochemical Society* **2002,** 149, (12), A1610-A1615.